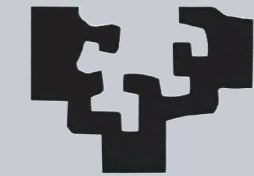




eman ta zabal zazu



U.P.V. E.H.U.



PhD Dissertation
**SU-8 MICROPROBES FOR BIOMEDICAL
APPLICATIONS**

Ane Altuna Letamendi

Supervisors: Dr. Luis José Fernández Ledesma and
Dr. Pedro Rolando Grandes Moreno

June 2012
© 2012, Ane Altuna Letamendi

eman ta zabal zazu



U.P.V. E.H.U.

IK4  IKERLAN
Research Alliance



PhD Dissertation
**SU-8 MICROPROBES FOR BIOMEDICAL
APPLICATIONS**

Ane Altuna Letamendi

Supervisors: Dr. Luis José Fernández Ledesma and
Dr. Pedro Rolando Grandes Moreno

June 2012

Eskerrak

Idatzi honen bitartez urte hauetan nire alboan izan ditudan guztien laguntza eskertu nahiko nuke.

There are many people to thank for their support and encouragement. I would like to acknowledge all the people that have trusted in me since the first day. The technical support and what is more important, the personal availability of all of them has been the engine during this long journey.

En primer lugar me gustaría agradecer a mi director de tesis, Dr. Luis Fernández, por su profesionalidad, entusiasmo y apoyo incondicional en todo momento. Él ha sido el gran partícipe de mi enriquecimiento profesional y espero que lo siga siendo en el futuro. Mil gracias.

Me gustaría agradecer a la Universidad del País Vasco y concretamente a Dr. Pedro Rolando Grandes del departamento de neurociencias por aceptar la dirección de esta tesis y adentrarse en el mundo de los microsistemas.

Gracias a Kepa Mayora por confiar en mí y darme la oportunidad de desarrollar este trabajo en el departamento de Microsistemas de Ikerlan S. Coop. Todo esto empezó cuando María Tijero me enseñó todo lo que sabía sobre las microagujas. Gracias por tu paciencia y consejos del día a día. Cómo no, agradecer al equipo de packaging, Javi, Rafa y Ander. Pero todo esto habría sido imposible sin la estrecha colaboración del departamento de Microsistemas. Todos ellos han contribuido en el buen trabajo; escuchando los problemas cada viernes, dándome consejo y compartiendo risas en la hora del café. Eskerrik asko guztioi, benetan. Lankideak eta lagunak aurkitu ditudalakoan nago.

Gracias a Liset Menéndez de la Prida por transmitir todos los conocimientos “neuro” con tanto entusiasmo y eficacia. Tus repetidas correcciones han entrado en lo más profundo de mí. Agradecer también a Elisa, Elena y Paloma por el gran interés que han mostrado en cada experimento.

Gracias a los del CNM; Gemma Gabriel, Antón Guimerà y Rosa Villa, por vuestra aportación y constancia. También, me gustaría agradecer a Antoni Ivorra por prestarme sus conocimientos escritos que tanto han agilizado la lectura de mi tesis.

Eta nola ez, egunerokotasunean horren garrantzitsuak diren pertsonak eskertu nahi nituzke. Ezer gutxi ulertuta ere, nire emozio eta saminak elkarbanatzen jakin dituztelako. Garar, Hirust, Nerea, Sujan, Laida, Jon Ander eta lagun guztiei. Hitz polittak baino bazkari eder batetara gonbidatzea hobe. Zuen interesa asko eskertzen da. Amamari eta bere ingurukoei, erregina bat bezala sentiarazten nautelako. 4D-koei, tio, Eider eta Josu, eskerrik asko izek. Tia Bego ta Jesusi. Ando, zure bizipoza ikaragarria da;

eskerrik asko egunak alaiagoak egitearren. Aitari, zure eguneroko bazkaria eta interesa ez dago ordaintzerik, milesker. Ama, eskerrik beroenak, zure euskarria deskribaezina da.

Mila esker guztioi!

LIST OF PUBLICATIONS

- 1- Tijero, M., Gabriel, G., Caro, J., **Altuna, A.**, Hernández, R., Villa, R., Berganzo, J., Blanco, F.J., Salido, R., Fernández, L.J. SU-8 microprobe with microelectrodes for monitoring electrical impedance in living tissues (2009) *Biosensors and Bioelectronics*, 24 (8), pp. 2410-2416
- 2- Fernández, L.J., **Altuna, A.**, Tijero, M., Gabriel, G., Villa, R., Rodríguez, M.J., Batlle, M., Vilares, R., Berganzo, J., Blanco, F.J. Study of functional viability of SU-8-based microprobes for neural applications (2009) *Journal of Micromechanics and Microengineering*, 19 (2), art. no. 025007
- 3- **Altuna, A.**, Guimerá, A., Tijero, M., Gabriel, G., Berganzo, J., De La Prida, L.M., Villa, R., Fernández, L.J. “SU-8 based microneedles for *in vitro* neural applications”, Proceedings of MME Conference, Toulouse, France, September 20-22, 2009
- 4- **Altuna, A.**, Gabriel, G., De La Prida, L.M., Tijero, M., Guimerá, A., Berganzo, J., Salido, R., Villa, R., Fernández, L.J. SU-8-based microneedles for *in vitro* neural applications (2010) *Journal of Micromechanics and Microengineering*, 20 (6), art. no. 064014
- 5- Patent. Ikerlan S.Coop. y Consejo Superior de Investigaciones Científicas, *SU-8 microneedles for monitoring and stimulating neurons*, **Ane Altuna Letamendi**, María Tijero Serna, Javier Berganzo Ruiz, Luis Fernández Ledesma, Rosa Villa Sanz, Gemma Gabriel Buguña, Antoni Guimerá Brunet, Liset Menéndez de la Prida, P200930430, A61M5/00 (2006.01) A61B5/05 (2006.01) 2010-11-24.
- 6- **Altuna, A.**, Gabriel, G., De La Prida, L.M., Guimerá, A., Berganzo, J., Villa, R., Fernández, L.J. “Novel SU-8 based microprobes for *in vitro* neural recording”, MNBS Conference, Arrasate, Spain, April 5-6, 2011
- 7- **Altuna, A.**, Gabriel, G., De La Prida, L.M., Guimerá, A., Berganzo, J., Villa, R., Fernández, L.J. “Novel SU-8 based microprobes for *in vitro* neural recording”, MMB Conference, Lucerne, Switzerland, May 4-6, 2011
- 8- **Altuna, A.** Menéndez De La Prida, L., Bellistri E., Gabriel, G., Guimerá, A., Berganzo, J., Villa, R., Fernández, L.J. “SU-8 based microprobes with integrated planar electrodes for enhanced neural depth recording”, accepted by Biosensors&Bioelectronics
- 9- **Altuna, A.**, Gabriel, G., Menéndez De La Prida, L., Tijero, M., Guimerá, A., Bellistri, E., Berganzo, J., Villa, R., Fernández, L.J. “SU-8 based microneedles for biomedical applications” sent to Microneedles Conference, Cork, Ireland, 13-15 May 2012
- 10- **Altuna, A.** Menéndez De La Prida, L., Bellistri E., Cid, E., Aivar, P., Gabriel, G., Guimerá, A., Berganzo, J., Villa, R., Fernández, L.J. “SU-8 based microprobes for simultaneous neural recording and drug delivery”, in preparation.

Abstract

The present thesis deals with the design, fabrication, packaging and characterization of polymer SU-8 made microprobes for medical applications. At present, there is a huge variety of probes for recording, stimulation and drug delivery; however, still some improvements have been demanded by physicians and biologists in relation with their size and structural material. Here, microprobes based on the SU-8 technology have been developed in order to overcome the current limitations. Firstly, accurate designs have been established, then reproducible fabrication procedures have been developed and finally the probes have been packaged in order to connect the miniaturized device with the outside. The effectiveness of this technology is then checked with the electric and fluidic characterization of the probe and, finally, experimental tests in living tissues are carried out in order to verify the real capability of the microprobes. The application of the probes is focused towards two biomedical fields: 1) the monitorization of a living tissue such as a kidney and 2) the recording of action potentials and drug delivery in neural tissue.

The first objective is to develop a minimally invasive probe in order to avoid deep damages in living tissues. Electrical measurements based on impedance monitoring, which have been demonstrated as a potential method to determine the physiological status of living tissues, can be modified, weakened or blocked when cells have been previously damaged. Here, probes based on micro electromechanical systems (MEMS) technology are developed in order to create miniaturized devices and, as a result, obtain reliable measurements. MEMS is the technology of miniaturized mechanical and electro-mechanical elements. The components range between 1-100 micrometers and the devices up to a millimeter. These elements are based on an already well-established technology which uses the tools and techniques that were developed for Integrated Circuit (IC) industry to build microscopic devices. The basic techniques are the deposition of material layers, patterning by photolithography and etching to obtain the required shapes. Silicon is the most popular material used to create MEMS devices, nevertheless, it has been demonstrated that the rigidity and brittleness of silicon are serious drawbacks for its use as structural material on tissue monitoring applications. Consequently, other materials such as polymers are emerging as an alternative to silicon. In this work, polymer SU-8 is used as a structural material due to its suitable features for the fabrication of microprobes. This polymer is so attractive because of its very low optical absorption in the near UV range. This leads to uniform exposure conditions as a function of thickness, which gives rise to vertical sidewall profiles and hence good dimensional control over the entire structure height. Thus, the rigidity of the probe can be controlled adjusting its thickness. Furthermore, the fabrication of the probes is a low-cost process, and its adequate biocompatibility has been already reported.

The second objective is to obtain the highest signal-to-noise ratio possible in order to understand the real status of the tissue. Microelectrodes have been integrated in the probes and their physical constitution, spatial configuration and superficial treatments have been studied in this thesis. A specific design for each application and the modification of standardized microfabrication techniques helped to obtain a proper sensing capability of the microelectrodes. As a result, the SU-8 probes enabled the monitorization of ischemia-reperfusion episodes in rat's kidney. New probe designs were also developed for neural applications in this thesis, where action potentials with peak-to-peak amplitudes of 400-500 μV over noise were recorded in rat's hippocampus. Furthermore, it was demonstrated the capability of the microelectrodes to distinguish different neuronal sources. Thus, it has been demonstrated the versatility of the polymer SU-8 to create sensing devices for several biomedical applications.

The last aim was to integrate microfluidic channels into the SU-8 probe in order to deliver drugs in neural applications. Simultaneous neural activity recording and drug delivery was pursued in order to understand better the behavior of the brain. Finally, 0.5 μl of a kainic acid solution was delivered into the rat's hippocampus to elicit epileptic seizures. Immediately after delivery started, the neural activity increased and, thus, it was verified the capability of the probe to record from changes in the neural activity while delivering. At present, there is huge expectancy for further testing in order to establish the technology already developed in this thesis.

Laburpena

Tesi honetan SU-8 erretxinaz eginiko mikro orratzen diseinua, fabrikazioa, muntaia eta karakterizazioa ikertu dira zenbait aplikazio klinikotarako. Egun, eskuragarri dauden orratzen artean zenbait hutsune nabari dira materialari eta dimentsioei dagokienez; horregatik, lan honetan ordeko mikro orratzak proposatzen dira. Horretarako lehenik eta behin, diseinu zehatz bat finkatu da; fabrikazio erreproduzigarri bat garatu da ondoren eta azkenik, orratzen enkapsulazio prozesua joratu da mikro eskalan kokatzen diren orratzak kanpoalde makroskopikoarekin konektatzeko asmoz. Ondoren, mikro orratzen ahalmen erreala ezagutzeko prozesu hauetan garatutako teknologia guztia jarduera elektriko eta fluidiko batzuen bidez karakterizatu da. Azkenik, mikro orratzak osasuna eta biologia tartekatzen dituen bi aplikaziotan trebatu dira: 1) ehun biologikoen monitorizazioa, giltzurruna kasu eta 2) akzio-potentzialen neurketa eta drogen isurketa ehun neuronalean.

Tesi honetako lehen helburua orratzek ehun biologikoetan ahalik eta urradura txikiena eragitea da. Ehun batek berezkoa duen izaera elektrikoak erlazio zuzena du ehunaren egoerarekin. Are gehiago, ikertzen ari garen ehuna osatzen duten zelulak urratuta badaude, erantzun elektrikoa aldatu, ahuldu edo suntsitu daiteke. Tesi honetan MEMS (micro electromechanical systems) teknologian oinarrituz mikro eskalan kokatzen diren orratzak garatu dira ehunetan eragindako urradura minimizatzeko asmoz eta ondorioz, erantzun elektriko fidagarri bat jasotzeko. MEMS teknologiak elementu nahiz gailu elektriko eta mekaniko miniaturizatuak batzen ditu iada ongi ezagunak diren mikrofabrikazio tekniketan oinarritzen direnak. Aldi berean mikrofabrikazio teknika hauek Zirkuitu Integratuen (IC) industrian dute jatorria. Orokorrean, MEMS teknologian oinarritutako elementuek 1-10 mikrometroko dimentsioak izaten dituzte eta gailuak berriz, 20 mikrometro eta milimetro batetako neurrietara mugatzen dira. Fabrikazio teknika nagusiak materialen deposizioa, fotolitografia eta etching izenez ezagutzen den egiturazio teknika dira. Egun, silizioa da material erabilgarriena izan ere silizioaren mikrofabrikazioa guztiz finkatua dago merkatuan; hala ere, zurruntasun eta hauskortasun joera dela eta beste material batzuk ikertu dira azken urteetan. Lan honetan SU-8 izenez ezagutzen den erretxina erabili da oinarritzeko material gisa honek aurkeztzen dituen hainbat propietateengatik. Erretxina honen abantaila nagusietako bat UV argiarekiko duen absortzio baxua da. Ondorioz, esposizio uniformeak lortzen dira eta elementuen lodiera ezberdinetarako kontrol dimentsional zuhurra lortzen da. Horrela, lodierekin jokatuz elementuen zurruntasuna kontrola daiteke. Bestalde, orratzen fabrikazio kostua baxua da eta azken publikazioek SU-8-aren biokonpatibilitate egokia ziurtatzen dute.

Bigarren helburua ikertzen ari garen ehunaren egoera erreala ezagutzeko asmoz ahalik eta seinalezarata erlazio altuena lortzea da. Horretarako mikroelektrodoak txertatu dira orratzetan eta hauen izaera fisikoa, egitura espaziala eta azaleko tratamenduak ikertu dira tesi honetan. Aplikazio

bakoitzera egokitutako diseinuek eta mikrofabrikazio tekniken moldaketek, mikroelektrodoen sentsoare ahalmena goratu dute. Ondorio gisa, arratoiaren giltzurrunean iskemia-erreperfuzio jarduera monitorizatzea lortu da. Aplikazio neurologikoei dagokionez, zarata maila gainditzen duten 400-500 μ V-tako akzio-potentzialak neurtu dira arratoiaren hipokanpoan. Are gehiago, mikroelektrodo bakoitza iturri neuronal ezberdin bat detektatzeko gai izan da. Horrela, SU-8 erretxinaren malgutasuna baieztatu da, izan ere hainbat aplikaziotan bere sentsoare ahalmena frogatu da.

Azken helburua orratzetan hodi mikrofluidikoak txertatzea izan da aplikazio fluidikoak jorratzeko xedeaz. Aplikazioari dagokionez, lehenengo saiakerak besterik ez dira gauzatu baina emaitz adierazgarriak lortu dira. Konkrétuki, drogen isurketak jarduera neurologikoan duen eragina ikertu da. Arratoiaren hipokanpoan 0.5 μ l-tako kainato disoluzioa isuri da eta berehala aktibitate neuronalaren igoera neurtu dute mikroelektrodoek. Atariko emaitza hauek mikro orratzen funtzionalitatea baieztatu dute; hala ere saiakera gehiago eta prozeduraren optimizazio beharra aurreikusten da. Egun, aplikazio honek garunaren ezagutzan izan dezakeen eragin onuragarriagatik, esperimentu gehiago jorratzen ari dira.

Resumen

La presente tesis doctoral aborda el diseño, fabricación, encapsulado, y caracterización de microagujas de SU-8 para aplicaciones médicas. En la actualidad existe una amplia variedad de agujas para el registro, estimulación y dispensado de drogas, pero se han observado algunas limitaciones en relación a su diseño y material estructural utilizados. En este trabajo se han desarrollado microagujas basadas en la tecnología de SU-8 como alternativa a las agujas actuales. Primeramente se diseñan las agujas para cada tipo de aplicación, después se determinan los procedimientos de fabricación y finalmente se desarrollan los encapsulados para conectar la aguja miniaturizada con el exterior macroscópico. La aplicación de las agujas se ha centrado en dos campos biomédicos: 1) la monitorización de órganos tal como el riñón, y 2) el registro de la actividad neuronal, añadiendo la posibilidad de realizar dispensado de drogas de forma simultánea.

El primer objetivo es crear microagujas que causen el menor daño posible en el tejido biológico. Las mediciones eléctricas que se llevan a cabo para conocer el estado real del tejido pueden resultar modificadas, debilitadas o destruidas si las células que constituyen el tejido han sido previamente dañadas. En este trabajo, se desarrollan microagujas basadas en la tecnología MEMS (micro electromechanical systems) para evitar daños profundos en el tejido y poder así realizar mediciones fidedignas. La tecnología MEMS integra elementos y dispositivos eléctricos, mecánicos y electrónicos miniaturizados, los cuales están basados en la industria consolidada de los Circuitos Integrados (IC). Generalmente, las dimensiones de los elementos basados en MEMS son de entre 1 y 100 micras y los dispositivos pueden variar entre 20 micras y 1 milímetro. Las técnicas base de esta tecnología son la deposición de materiales en láminas, la fotolitografía y el grabado. El silicio es el material más utilizado para crear los múltiples dispositivos MEMS, sin embargo, su rigidez y fragilidad ha motivado el estudio de otros materiales tales como los polímeros. En esta tesis se ha utilizado el polímero SU-8 como material estructural debido a sus propiedades favorables para la fabricación de microagujas. Además, la fabricación de microagujas con este polímero permite el uso de procesos de bajo coste. Esta fotoresina presenta una baja absorción a la luz UV, posibilitando exposiciones uniformes en función del espesor del polímero. Así, se obtienen perfiles verticales y un buen control dimensional para toda la estructura. Además, estudios recientes muestran una adecuada biocompatibilidad del polímero SU-8.

El segundo objetivo es obtener la más alta relación señal-ruido posible en las mediciones eléctricas. Para ello se han integrado microelectrodos en las agujas y se ha estudiado la constitución física, la configuración espacial y los tratamientos superficiales de los mismos. Un determinado diseño para cada aplicación y la modificación de las técnicas de fabricación han dado como resultado una óptima

capacidad sensora de los electrodos. Así, se ha demostrado su uso a través de la monitorización de episodios de isquemia y reperfusión en riñón de rata. En cuanto a las aplicaciones neuronales, se han registrado potenciales de acción con una amplitud de hasta 400-500 μV en hipocampo de rata. Además, se ha demostrado que los microelectrodos son capaces de discriminar diferentes fuentes neuronales. Todos estos resultados han demostrado la versatilidad del polímero para crear dispositivos sensores con aplicación en diversas áreas biomédicas.

El último objetivo de esta tesis ha sido integrar canales microfluídicos en la aguja para poder dispensar drogas en aplicaciones neuronales y como resultado, detectar cambios en la actividad neuronal. Finalmente, se han llevado a cabo los primeros experimentos fluídicos *in vivo* en hipocampo de rata como prueba de concepto. Se dispensan 0.5 μl de una disolución de kainato y a continuación se registra un incremento en la actividad neuronal. Los resultados preliminares han demostrado la funcionalidad de la aguja para dispensar y monitorizar de forma simultánea aunque se tienen que realizar más experimentos y optimizar el protocolo experimental para verificar el buen funcionamiento de la aguja. En estos momentos, se están realizando más experimentos neuronales para llegar a establecer la tecnología desarrollada en esta tesis.

Contents

1. INTRODUCTION	1
1.1 General introduction: latest trends in BioMEMS.....	1
1.2 Motivation.....	3
1.3 References.....	5
2. STATE OF THE ART	6
2.1 Introduction.....	7
2.2 Classification of microprobes.....	8
2.2.1 Microprobes for the monitoring of living tissues.....	8
2.2.2 Microprobes for neural monitoring.....	10
2.2.3 Microprobes for neural drug delivery.....	12
2.3 Proposal: SU-8 based microprobes.....	15
2.4 SU-8 MEMS technology.....	17
2.4.1 Patterning processes.....	18
2.4.2 Deposition techniques: metallization by sputtering.....	20
2.4.3 Surface treatments: O ₂ plasma treatment.....	21
2.4.4 Bonding.....	21
2.4.5 Release techniques.....	22
2.5 References.....	24
3. SU-8 BASED MICROPROBES FOR THE MONITORING OF LIVING TISSUES: ISCHEMIA DETECTION IN RAT'S KIDNEY	30
3.1 Background.....	31
3.2 Design.....	33
3.2.1 The design of the probe.....	35
3.2.2 The location of the electrodes.....	37
3.3 Fabrication.....	37
3.3.1 First fabrication procedure.....	39
3.3.2 Problems and solutions related to the first fabrication procedure.....	40
3.3.3 Second fabrication procedure.....	40
3.3.4 Achievements, problems and solutions related to the second fabrication procedure.....	40
3.4 Packaging.....	46
3.5 Characterization.....	46
3.5.1 Impedance spectroscopy: SU-8 probe vs. Si and SiC probes.....	46
3.5.2 Electrochemical deposition of platinum black.....	48
3.6 Experimental procedures.....	52
3.6.1 In vivo monitoring of ischemia-reperfusion episode in rat's kidney.....	52
3.7 Conclusions.....	54
3.8 References.....	55
4. FIRST SU-8 MICROPROBE PROTOTYPE FOR NEURAL MONITORIZATION AND DRUG DELIVERY	58
4.1 Design.....	59
4.2 Fabrication.....	60
4.2.1 Fabrication procedure.....	60
4.2.2 Problems and solutions related to the fabrication procedure.....	62
4.3 Packaging.....	64
4.4 Characterization.....	65
4.4.1 Fluid delivery characterization.....	65
4.4.2 Impedance monitoring while delivering in the agarose gel.....	66
4.5 Experimental procedures.....	67
4.5.1 Mechanical and fluidic capability evaluation of the SU-8 probes by means of ex vivo tests.....	67
4.5.2 Evaluation of the damage evoked by the SU-8 probes by means of in vivo tests.....	68

4.6 Conclusions	70
4.7 References	71
5. SECOND SU-8 MICROPROBE PROTOTYPE FOR NEURAL ACTIVITY RECORDING	73
5.1 Background	74
5.1.1 Neuron- electrode interface	74
5.1.2 In vitro and in vivo neural recording procedures	76
5.2 Design	78
5.3 Fabrication.....	79
5.3.1 First fabrication procedure: 20 μm embedded electrodes	79
5.3.2 Achievements, problems and solutions related to the first fabrication procedure.....	81
5.3.3 Experimental limitations related to the first fabrication procedure	83
5.3.4 Second fabrication procedure:electrodes 2-3 μm embedded into a layered probe.....	89
5.3.5 New concepts on the fabrication sequence.....	91
5.3.6 Third fabrication procedure: electrodes at the probe surface level	92
5.3.7 Achievements related to the third fabrication procedure	94
5.3.8 Resume of the most relevant features of the first, second and third fabrication procedures	96
5.4 Packaging	97
5.5 Characterization of the sensing sites	97
5.5.1 Impedance spectroscopy	97
5.5.2 Platinum black electrochemical deposition.....	99
5.5.3 Single walled carbon nanotubes (SWNTs) coating.....	100
5.6 Experimental procedures: extracellular neural activity recording.....	102
5.6.1 In vitro tests.....	102
5.6.2 In vivo tests	104
5.7 Conclusions	105
5.8 References	107
6. THIRD SU-8 MICROPROBE PROTOTYPE FOR SIMULTANEOUS DRUG DELIVERY AND NEURAL ACTIVITY RECORDING	109
6.1 Design	110
6.1.1 A tetrode and a fluidic channel integration	111
6.1.2 Eight electrodes and two fluidic channels integration.....	112
6.1.3 Eight electrodes and eight fluidic channels integration design	113
6.2 Fabrication.....	114
6.2.1 Initial fabrication procedure	114
6.2.2 Modifications, problems and solutions related to the initial fabrication procedure .	114
6.2.3 Final fabrication procedure	119
6.3 Packaging	121
6.4 Characterization	121
6.4.1 Impedance spectroscopy	121
6.5 Experimental procedures.....	122
6.5.1 Simultaneous neural activity recording and drug delivery by means of in vivo testing	122
6.6 Conclusions	123
6.7 References	125
7. CONCLUSIONS AND FUTURE WORK	126
7.1 General conclusions	127
7.2 Costs' evaluation.....	130
7.3 Discussion	130
7.4 Future work	132
7.5 References	135

1. INTRODUCTION

Contents

1. INTRODUCTION	1
1.1 GENERAL INTRODUCTION: LATEST TRENDS IN BIOMEMS	1
1.2 MOTIVATION	3
1.3 REFERENCES	5

1.1 General introduction: latest trends in BioMEMS

Historically, the field of biomedical instrumentation has always been of great importance in the clinical field. The increasing demand for “high-quality” medical care has led to a constant development of new technologies. MEMS technology has already demonstrated to have the potential to fulfill this demand¹. In the last decades, MEMS technology has emerged as a global industry and has been mainly focused on large markets such as automotive or information technology industries. However, MEMS technology is projected to have a growing impact on biomedical applications. Particularly, four fields have been studied and reported by BIOMEMS 2010²: medical devices, home care, *in vitro* diagnostics and, pharmaceutical and biological research. As shown in figure 1.1 there is a clear increasing tendency in all the fields, specifically, *in vitro* diagnostics is the most relevant one. It is expected that microsystems technologies market for healthcare applications will grow from \$1.2 B in 2009 to \$4.5 B in 2015 representing over 1B units per year in 2015. According to the aforementioned report, these sensors are fast going wireless and it is expected the 30% of all biomedical systems to be autonomous wireless units by 2015. Briefly, the manufacturing techniques used in the microelectronics industry may lead to greater uniformity and reproducibility of miniaturized devices than is currently available for the biomedical and pharmaceutical industries.

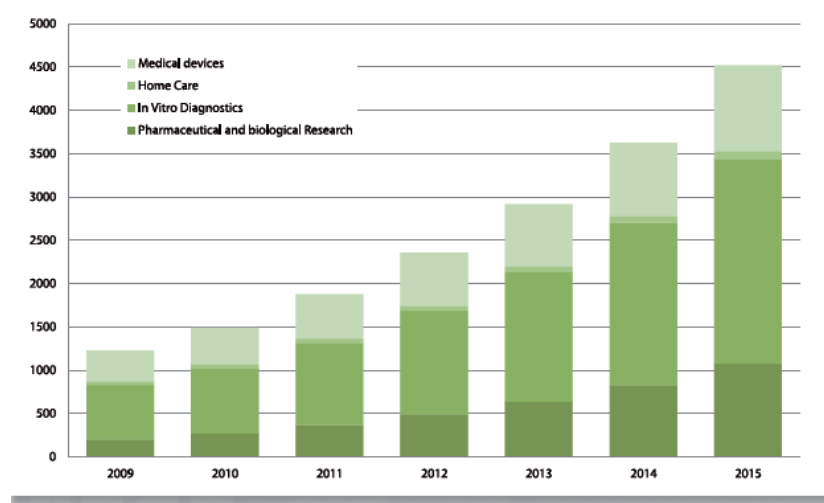


Figure 1.1 Microsystems devices for healthcare applications market 2009-2015 in \$M

New *in vitro* diagnostic systems, new therapy strategies, genetic disease treatment, targeted and intelligent drug delivery, artificial pancreas, drug discovery processes... are healthcare improvements that will be dealt in future generations, figure 1.2. Medical trends are focused toward implantable devices capable of making diagnostic and delivering drugs according to the diagnostic of the patients. Home care improvements are based on the shelf assistance and autonomy of patients thanks to portable technology. Finally, the advance in *in vitro* diagnostics involves combining biosensors and dispensing systems in a single and portable device.

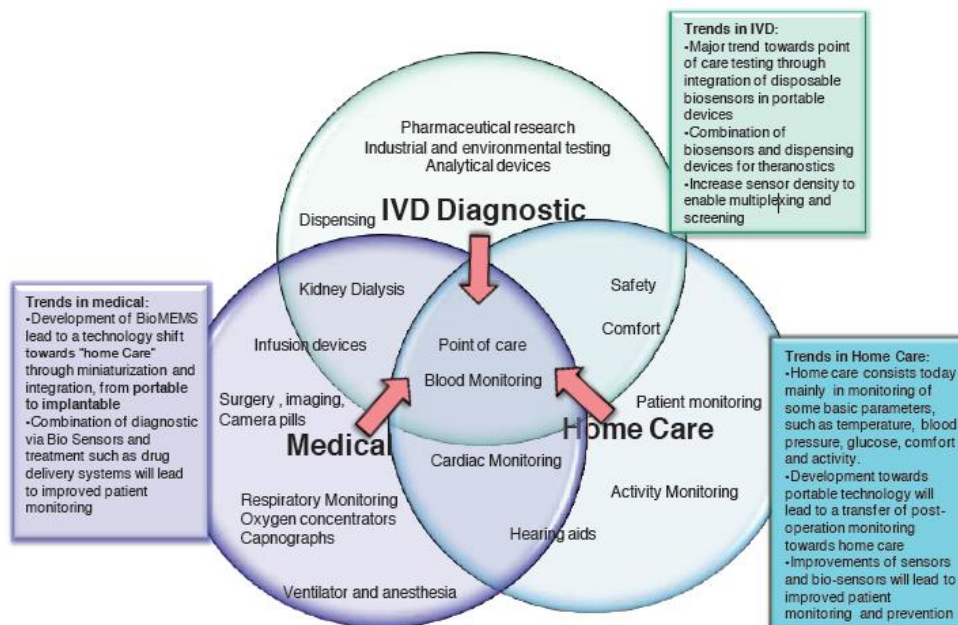


Figure 1.2 Latest trends in medical and home care, and *in vitro* diagnostic

1.2 Motivation

In connection with the predictions, it is believed that miniaturized probes can be of great relevance for the sensing of accurate biological activity and drug delivery within a wireless system. Microprobes based on MEMS fabrication techniques have already demonstrated to be an exceptional biomedical tool, in a large extent, due to their size. The acceptance of miniaturized probes has been motivated by several reasons: 1) disposability (limits the possibility of contamination), 2) reduced invasiveness, 3) high-volume production and consequently potential low cost and 4) proved characteristic of reliability and reproducibility. All these features make us think that miniaturized probes may be a suitable tool to fulfill some of the future prospects.

Microelectrodes integrated in probes allow to record from multiple recording sites and the stimulation of a small area of tissue. These measurements detect the state of the tissue, organ or body liquids by variations in the impedance values. For example, under current transplantation protocols, one of the most critical and unaddressed phases of the transplant process is organ transportation from donor to recipient, during which the elapsed time and preserving conditions must be thoroughly controlled. In this phase, the organ remains immersed in a sterile, organ-preservation solution at a temperature of 2-8°C. During this time, it is essential to maintain organ viability to ensure the complete restoration of organ function following transplantation. Unfortunately, direct evaluation of organ function after transplantation is to date the only reliable procedure for the assessment of correct preservation during transportation. Although some viability indicators have been proposed and tested, they are extremely invasive and time-consuming. Moreover, experimental results suggest that the measurements have to be carried out in a continuous monitoring scheme to accurately predict organ viability. All these factors create a demand for an objective and practicable organ-viability indicator during the transportation phase. In this thesis a minimally invasive microprobe for a continuous monitoring of tissue impedance is developed. As a proof of concept, an ischemia-reperfusion episode is evoked in a rat's kidney and impedance variations are monitorized.

Microelectrodes integrated in a probe hold also a great potential on neural applications. In fact, the increasing interest in understanding and controlling brain functions has resulted in the development of multiple microprobe strategies for neural activity recording and stimulation. Multi-neuronal recording is a powerful electrophysiological technique that has revealed much of what is known about the neuronal interactions in the brain. Basically, an action potential is fired in a neuron when the ions move across the neuronal membrane. Characteristic voltage traces reflecting ion currents through the cell membrane of the soma and nearby dendrites give a reliable measure of its firing activity. In typical extracellular recordings of neurons firing action potentials, microelectrodes are placed next to the soma of the cell in question in order to detect those firings. Field potentials generally refer to changes

of larger amplitude and longer duration in the extracellular voltage (1-10mV vs. 50-200 μ V, 10-100ms vs. 1ms). These potentials can be generated by synchronous action potentials in groups of neurons as well as synaptic currents which may often be too small to be detected in the background noise when they occur as isolated events. Spike-waves are a typical example of field potential generated by synchronous firing in group of neurons. In the current days, it is difficult to detect precise spike timings, especially synchronized simultaneous firings, among closely neighboring neurons recorded by one common electrode because spike waveforms overlap on the electrode when two or more neurons fire simultaneously. This limitation makes us think that an accurate miniaturized tool has to be available for further research. In this thesis, an alternative microprobe with multiple recording sites is presented for several neural applications.

Additionally, drug delivery systems have already had an enormous impact on medical technology. Nowadays, there is huge hope on delivering precise quantities of drugs at the right time and as close to the region of interest as possible. Particularly, drug delivery into the central nervous systems has been limited since Ehrlich first described the blood brain barrier (BBB) in 1885³. Tight junctions of endothelial cells that form the BBB protect the brain, but they also restrict the delivery of high-molecular-mass and polar molecules^{4,5}. Many therapeutic agents present such characteristics and they cannot reach the affected area of the brain. Consequently, a variety of neurological diseases, brain tumors among others, do not have a successful treatment. For example, conventional therapy for brain tumors includes surgical biopsy for pathological diagnosis and, if it is possible, the first treatment is tumor resection, followed by radiotherapy and chemotherapy. Despite these treatments, the prognosis for patients with brain tumor has remained largely unchanged over the last three decades^{6,7,8,9}. Advances in neuropharmacology have led to the use of chemical modification techniques to make drugs more likely to reach the brain parenchyma in the setting of an intact BBB, however, to date, the bulk clinical investigation has focused on methods to either disrupt or circumvent the BBB.

Convection-enhanced delivery (CED) technique is a novel approach to deliver drugs into brain tissue and is defined as the continuous injection of a therapeutic fluid agent by positive pressure. It has been shown that fluid convection can supplement simple diffusion to enhance the distribution of small and large molecules in the brain. Based in the CED technique, drug delivery *in vivo* tests in rat's hippocampus have been carried out in this thesis. For that, microprobes with multiple fluidic channels have been developed. It is believed that the integration of delivering capability into a microprobe can open new opportunities in the urgent treatments for brain diseases.

1.3 References

¹<http://www.mems-exchange.org/MEMS/applications.html>

²http://www.i-micronews.com/upload/Rapports/Yole_BioMEMS_Report_October_2010_flyer_Web.pdf

³Hunt Bobo, R., Laske, D.W., Akbasak, A., Morrison, P.F., Dedrick, R.L., Oldfield, E.H. Convection-enhanced delivery of macromolecules in the brain (1994) *Proceedings of the National Academy of Sciences of the United States of America*, 91 (6), pp. 2076-2080

⁴Oldendorf, W.H. Lipid solubility and drug penetration of the blood brain barrier (1974) *Proceedings of the Society for Experimental Biology and Medicine*, 147 (3), pp. 813-816

⁵Rapoport, S.I., Blood-Brain Barrier in Physiology and Medicine (1976) Rave, New York, pp. 99-111.

⁶Allard, E., Passirani, C., Benoit, J.-P. Convection-enhanced delivery of nanocarriers for the treatment of brain tumors (2009) *Biomaterials*, 30 (12), pp. 2302-2318

⁷Mason, W.P. Progress in clinical neurosciences: Advances in the management of low-grade gliomas (2005) *Canadian Journal of Neurological Sciences*, 32 (1), pp. 18-26

⁸Lonardi, S., Tosoni, A., Brandes, A.A. Adjuvant chemotherapy in the treatment of high grade gliomas (2005) *Cancer Treatment Reviews*, 31 (2), pp. 79-89

⁹Nieder, C., Adam, M., Molls, M., Grosu, A.L. Therapeutic options for recurrent high-grade glioma in adult patients: Recent advances (2006) *Critical Reviews in Oncology/Hematology*, 60 (3), pp. 181-193

2. STATE OF THE ART

The objectives of this chapter are to place the microprobes developed in this work among analogous microprobes already created by other researchers, justify the structural material chosen for the fabrication of the probes and explain the techniques of microfabrication in order to understand in an easy way the following chapters. To date, huge achievements have been obtained in terms of probe design, materials, components and integration establishing high fidelity as a biosensor device. In this chapter, a short review of them is added in order to demonstrate that there is still need to continue creating highly advanced probes. Concerning the areas of application, two biomedical fields are highlighted here: the monitorization of living tissues and, neural applications. In addition, working at micro scale dimensions is justified and the properties of polymer materials are emphasized suggesting them as a new generational material. Specifically, the promising features of the polymer SU-8 are described and MEMS techniques for the fabrication of SU-8 microprobes are explained.

Contents

2. STATE OF THE ART	6
2.1 INTRODUCTION	7
2.2 CLASSIFICATION OF MICROPROBES	8
2.2.1 Microprobes for the monitoring of a living tissue.....	8
2.2.2 Microprobes for neural monitoring.....	10
2.2.3 Microprobes for neural drug delivery	12
2.3 PROPOSAL: SU-8 BASED MICROPROBES.....	15
2.4 SU-8 MEMS TECHNOLOGY.....	17
2.4.1 Patterning processes.....	18
2.4.2 Deposition techniques: metallization by sputtering	20
2.4.3 Surface treatments: O ₂ plasma treatment.....	21
2.4.4 Bonding.....	21
2.4.5 Release techniques	22
2.5 REFERENCES.....	24

2.1 Introduction

Conventional small-scale biomedical tools that are manufactured by traditional machining are limited to a scale between a millimeter and a few hundred micrometers¹. Such instruments do not permit surgery on small tissue structures nor at cellular level. In addition, the conventional surgery tools do not allow to reach all the areas of the human body that could be affected by a disease. In order to overcome this limitation, micro scale devices have been developed in recent decades. The earliest of these biomedical devices are providing unprecedented access for manipulation, monitoring and drug delivery whereas take advantage of small-length scales to act in specific areas with accuracy.

One of the most prominent small-scale device used in electrophysiology is the microprobe, mainly designed to perform *in vivo* recording and stimulation^{2,3,4,5}. Nevertheless, the most traditional and popular probe is the metal-wire neural probe. It is a sharpened wire, normally less than 100 μm in diameter which is insulated to define an exposed recording area tip⁶. Although the microwire electrode is still being used nowadays, it has several disadvantages like its limited number of possible geometries, the ductility of the metal, and its low reproducibility. In order to find a solution to these limitations, microprobes based on MEMS technology have been developed during the last decades. In this particular case, microprobes with onboard metal electrode pads positioned at specific locations along the probes have been fabricated using this technique. These probes can be inserted in living tissue where precisely located electrodes can stimulate or record from the affected area. In addition to recording and stimulating from living tissue, the possibility of drug delivery can contribute positively in the field of research. Currently, the smallest needles available for injections are approximately 30 gauge and they are mostly made of stainless steel⁷. In order to minimize the size of the needle, MEMS technology enables the integration of micro-scale channels into the probe.

As a clear example, although it is not a topic discussed in this work, it has to be mentioned that many researchers are focused on the development of microneedles for transdermal delivery of drugs. They offer a convenient way to administer drugs without the drawbacks that standard hypodermic injections present related to issues such as patient acceptability and injection safety⁸. As a first-generation transdermal microneedle, arrays of bulk micromachined solid silicon microneedles were fabricated and shown to increase skin permeability to a variety of different molecules by orders of magnitude, including macromolecules. Since then, several improvements have been done concerning the skin permeability and delivery efficiency.

Certainly, silicon has been the most widely used material for the fabrication of sharp probes. Silicon micromachining-based devices include several favorable features: batch fabrication, high reproducibility of geometrical and electrical characteristics, easy configuration of recording site placements and substrate shape, and the ability to include on-chip electronics for signal conditioning⁹. In addition, they can be microassembled into three dimensional arrays. Briefly, due to the capability of miniaturization and its relative biocompatibility, silicon based microprobes have been used for many different biomedical applications. However, the main drawbacks of the material are its rigidity and brittleness. It has been reported that tissue is injured during the use of silicon based microprobes, the rigidity of the silicon being the cause^{10,11}. Furthermore, there is a high risk of breaking during the manipulation of silicon based probes. In addition, in some cases undesirable cross talk happens between the recording sites and substrate¹². Recent studies suggest that polymers could be an alternative to silicon^{10,11,13,14,15}.

In the present work microprobes made exclusively of polymer SU-8 (MicroChem Corp., Newton, MA) have been developed for enhanced living tissue monitoring, neural activity recording and drug delivery. It is thought that the polymer SU-8 can positively contribute to the current state of the art of microprobes. The study of the SU-8 behavior and the optimization of the already well-established microfabrication techniques have been the key to create such probes. Additionally, suitable designs, handling packgings, electric and fluidic characterizations and accurate experimental approaches have addressed the SU-8 microprobes towards unprecedented achievements.

2.2 Classification of microprobes

2.2.1 Microprobes for the monitoring of living tissues

Needle-shaped microprobes have been widely used for neural applications but other application areas can also make use of these devices for other purposes. In recent years, there has been a high demand for fast, reliable and continuous measurements in medicine and surgery, in particular during major operations such as open-heart surgery¹⁶. MEMS technology has enabled a minimally invasive system,

specifically a microprobe to monitor physiological parameters on-line at low cost. Electrical impedance measurements have proved potentially useful method to determine the physiological status of living tissues. The changes induced by some pathology are associated with variations of essential tissue parameters such as the physical structure or the ionic composition that can be reflected as changes in passive electrical properties. The range of applications derived from this fact is wide, for example tumor detections, ischemia monitoring during cardiac surgery or transplantation among others¹⁷.

Impedance silicon-based probes used in most *in vivo* studies in the past consisted of a linear array of four metallic needle electrodes placed at a constant inter-electrode separation distance¹⁸, as shown in figure 2.1 a) i). Although this classical configuration can be easily adapted to many experimental studies, it cannot be considered a minimally invasive probe since four needles are inserted into the tissue for a single point impedance measurement. Ivorra et al. proposed a planar probe configuration to overcome this drawback as seen in figure 2.1 a) ii). This configuration showed two main advantages: the reduction of damage induced to tissue during insertion and the possibility to perform depth measurements without losing spatial resolution. In addition, experimental results showed its potential in detecting structural alterations, anoxic edema and functional impairment in rat's kidney after sustained ischemia^{19,20,21,22}.

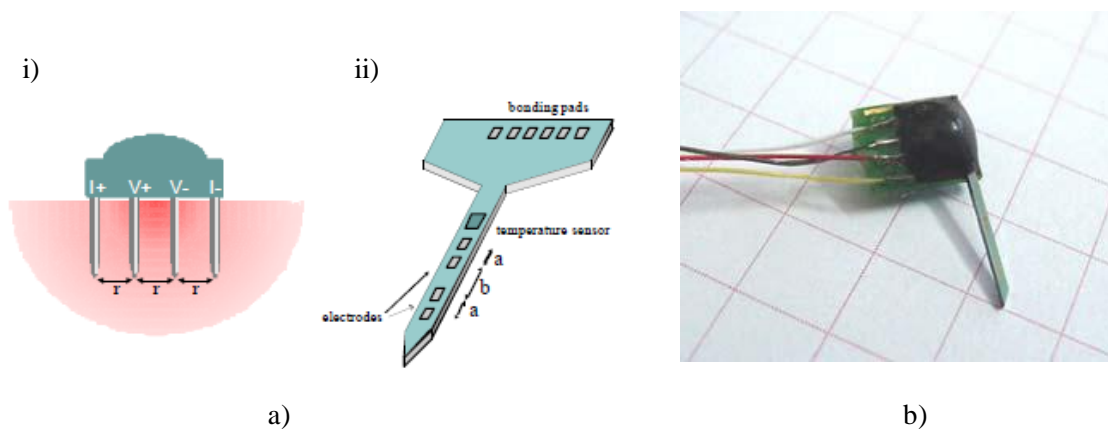


Figure 2.1 a) Drawing of a microprobe with (i) single shanks for each recording site and (ii) a planar electrode-configuration. b) A packaged needle-shaped silicon probe.

Nevertheless, the main shortcoming of the aforementioned sensor was its production using silicon substrates, figure 2.1 b). At high frequencies, the substrate partially short-circuited the system with the injected current leaking out across the substrate and generating a false image of the measurements²³.

In order to prevent current leakages, the semiconductor silicon carbide (SiC) was proposed as a structural material. Many suitable properties of SiC, such as the possibility of processing using standard semiconductor processes, its higher mechanical resistance to stress and a high electrical breakdown constant made it candidate for the fabrication of the microdevice without the need to revert to complex insulation processes. *In vivo* experiments were carried out for Si-based and SiC-based probes and the results showed that the effective operational range of semiconductor based probes was higher while Si-based probes lost their functionality at high frequency measurements. However, accurate monitoring of ischemia in rat's kidney was demonstrated for both types of probe.

2.2.2 Microprobes for neural monitoring

In the early 70s Wise, Starr and Angell developed one of the first silicon based multielectrode array at the University of Michigan^{24,25}. Since then, numerous designs and configurations have been conceived, fabricated and tested for various acute and chronic neural applications, figure 2.2 a). The key advantage of such devices compared to traditional recording probes is the possibility to integrate a large number of electrodes in a single device and place them at the desired location within the tissue. Such devices can also be custom configured to serve specific experimental needs while maintaining the advantage of mass reproduction. Concerning the connection with the outside, flexible cables have been used so that the device can withstand surgical manipulation and permits long term recording. Recently, alternative methods of fabricating silicon based arrays have been developed. For example, the University of Utah invented a new method to fabricate multiple electrode arrays²⁶. The Utah Electrode Array is a three dimensional electrode array which consists of 100 sharp silicon needles built in a perpendicular direction to the substrate, figure 2.2 b). Also, an alternative method to fabricate planar silicon-based arrays using silicon-on-insulator (SOI) technology was developed after silicon plasma etching was invented²⁷, figure 2.2 c). Nevertheless, all the probes made of silicon present the same problems in relation to the intrinsic properties of the material. As an alternative to semiconductor-based probes, ceramic probes have been fabricated¹². The main aim of these devices is to decrease the cross talk between recording sites and reduce shunt capacitance between the metallization layer and substrate. However, latest research suggests the replacement of silicon by flexible polymers in order to reduce tissue damage and avoid current leakages^{10, 12}. Among several polymers, microprobes based on polyimide, parylene or benzocyclobutene (BCB) have already been fabricated and tested^{28,29,30,31}. The three of them offer a low elastic modulus, which makes them suitable materials to adapt their shape to the neural environment and, consequently, reduce the damage induced to the tissue. Polyimide and BCB have been mainly used for the fabrication of probes for neural activity recording, whereas parylene based probes have additionally integrated microchannels for applications where simultaneous monitoring and drug delivery was required.

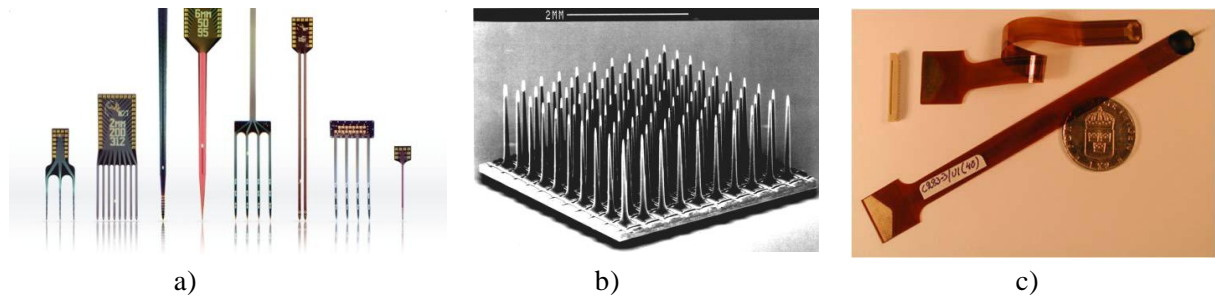


Figure 2.2 a) Michigan probes, b) SEM picture of Utah electrode array and c) SOI neural probe fixed to a flexible PCB.

During the last decade, a huge effort has been made to develop polyimide based microprobes for acute and chronic neural recording. However, at first polyimide-metal-polyimide sandwich structures were fabricated due to the lack of stiffness of this polymer^{32,33}. Although polyimide presents relevant advantages, such as biocompatibility and easy microfabrication technology, there were some problems associated with its excessive flexibility. For example, Lee et al. attached a silicon backbone just in the desired region of the probe to increase the stiffness, while the rest of the device was just made of polymer in order to absorb stress from any micromotion between the brain tissue and the electrode¹⁵, figure 2.3 a). Thus, the electrodes could penetrate the pia of a rat without buckling. The electrical measurements showed stable impedance values, and biocompatibility tests proved the non-toxicity of the electrodes, allowing cell adhesion and growth. Nevertheless, recently, a fully polyimide probe has been developed for cortical recording³⁴, figure 2.3 b). A flexible and biocompatible device has been achieved based on polyimide microfabrication techniques. This device contains a high density of electrode sites, which have made possible the discrimination between two single neurons sending signals at the same time. Histology tests have been carried out and since a low inflammatory response has been verified, the authors comment that future work will concentrate on chronic cortical recordings.

Concerning other polymers, BCB-based microprobes cannot penetrate the brain tissue on their own because the electrodes buckle under insertion force³⁵ as seen in figure 2.3 c). Although different coatings have been tested to overcome the problem related to buckling strength, the microprobes tested on neural tissue are made of BCB and silicon backbone³⁶. The measurements verify that the recordings are of multiunit neural activity originated from neurons in the barrel cortex. The authors reported that the damage trauma is minimal, so future studies will be pursued to observe chronic recording capabilities.

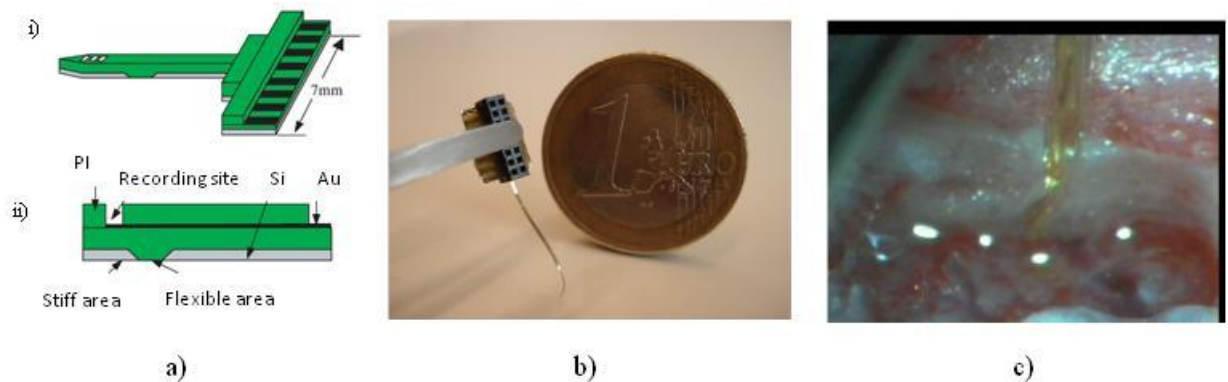


Figure 2.3 a) Schematic diagrams of the polyimide-based neural probe: (i) top view and (ii) cross-sectional view. The stiff portion with Si backbone layer remains inside the brain. Flexible portion without silicon backbone layer is to accommodate micro-motion between brain tissues and skull. b) A packaged polyimide made probe device. c) BCB electrode (yellow) buckling during insertion into the brain.

Polymer SU-8 technology has already been used as structural material to create microprobes for other purposes such as to record fiber spike signals from regenerated axons within peripheral nerves³⁷. Also, it has been already reported parylene based microprobes technology for neural activity recording which takes advantage of the mechanical properties of the SU-8 to obtain robustness³⁸.

2.2.3 Microprobes for neural drug delivery

The two most common methods of drug delivery into the human body are injections and oral formulations. Injections allow the release of drugs directly into the bloodstream but they involve a painful delivery, can cause infection and often require medical personnel. Oral drug delivery only involves swallowing a pill, however there are some limitations such as the poor absorption and the drug degradation that occurs in the gastrointestinal track and liver^{39,40}. An optimal delivery route for biopharmaceuticals to be effective and minimally invasive is through the skin or by means of transdermal drug delivery. Nowadays, many kinds of minimally invasive microneedles are being developed for transdermal drug delivery⁴¹. They are large enough to insert into the skin but short enough to avoid reaching the deep layers of the skin responsible of the stimulation of the nerves and, consequently, cause pain⁴². In addition, they enable a systemic distribution of the drugs and they are easy to use. Nevertheless, drug delivery for neural applications presents an additional drawback. It is particularly difficult that drugs could reach the affected area of the brain due to the presence of the BBB, which is formed by tight junctions of the epithelium that lines capillaries in the brain⁴³. Generally, only low-molecular-mass lipid-soluble molecules and few peptides and nutrients can cross this barrier to a significant extent, either by passive diffusion or using specific transport mechanisms.

Therefore, motivated by the difficulties associated with improving effective treatments for neural diseases other methods have been developed.

Convection enhanced delivery (CED) is based on the continuous injection under positive pressure of a fluid containing a therapeutic agent. This method was proposed and introduced by researchers from the US National Institute of Health (NIH) in the early 1990s^{44,45,46}. CED is a promising therapeutic method for treating brain diseases, such as tumors, neurodegenerative diseases, Parkinson or epilepsy⁴⁷. The results of different studies and clinical trials indicate that convection can be used to distribute molecules regardless of their size or molecular weight^{48,49,50}.

Traditional CED involves inserting a needle or a catheter into a disease-afflicted tissue and pumping at a constant flow rate via an external pump. As the agent is pumped out of the tip directly into the parenchymal tissues, the resulting pressure gradient drives the fluid through the interstitial space. This method has been effective in proving that higher drug concentrations can be achieved by direct infusion than by systemic delivery. However delivering therapeutics over several centimeters requires relatively high pressures that may result in irreversible tissue damage, uncontrolled drug distribution and backflow up the needle⁵¹. In order to improve the problems related to traditional needles and fulfill the requirements for CED, silicon micromachining-based microfluidic devices have been developed during the last 15 years. In the late 90s, Chen et al. developed a silicon probe capable of selectively delivering chemicals at the cellular level as well as electrically recording from and stimulating neurons *in vivo*², figure 2.4 a). Initial experiments consisted of delivering chemicals in the central nervous system of guinea pigs for acute applications. The microprobe showed its viability to detect how the neuron discharge rate increases when injecting a neural stimulant, and decreases when injecting a depressant. More sophisticated microprobes have been developed in recent years. Rohatgy et al. validated a neural probe design capable of simultaneous drug delivery and electrophysiology recordings *in vivo*⁵², figure 2.4 b). A 16-channel microfabricated silicon electrode array fixed to a silica catheter could measure individual spikes as well as local field potentials during real-time drug delivery. Also, Spieth et al. have recently developed a novel 3D microprobe system for neural applications⁵³. First steps towards a multifunctional floating array which combines drug delivery and electrical recording have been reported. As the delivery requirements have become more demanding, additional components for the control and monitoring of fluid flow such as shutters for reducing unintended drug delivery, integrated flowmeters, or microvalves and micropumps for on-chip realization have been particularly studied⁵⁴, figure 2.4 c).

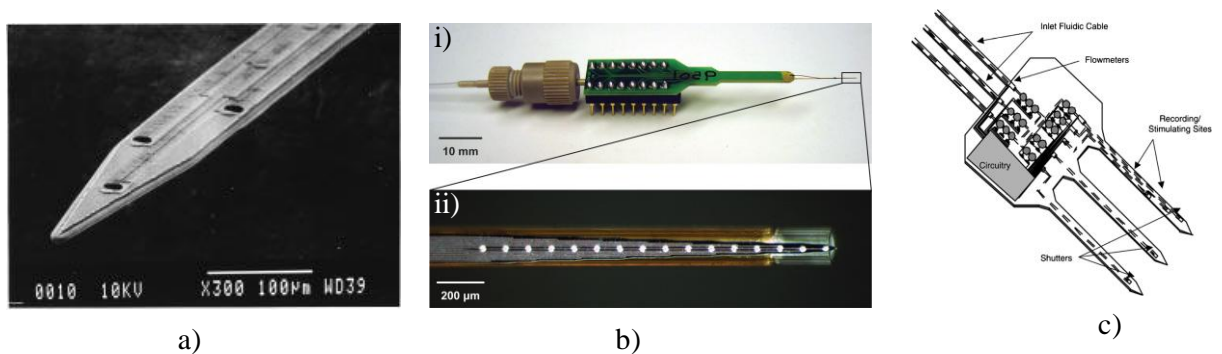


Figure 2.4 a) Overall SEM view of a probe containing three drug delivery channels. Each outlet orifice has a recording site beside it. The site at the tip of the probe has a large area and can serve both for recording and stimulation. b) (i) Photograph showing the full neural probe and attached fluidic line, (ii) a magnified view showing the electrode sites on the array. The catheter is made of fused silica covered in a polyimide sheath, with an outer diameter of 165 μm and an inner diameter of 127 μm . c) Drawing of a chronically implantable probe for electrical recording, stimulation and chemical drug delivery.

Concerning polymer based microprobes, polyimide based microprobes have already been described for simultaneous drug delivery and monitoring. The key component of the Metz et al. system was a flexible polyimide substrate with embedded microchannels that were batch-fabricated combining polyimide micromachining and lamination technique²⁸, figure 2.5. Microelectrodes were characterized by electrical impedance and by pressure drop experiments and the best fluid delivery scheme was found. Authors focused future work on the study of the influence of chemical compounds on intracellular information exchange under simultaneous electrophysiological monitoring.

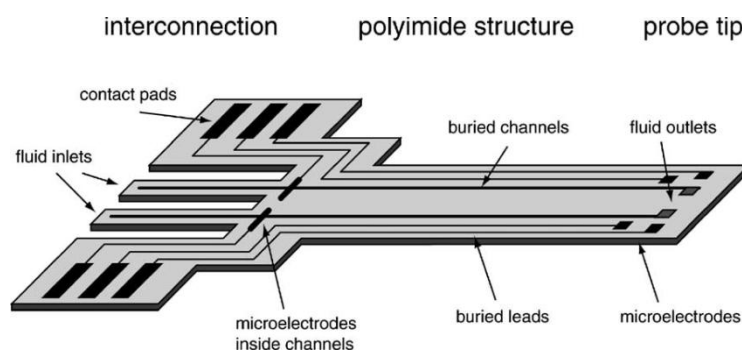


Figure 2.5 Illustration of implantable, flexible polyimide probe with microelectrodes and microfluidic channels.

Instead of polyimide, Takeuchi et al. developed a parylene based probe with integrated microchannels and first neural recordings have already been carried out³⁰. In this particular case, the channel was

proposed for more than one function. Firstly to inject chemicals to the tissue, secondly to measure the neural signals from the tissue when filled with biological saline and finally, to improve the stiffness of the flexible probe when filled with solid material. According to this last aim, the novel process consists of filling the channel with melted PEG and as it gets colder the material solidifies and permits the probe to be inserted into the neural tissue as shown in figure 2.6 a) ii). Once the probe is penetrated, the initial flexibility is recovered because the PEG is dissolved. Also, Ziegler et al. have described the technology and characterization of fully parylene based neural probes with built-in microfluidic channels¹³, figure 2.6 b). First attempts at micromolding and thermal bonding have been carried out to optimize the fabrication procedure of microchannels. The fluidic tests checked that there were no leakages along the microfluidic system and demonstrated a lineal relationship between the flow rate and the applied pressure. The electrodes were characterized by electrical impedance measurements in which impedance sufficiently low for neural recording was observed.

Other polymers like BCB have been used to fabricate neural implants and the functionality of the channels has been verified. However, in order to achieve an easy handling of the device, the attachment of a silicon backbone was essential³¹. As seen, several polymers have been suggested to replace silicon but as far as we know, there are no results on only polymer based microprobes for simultaneous electrical monitoring and drug delivery tested in living neural tissue.

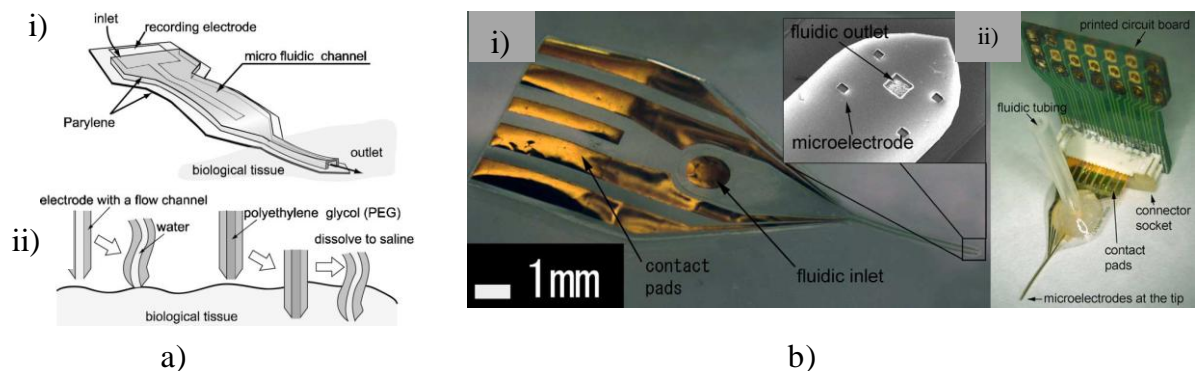


Figure 2.6 a) (i) Parylene neural probe integrated with a microfluidic channel. (ii) The mechanism of the insertion into biological tissue. b) (i) Overall view of the parylene neural probe; the SEM photograph (middle) shows only the tip of the probe; four recording electrodes and the fluidic outlet are visible and (ii) the entire assembled neural probe with fluidic and electrical connections.

2.3 Proposal: SU-8 based microprobes

As discussed in previous sections, silicon based probes have well-recognized advantages compared to traditional metal-wire probes. One of the most important advantages conferred by going toward the

microscale is the favorable scaling of material strength and stiffness versus mass⁵⁵. For any given object, as the size shrinks, the device keeps its robustness while remarkably decreasing its weight. Consequently, microdevices can be constructed with less material and less structural reinforcements than a macroscale device would require for an analogous purpose. In addition, silicon and silicon-based compounds used in microfabrication have the benefit of exhibiting no plastic deformation as many conventional metals do. Nevertheless, structural limits have to be taken into account because if the device is stressed beyond its ultimate strength, it may break. Also, it has been demonstrated that, due to its rigidity, tissue damage occurs. Mainly these facts have made researchers think about less fragile and more flexible materials such as polymers.

The introduction of new polymers has permitted the fabrication of flexible devices. One of the advantages of flexible microprobes is that they adapt their shape as the tissue deforms and therefore, the injury caused to the tissue is less than the damage induced by silicon based probes. During long time trials, implanted electrodes may lose their functionality due to the glial scar that blocks signals from cells. Since scarring is exacerbated by micromotion between the rigid electrode and the soft neural tissue, the development of more flexible probes is essential for improving their biocompatibility. Also, initial studies suggest that polymers are more biocompatible than silicon, which makes us think that polymer based probes could benefit chronic applications⁵⁶.

As mentioned before, polyimide, parylene and BCB based microprobes have been optimally fabricated and tested for various neural applications. As seen in table 2.1, contrary to silicon, the three of them present a low dielectric constant which makes them candidates to avoid possible current leakages. Also, they present a low Young's modulus which makes them suitable to obtain flexible devices. Nevertheless, since the processes available for these polymers do not allow the fabrication of thicknesses higher than ten microns, the microprobes are too flexible to penetrate the brain tissue on their own. Concerning other features of interest, polyimide has a relatively high water uptake compared to parylene or BCB which leads to a rapid fall in the electrode impedance and therefore, it may not be suitable for chronic applications.

Table 2.1. Selected properties for parylene, BCB, polyimide (PI) and SU-8 polymers

	Parylene	BCB	PI	SU-8
Dielectric constant	2.6-3.1	2.65	3.5	3-10
Water uptake (wt %)	<0.1	0.12	4	0.3
Young 's modulus (GPa)	2.42-2.76	3.1	2.8	4.5
Thickness (μm)	1-10	1-10	1-10	200

In order to overcome the drawbacks of materials like silicon, parylene, BCB and polyimide microprobes made exclusively of SU-8 are proposed here. Firstly, it should be noted that the fabrication of the device is a low-cost process and at the same time the device is reusable. The elastic modulus of this polymer is in the same order as the parylene, polyimide and BCB, but the SU-8 allows the fabrication of devices within a wider range of thickness. Therefore, the rigidity of the microprobe can be controlled by adjusting its thickness. Additionally, a suitable degree of biocompatibility of SU-8 has already been reported although a deeper study could benefit further applications³⁷. Apart from these features, the polymer SU-8 has been chosen because of its high-aspect-ratio capability⁵⁷. Vertical sidewall profiles can be patterned on devices with a length in the order of centimeters while still being narrow (< 100 μm). The use of microfabrication techniques, such as photolithography, enables good dimensional control over the entire thickness, and thus, a needle-shaped device can be obtained.

2.4 SU-8 MEMS technology

In this section the most relevant techniques for the fabrication of SU-8 based microprobes are highlighted. These techniques deal with the patterning of the polymer and sensing areas, construction of microchannels and releasing methods of the probes. Although these processes are already very well established, several optimizations and new approaches are required to adapt them for the development of SU-8 microprobes as it will be explained in next chapters.

2.4.1 Patterning processes

2.4.1.1 Photolithography

Photolithography is a process used in microfabrication to selectively remove parts of a thin film or the bulk of a substrate. It uses UV light to transfer a geometric pattern from a photomask to a light-sensitive resin on a substrate. The photoresin can be positive or negative; the positive resin becomes soluble in the basic developer when exposed and the negative photoresist becomes insoluble in the (organic) developer, figure 2.7. The standard photolithography process for the SU-8 negative resin consists of the following basic steps: substrate preparation, photoresist coating, soft baking, UV light exposition, post-exposure baking and developing.

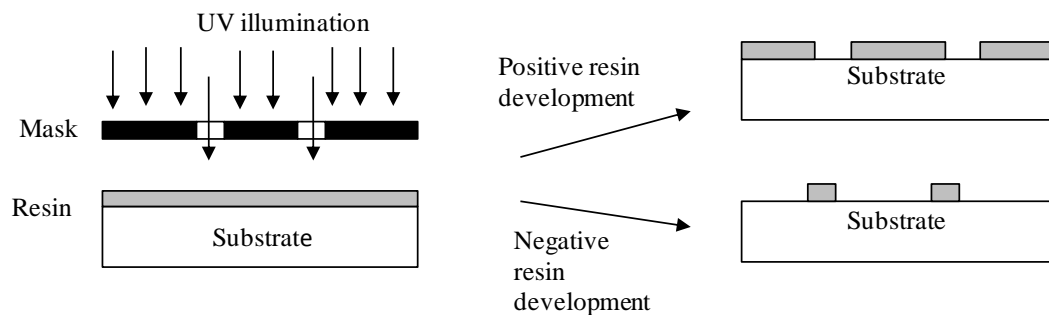


Figure 2.7 Schematic diagram of a photolithography process for positive and negative resins

- 1- Substrate preparation: the contaminants are removed from the wafer surface by solvent cleaning or piranha etch. If necessary the wafer is dehydrated to obtain better process reliability.
- 2- Spin coating: a small puddle of a fluid resin is deposited onto the center of a substrate while the substrate is turning at low speed. As the speed increases, the resin is spread all over the substrate and a thin film of resin covering the substrate is obtained. Final film thickness and other properties depend on the nature of the resin and the parameters chosen for the spin process.
- 3- Soft bake: after the spin coating, the resin is kept at a specific temperature to evaporate the solvent and obtain a dry film. Lower initial baking temperatures allow the solvent to evaporate out of the film and at a more controlled rate, which results in better coating fidelity, reduces edge bead and improves resin-substrate adhesion.
- 4- UV exposition: the resin is exposed to a controlled UV light. During the illumination the cationic polymerization starts.

- 5- Post-bake: during this step the illuminated SU-8 areas are crosslinked through a cationic photoamplification mechanism. This can be done at room temperature but in order to increase the process speed a higher temperature is preferred.
- 6- Development: the substrate is immersed in a solvent that eliminates the areas which have not been illuminated. Finally the substrate is rinsed with IPA.

2.4.1.2 Lift off

Lift off is a method for the patterning of thin films. First, an inverse pattern of the desired structure is transferred to a resin by photolithography as seen in figure 2.8 I). Then, the deposition of the thin film is carried out, figure 2.8 II). Next, the substrate is immersed in a dissolution that dissolves the resin, figure 2.8 III). As a result, the thin film remains only at the areas where it is in a direct contact with the substrate, figure 2.8 IV).

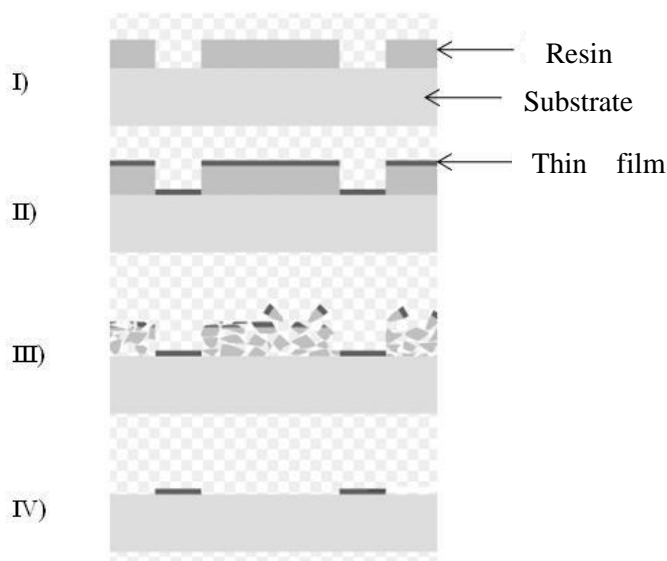


Figure 2.8 Schematic diagram of a lift off

2.4.1.3 Wet chemical etch

Etching process is used in microfabrication to chemically remove layers from selected areas of the wafer. After depositing the thin film on top of the wafer, figure 2.9 I), a sacrificial resin is photopatterned so that the desired areas of the material are covered as seen in figure 2.9 II). Then, the substrate is immersed in a bath of etchant where the unprotected areas of the thin film react and are dissolved, figure 2.9 III). Thus, the thin film is patterned but the sacrificial resin is still on top, figure 2.9 IV). Finally, the resin that is covering the thin film is removed by its specific solvent as shown in figure 2.9, V).

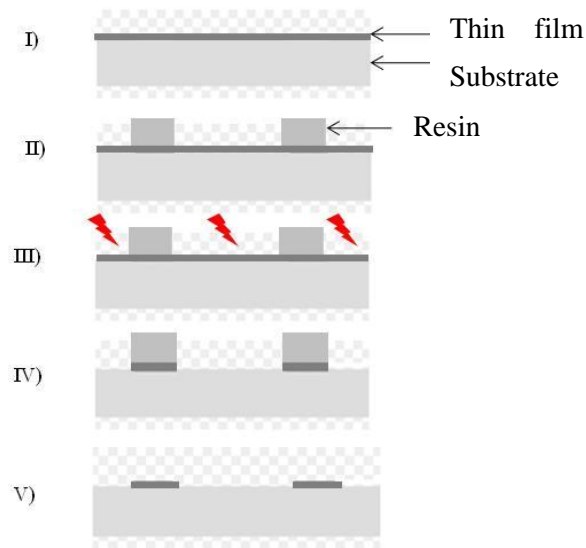


Figure 2.9 Schematic diagram of a wet chemical etching

2.4.2 Deposition techniques: metallization by sputtering

The so called “sputtering” process is a physical vapor deposition (PVD) method for the deposition of thin films. Substrates are placed in a chamber where first a high vacuum is reached (10^{-5} - 10^{-6} bar), figure 2.10. Then, a small flow of an inert gas (typically argon) is introduced till a pressure in the order of 10^{-3} bar is obtained. Plasma of the inert gas is then ignited. The energetic ions of the plasma bombard the surface of the target. The energy of the bombarding ions (\approx KeV) is sufficient to make some of the target atoms escape from the surface. Some of these atoms land on the sample surface and form a thin film. The heat generated during the sputtering process is dissipated by refrigeration to avoid the cathode overheating. Most elements from the periodic table can be sputtered, as well as inorganic and organic compounds. The structure of sputtered films is mainly amorphous, and its stress and mechanical properties are sensitive to specific sputtering conditions. Some atoms of the inert gas can be trapped in the film causing anomalies in its mechanical and structural characteristics. Therefore, each property of a thin film varies according to the precise conditions under which it was made.

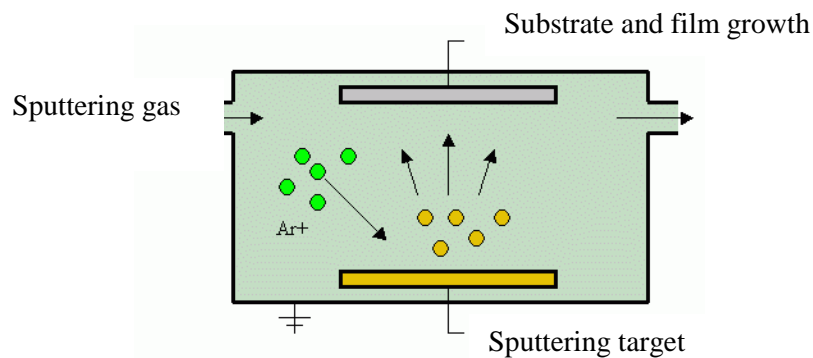


Figure 2.10 Drawing of a sputtering process

2.4.3 Surface treatments: O_2 plasma treatment

Over the last decades, plasma has become very useful by means of removing small quantities of material from a variety of substrates quickly and efficiently. The plasmas employed at room temperature are typically generated in a vacuum chamber. To generate plasma, the chamber is pumped to a pre-set base pressure, process gas is introduced and a radio frequency electromagnetic field is applied to produce glow-discharge plasma. In the plasma, there are many species such as ions, free radicals, electrons, photons, neutrals and reaction by-products. These species make highly active, low temperature plasma that can act on a material selectively and quickly.

In this case, oxygen plasma treatment has been used to activate the SU-8 surface. In this way, the adhesion between SU-8 and the following layer improves. Specifically, oxygen ions react with the homopolar surface of SU-8 and as a result, the SU-8 becomes hydrophilic. A hydrophilic surface is generally beneficial to get good adhesion and good uniformity with regard to the following deposition.

2.4.4 Bonding

In microfluidics, the bonding technology is essential to create cavities. Among microfabrication techniques, one of the methods to create 3D microchannel pads is based on the adhesive bonding. First of all, two SU-8 layers are patterned by photolithography. Then, both layers are brought into contact, pressed together and heated above the glass transition temperature of the SU-8. In this way, the two layers get bonded as seen in figure 2.11.

There are three main processes involved in the fabrication of 3D microchannels: i) the spin coating process to obtain high quality and uniformity of SU-8 thick films, ii) the photolithography process to obtain photopatterned thick films suitable for bonding applications and iii) the bonding process^{58,59,60}. Good planarity level of the resin is important to obtain a proper bonding process. This is mainly influenced by the speed, acceleration and duration of the spin coating. Also, UV dose, temperature and

cross-linking time have to be controlled in both substrates so that the polymerization degree is low enough. Finally, both substrates are aligned, and temperature and pressure are applied. The crosslinking reactions continue until a strong adhesion between the two layers of SU-8 occurs and thus, the channels are created.

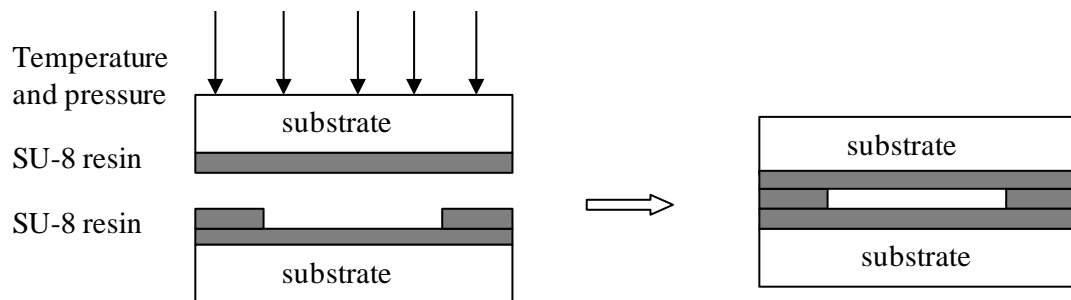


Figure 2.11. Schematic diagram of a SU-8 to SU-8 bonding process

2.4.5 Release techniques

The large majority of MEMS are fabricated on silicon, glass or Pyrex™ substrates. However, their final application often requires removal from the fabrication substrate or at least a partial release of some section of the device⁶¹. In this particular case, the last fabrication process is the separation of the microprobes from the substrate avoiding the use of common cutting processes usually employed in MEMS technology.

2.4.5.1 Mechanical release

One of the methods used to detach SU-8 devices from the substrate is the mechanical release. It consists of using a substrate with low adhesion properties with respect to SU-8, like the polyimide film called Kapton™. Once the whole SU-8 fabrication process is performed on top of a substrate with such a low adhesion, the probes are manually peeled off. However, this method is not always viable. When the devices are a few microns wide and various centimeters long the mechanical method does not work since the devices tend to break during manipulation. In order to overcome this problem, other release methods have been employed.

2.4.5.2 Wet chemical etching and electrochemical etching

In the fabrication procedure of the microprobes, the wet chemical etching involves firstly, the deposition of a metallic layer on top of the substrate, then the fabrication of the SU-8 probes on top of this layer and finally the removal of the sacrificial layer once the fabrication of the devices has finished. The dissolution of the metal in its specific etchant is essentially diffusion-limited and consequently the duration of the process may last up to days. Mainly for long underetching distances,

the structures that will be finally liberated have to be exposed to the etchant for a long time which may result in device damaging. As an alternative, the electrochemical etch is employed, which is a faster and less damaging method⁶⁰.

The electrochemical etching is based on the anodic metal dissolution. A small and positive potential is applied to the sacrificial metallic layer and therefore, the dissolution of the metal takes place in a neutral salt solution, figure 2.12. As a result, the probes are separated from the substrate without using any mechanical force. Among the advantages, it should be mentioned that most of the metals that are of interest in MEMS industry can be anodically dissolved in neutral salt solutions and that it is a non-aggressive system from the environmental point of view.

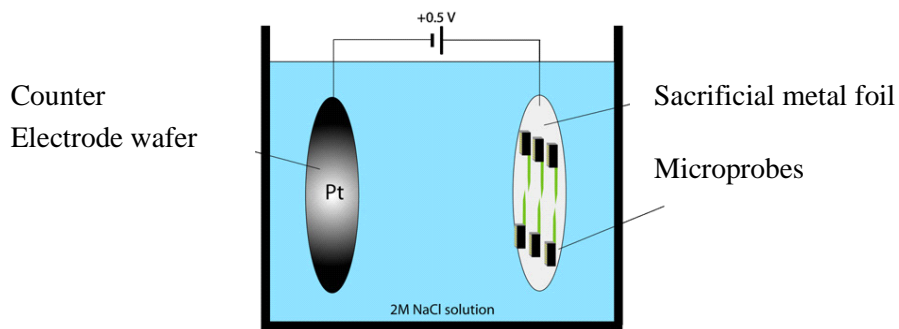


Figure 2.12 Schematic diagram of the electrochemical process for the release of the probes

2.5 References

- ¹Chang, W.C., Sretavan, D.W. Microtechnology in medicine: the emergence of surgical microdevices. (2007) *Clinical neurosurgery*, 54, pp. 137-147
- ²Chen, J., Wise, K.D., Hetke, J.F., Bledsoe Jr., S.C. A multichannel neural probe for selective chemical delivery at the cellular level (1997) *IEEE Transactions on Biomedical Engineering*, 44 (8), pp. 760-769
- ³Hoogerwerf, A.C., Wise, K.D. A three-dimensional microelectrode array for chronic neural recording (1994) *IEEE Transactions on Biomedical Engineering*, 41 (12), pp. 1136-1146
- ⁴Kipke, D.R. Multifunctional Neuroprobes with Integrated Chemical and Electrical Neural Interfaces (2003) *Annual International Conference of the IEEE Engineering in Medicine and Biology - Proceedings*, 4, pp. 3337-3339
- ⁵Wise, K.D. Silicon microsystems for neuroscience and neural prostheses (2005) *IEEE Engineering in Medicine and Biology Magazine*, 24 (5), pp. 22-29
- ⁶Strumwasser, F. Long-term recording from single neurons in brain of unrestrained mammals (1958) *Science*, 127 (3296), pp. 469-470
- ⁷McAllister, D.V., Allen, M.G., Prausnitz, M.R. Microfabricated microneedles for gene and drug delivery (2000) *Annual Review of Biomedical Engineering*, 2 (2000), pp. 289-313
- ⁸Levine, M.M. Can needle-free administration of vaccines become the norm in global immunization? (2003) *Nature Medicine*, 9 (1), pp. 99-103
- ⁹ Kipke, D.R., Vetter, R.J., Williams, J.C., Hetke, J.F. Silicon-substrate intracortical microelectrode arrays for long-term recording of neuronal spike activity in cerebral cortex (2003) *IEEE Transactions on Neural Systems and Rehabilitation Engineering*, 11 (2), pp. 151-155
- ¹⁰ Subbaroyan, J., Martin, D.C., Kipke, D.R. A finite-element model of the mechanical effects of implantable microelectrodes in the cerebral cortex (2005) *Journal of Neural Engineering*, 2 (4), pp. 103-113
- ¹¹Cheung, K.C., Renaud, P. BioMEMS for medicine: On-chip cell characterization and implantable microelectrodes (2006) *Solid-State Electronics*, 50 (4), pp. 551-557
- ¹²Burmeister, J.J., Moxon, K., Gerhardt, G.A. Ceramic-based multisite microelectrodes for electrochemical recordings (2000) *Analytical Chemistry*, 72 (1), pp. 187-192
- ¹³Ziegler, D., Suzuki, T., Takeuchi, S. Fabrication of flexible neural probes with built-in microfluidic channels by thermal bonding of Parylene (2006) *Journal of Microelectromechanical Systems*, 15 (6), pp. 1477-1482

- ¹⁴O'Brien, D.P., Nichols, T.R., Allen, M.G. Flexible microelectrode arrays with integrated insertion devices (2001) *Proceedings of the IEEE Micro Electro Mechanical Systems (MEMS)*, pp. 216-219
- ¹⁵ Lee, K.-K., He, J., Singh, A., Massia, S., Ehteshami, G., Kim, B., Raupp, G. Polyimide-based intracortical neural implant with improved structural stiffness (2004) *Journal of Micromechanics and Microengineering*, 14 (1), pp. 32-37
- ¹⁶ Dario, P., Carrozza, M.C., Benvenuto, A., Menciassi, A. Micro-systems in biomedical applications (2000) *Journal of Micromechanics and Microengineering*, 10 (2), pp. 235-244
- ¹⁷ A. Benvenuto, L. Beccai, F. Valvo, A. Menciassi, P. Dario, M. C. Carrozza, J. Aguiló, A. Ivorra, R. Villa, J. Millán, P. Godignon, J. Bausells, A. Errachid, Impedance Microprobes for Myocardial Ischemia Monitoring, (2000) Proceedings of the 1st Annual International IEEE-EMBS Special Topic Conference on Microtechnologies in Medicine and Biology, Lyon, France, pp. 234-238.
- ¹⁸ Suesserman, M.F., Spelman, F.A. Quantitative in vivo measurements of inner ear tissue resistivities: I. In vitro characterization (1993) *IEEE Transactions on Biomedical Engineering*, 40 (10), pp. 1032-1047
- ¹⁹ Ivorra, A., Gómez, R., Noguera, N., Villa, R., Sola, A., Palacios, L., Hotter, G., Aguiló, J. Minimally invasive silicon probe for electrical impedance measurements in small animals (2003) *Biosensors and Bioelectronics*, 19 (4), pp. 391-399
- ²⁰ Ivorra, A., Genescà, M., Sola, A., Palacios, L., Villa, R., Hotter, G., Aguiló, J. Bioimpedance dispersion width as a parameter to monitor living tissues (2005) *Physiological Measurement*, 26 (2), pp. S165-S173
- ²¹ Sola, A., Palacios, L., López-Martí, J., Ivorra, A., Noguera, N., Gómez, R., Villa, R., Aguiló, J., Hotter, G. Multiparametric monitoring of ischemia-reperfusion in rat kidney: Effect of ischemic preconditioning (2003) *Transplantation*, 75 (6), pp. 744-749
- ²² Genescà, M., Ivorra, A., Sola, A., Palacios, L., Goujon, J.-M., Hauet, T., Villa, R., Aguiló, J., Hotter, G. Electrical bioimpedance measurement during hypothermic rat kidney preservation for assessing ischemic injury (2005) *Biosensors and Bioelectronics*, 20 (9), pp. 1866-1871
- ²³ Gómez, R., Ivorra, A., Villa, R., Godignon, P., Millán, J., Erill, I., Solà, A., Hotter, G., Palacios, L. A SiC microdevice for the minimally invasive monitoring of ischemia in living tissues (2006) *Biomedical Microdevices*, 8 (1), pp. 43-49
- ²⁴ Wise, K.D., Angell, J.B., Starr, A. An integrated-circuit approach to extracellular microelectrodes (1970) *IEEE Transactions on Biomedical Engineering*, 17 (3), pp. 238-247
- ²⁵ Wise, K.D., Angell, J.B. A low capacitance multielectrode probe for use in extracellular neurophysiology (1975) *IEEE Transactions on Biomedical Engineering*, BME-22 (3), pp. 212-220

- ²⁶Campbell, P.K., Jones, K.E., Huber, R.J., Horch, K.W., Normann, R.A. A silicon-based, three-dimensional neural interface: Manufacturing processes for an intracortical electrode array (1991) *IEEE Transactions on Biomedical Engineering*, 38 (8), pp. 758-768
- ²⁷Cheung, K.C., Djupsund, K., Dan, Y., Lee, L.P. Implantable multichannel electrode array based on SOI technology (2003) *Journal of Microelectromechanical Systems*, 12 (2), pp. 179-184
- ²⁸Metz, S., Bertsch, A., Bertrand, D., Renaud, Ph. Flexible polyimide probes with microelectrodes and embedded microfluidic channels for simultaneous drug delivery and multi-channel monitoring of bioelectric activity (2004) *Biosensors and Bioelectronics*, 19 (10), pp. 1309-1318
- ²⁹Metz, S., Holzer, R., Renaud, P. Polyimide-based microfluidic devices (2001) *Lab on a Chip - Miniaturization for Chemistry and Biology*, 1 (1), pp. 29-34
- ³⁰Takeuchi, S., Ziegler, D., Yoshida, Y., Mabuchi, K., Suzuki, T. Parylene flexible neural probes integrated with microfluidic channels (2005) *Lab on a Chip - Miniaturisation for Chemistry and Biology*, 5 (5), pp. 519-523
- ³¹Lee, K., Massia, S., He, J. Biocompatible benzocyclobutene-based intracortical neural implant with surface modification (2005) *Journal of Micromechanics and Microengineering*, 15 (11), pp. 2149-2155
- ³²Boppart, S.A., Wheeler, B.C., Wallace, C.S. A flexible perforated microelectrode array for extended neural recordings(1992) *IEEE Transactions on Biomedical Engineering*, 39 (1), pp. 37-42
- ³³Meyer, J.-U. Retina implant - A bio MEMS challenge (2002) *Sensors and Actuators, A: Physical*, 97-98, pp. 1-9
- ³⁴Mercanzini, A., Cheung, K., Buhl, D.L., Boers, M., Maillard, A., Colin, P., Bensadoun, J.-C., Bertsch, A., Renaud, P. Demonstration of cortical recording using novel flexible polymer neural probes (2008) *Sensors and Actuators, A: Physical*, 143 (1), pp. 90-96
- ³⁵Singh, A., Zhu, H., He, J.Improving mechanical stiffness of coated benzocyclobutene (BCB) based neural implant (2004) *Annual International Conference of the IEEE Engineering in Medicine and Biology - Proceedings*, 26 VI, pp. 4298-4301
- ³⁶Clement, R.S., Singh, A., Olson, B., Lee, K., He, J. Neural Recordings from a Benzocyclobutene (BCB) Based Intra-Cortical Neural Implant in an Acute Animal Model (2003) *Annual International Conference of the IEEE Engineering in Medicine and Biology - Proceedings*, 3, pp. 2176-2179
- ³⁷Cho, S.-H., Lu, H.M., Culler, L., Romero-Ortega, M.I., Lee, J.-B., Hughes, G.A. Biocompatible SU-8-based microprobes for recording neural spike signals from regenerated peripheral nerve fibers (2008) *IEEE Sensors Journal*, 8 (11), art. no. 4658118, pp. 1830-1836

- ³⁸ Chen, C.-H., Chuang, S.-C., Su, H.-C., Hsu, W.-L., Yew, T.-R., Chang, Y.-C., Yeh, S.-R., Yao, D.-J. A three-dimensional flexible microprobe array for neural recording assembled through electrostatic actuation (2011) *Lab on a Chip - Miniaturisation for Chemistry and Biology*, 11 (9), pp. 1647-1655
- ³⁹ Cleland, J.L., Daugherty, A., Mersny, R. Emerging protein delivery methods (2001) *Current Opinion in Biotechnology*, 12 (2), pp. 212-219
- ⁴⁰ Langer, R. Drug delivery and targeting (1998) *Nature*, 392 (6679 SUPPL.), pp. 5-10
- ⁴¹ Ashraf, M.W., Tayyaba, S., Afzulpurkar, N., Nisar, A., Bohez, E.L., Tuantranont, A. Structural and microfluidic analysis of MEMS based out-of-plane hollow silicon microneedle array for drug delivery (2010) *2010 IEEE International Conference on Automation Science and Engineering, CASE 2010*, art. no. 5584012, pp. 258-262
- ⁴² Gill, H.S., Denson, D.D., Burris, B.A., Prausnitz, M.R. Effect of microneedle design on pain in human volunteers (2008) *Clinical Journal of Pain*, 24 (7), pp. 585-594
- ⁴³ Siepmann, J. Local controlled drug delivery to the brain (2006) *International Journal of Pharmaceutics*, 314 (2), pp. 99-100
- ⁴⁴ Lonser, R.R., Walbridge, S., Garmestani, K., Butman, J.A., Walters, H.A., Vortmeyer, A.O., Morrison, P.F., Brechbiel, M.W., Oldfield, E.H. Successful and safe perfusion of the primate brainstem: In vivo magnetic resonance imaging of macromolecular distribution during infusion (2002) *Journal of Neurosurgery*, 97 (4), pp. 905-913
- ⁴⁵ Morrison, P.F., Laske, D.W., Bobo, H., Oldfield, E.H., Dedrick, R.L. High-flow microinfusion: Tissue penetration and pharmacodynamics (1994) *American Journal of Physiology - Regulatory Integrative and Comparative Physiology*, 266 (1 35-1), pp. R292-R305
- ⁴⁶ Nguyen, T.T., Pannu, Y.S., Sung, C., Dedrick, R.L., Walbridge, S., Brechbiel, M.W., Garmestani, K., Beitzel, M., Yordanov, A.T., Oldfield, E.H. Convective distribution of macromolecules in the primate brain demonstrated using computerized tomography and magnetic resonance imaging (2003) *Journal of Neurosurgery*, 98 (3), pp. 584-590
- ⁴⁷ Saltzman, W.M., Olbricht, W.L. Building drug delivery into tissue engineering (2002) *Nature Reviews Drug Discovery*, 1 (3), pp. 177-186
- ⁴⁸ Hunt Bobo, R., Laske, D.W., Akbasak, A., Morrison, P.F., Dedrick, R.L., Oldfield, E.H. Convection-enhanced delivery of macromolecules in the brain (1994) *Proceedings of the National Academy of Sciences of the United States of America*, 91 (6), pp. 2076-2080
- ⁴⁹ Hall, W.A., Rustamzadeh, E., Asher, A.L. Convection-enhanced delivery in clinical trials (2003) *Neurosurgical focus [electronic resource]*, 14 (2)

- ⁵⁰Black, K.L., Ningaraj, N.S. Modulation of brain tumor capillaries for enhanced drug delivery selectively to brain tumor (2004) *Cancer Control*, 11 (3), pp. 165-173
- ⁵¹Raghavan, R., Brady, M.L., Rodríguez-Ponce, M.I., Hartlep, A., Pedain, C., Sampson, J.H. Convection-enhanced delivery of therapeutics for brain disease, and its optimization (2006) *Neurosurgical focus*, 20 (4)
- ⁵²Rohatgi, P., Langhals, N.B., Kipke, D.R., Patil, P.G. In vivo performance of a microelectrode neural probe with integrated drug delivery laboratory investigation (2009) *Neurosurgical Focus*, 27 (1)
- ⁵³Spieth, S., Brett, O., Seidl, K., Aarts, A.A.A., Erismis, M.A., Herwik, S., Trenkle, F., Tätzner, S., Auber, J., Daub, M., Neves, H.P., Puers, R., Paul, O., Ruther, P., Zengerle, R. A floating 3D silicon microprobe array for neural drug delivery compatible with electrical recording (2011) *Journal of Micromechanics and Microengineering*, 21 (12), art. no. 125001
- ⁵⁴Papageorgiou, D.P., Shore, S.E., Bledsoe Jr., S.C., Wise, K.D. A shuttered neural probe with on-chip flowmeters for chronic in vivo drug delivery (2006) *Journal of Microelectromechanical Systems*, 15 (4), pp. 1025-1033
- ⁵⁵Petersen, Kurt E. Silicon as a mechanical material (1982) *Proceedings of the IEEE*, 70 (5), pp. 420-457
- ⁵⁶ Voskerician, G., Shive, M.S., Shawgo, R.S., Von Recum, H., Anderson, J.M., Cima, M.J., Langer, R. Biocompatibility and biofouling of MEMS drug delivery devices (2003) *Biomaterials*, 24 (11), pp. 1959-1967.
- ⁵⁷Despont, M., Lorenz, H., Fahrni, N., Brugger, J., Renaud, P., Vettiger, P. High-aspect-ratio, ultrathick, negative-tone near-UV photoresist for MEMS applications (1997) *Proceedings of the IEEE Micro Electro Mechanical Systems (MEMS)*, pp. 518-522
- ⁵⁸Blanco, F.J., Agirregabiria, M., Garcia, J., Berganzo, J., Tijero, M., Arroyo, M.T., Ruano, J.M., Aramburu, I., Mayora, K. Novel three-dimensional embedded SU-8 microchannels fabricated using a low temperature full wafer adhesive bonding (2004) *Journal of Micromechanics and Microengineering*, 14 (7), pp. 1047-1056
- ⁵⁹Arroyo, M.T., Fernández, L.J., Agirregabiria, M., Ibáñez, N., Aurrekoetxea, J., Blanco, F.J. Novel all-polymer microfluidic devices monolithically integrated within metallic electrodes for SDS-CGE of proteins (2007) *Journal of Micromechanics and Microengineering*, 17 (7), art. no. 011, pp. 1289-1298
- ⁶⁰Agirregabiria, M., Blanco, F.J., Berganzo, J., Arroyo, M.T., Fullaondo, A., Mayora, K., Ruano-López, J.M. Fabrication of SU-8 multilayer microstructures based on successive CMOS compatible

adhesive bonding and releasing steps (2005) *Lab on a Chip - Miniaturisation for Chemistry and Biology*, 5 (5), pp. 545-552

⁶¹Metz, S., Bertsch, A., Renaud, P. Partial release and detachment of microfabricated metal and polymer structures by anodic metal dissolution (2005) *Journal of Microelectromechanical Systems*, 14 (2), pp. 383-391

3. SU-8 BASED MICROPROBES FOR THE MONITORING OF LIVING TISSUES: ISCHEMIA DETECTION IN RAT'S KIDNEY

In this chapter SU-8 based microprobes for the monitoring of living tissues are introduced. The novelty of this chapter is the evolution of the already developed silicon based planar microprobes concerning the structural material and fabrication procedure of the probe. Commonly used microfabrication techniques have been modified in order to integrate platinum electrodes into the SU-8 probe. Impedance spectroscopy results show constant impedance values in a wide range of frequencies suggesting the elimination of possible current leakages related to silicon based probes.

Additionally, platinum black coating has been implemented on top of the electrodes by electrochemical deposition to increase roughness and, consequently, reduce electrode-electrolyte impedance. Finally, *in vivo* experimental trials in rat's kidney have been carried out. Using SU-8 based probes the effects of an ischemia-reperfusion episode have been detected by visible changes in the impedance measurements.

Contents

3. SU-8 BASED MICROPROBES FOR THE MONITORING OF LIVING TISSUES: ISCHEMIA DETECTION IN RAT'S KIDNEY	30
3.1 BACKGROUND	31
3.2 DESIGN	33
3.2.1 The design of the probe.....	33
3.2.2 The location of the electrodes	35
3.3 FABRICATION	37
3.3.1 First fabrication procedure	37
3.3.2 Problems and solutions related to the first fabrication procedure	39
3.3.3 Second fabrication procedure.....	40
3.3.4 Achievements, problems and solutions related to the second fabrication procedure.....	40
3.4 PACKAGING	46
3.5 CHARACTERIZATION.....	46
3.5.1 Impedance spectroscopy: SU-8 probe vs. Si and SiC probes.....	46
3.5.2 Electrochemical deposition of platinum black	48
3.6 EXPERIMENTAL PROCEDURES	52
3.6.1 In vivo monitoring of ischemia-reperfusion episode in rat's kidney	52
3.7 CONCLUSIONS	54
3.8 REFERENCES	55

3.1 Background

Ischemia is a physiological term denoting insufficient blood flow for normal cellular function. It impedes the delivery of the necessary oxygen (hypoxia) and nutrients to the tissue cells. In a non-ischemic animal tissue, cells primarily use aerobic respiration where glucose is converted with the presence of O₂ into water, CO₂ and energy. The energy is used to build up a molecule called Adenosine Tri-Phosphate (ATP). ATP can provide energy for other processes such as muscle contractions. CO₂ is a byproduct of the reaction that is removed by blood circulation. During ischemia, there is a decrease in the oxygen and glucose available to the tissue as well as a decrease in the removal of carbon dioxide from the tissue due to inadequate blood flow. As a result of the decrease of the available oxygen, the tissue employs an anaerobic metabolic pathway. In this process glucose is also broken down to generate ATP but the efficiency is reduced (less ATP is obtained per glucose molecule) and lactic acid is generated, causing a decrease in the tissue pH. The reduced availability of ATP implies also a decrease in the available metabolic energyⁱ.

Animal cells keep their volume constant by means of an active mechanism that implies the consumption of ATP. Almost one-third of the energy requirement of a typical animal cell is consumed in fueling this mechanism. Briefly, the content of proteins and other non-diffusible macro-molecules

ⁱ This information has been copied from Ivorra, Antoni. *Contributions to the measurement of electrical impedance for living tissue ischemia injury monitoring* (2005) Universitat Politècnica de Catalunya

within cells create an osmotic pressure that is counter-balanced by an extracellular concentration of sodium ions. The extracellular concentration of sodium, however, is not the result of an impermeability of plasma membranes to sodium ions, but the consequence of a continuous active extrusion of sodium from the cell interior to the exterior in order to compensate for the influx diffusion of sodium. This fact is due to the low intracellular concentration of sodium and the electro-negativity of the non-diffusible molecules and proteins inside the cell. When the supply of metabolic energy becomes insufficient to sustain the usual rate of extrusion of sodium from the cell, as in the case of ischemia, sodium ions permeate into the cell and are not removed by active ion pumps. As a result, a net gain in intracellular sodium and chloride concentration takes place. This increase in solutes within the cell draws water osmotically from the extracellular compartment into the cell, resulting in a marked swelling of cellsⁱ.

An indirect relationship between ischemia and bioimpedance is generally accepted: the cell swelling resulting from inhibition of energy metabolism narrows the extracellular space and consequently, reduces the width of the electrical path for low frequency currents (plasma membranes are considered as dielectric), thus decreasing conductance and increasing resistance. However, the electrical bioimpedance characteristics still lack a complete explanation in terms of biological structures and physiological eventsⁱ.

The optimum frequencies or frequency bands for electrical bioimpedance measurements related to ischemia are located within the so called β dispersion region¹. This broad frequency band goes from some tens or hundreds of Hz to some tens of MHz and two main reasons are argued in its favour: 1) it is a 'comfortable' frequency range, not too high and not too low, to develop the necessary electronic instrumentation and probes and 2) the impedance measurements performed in these frequency regions have demonstrated a high sensitivity to ischemia, whilst higher frequencies do not seem to show much sensitivity^{2,3}. However, it must be mentioned that the α dispersion region (< 10 Hz) could be especially valuable in some tissues, such as liver⁴ⁱ.

Tissue impedance can be measured by a couple of electrodes attached to the surface of the sample under study. Both electrodes can be used to inject the current and to measure the voltage drop. However, the electrode-electrolyte interface impedances are in series with the sample impedance and, therefore, the measured impedance, Z_{MEAS} , is the sum of the three impedances Z_x , Z_{e1} and Z_{e2} where Z_x is the impedance of the sample and Z_{e1} and Z_{e2} are the impedances of both wires connecting the voltmeter to the component being measured, figure 3.1. Unfortunately, these parasitic impedances are sufficiently large to disturb the measurements, especially at low frequencies. Because of that, an alternative measuring method is used: four-electrode method or Kelvin method. By means of this

method the current is injected with a couple of electrodes and the resulting voltage drop is measured with another couple of electrodes. This method involves the use of both an ammeter and a voltmeter. At first it appears that a stray impedance is introduced into the circuit, however, voltmeter's wires carry minuscule current and the influence of the wires connecting the voltmeter across the sample drops insignificant amounts of voltage. Thus, it cancels the influence of the electrode-electrolyte interface impedance resulting in a voltmeter indication that is very nearly the same as if it was connected directly across the sample impedance. Therefore, the four-electrode method was used with the probes presented in this chapterⁱ.

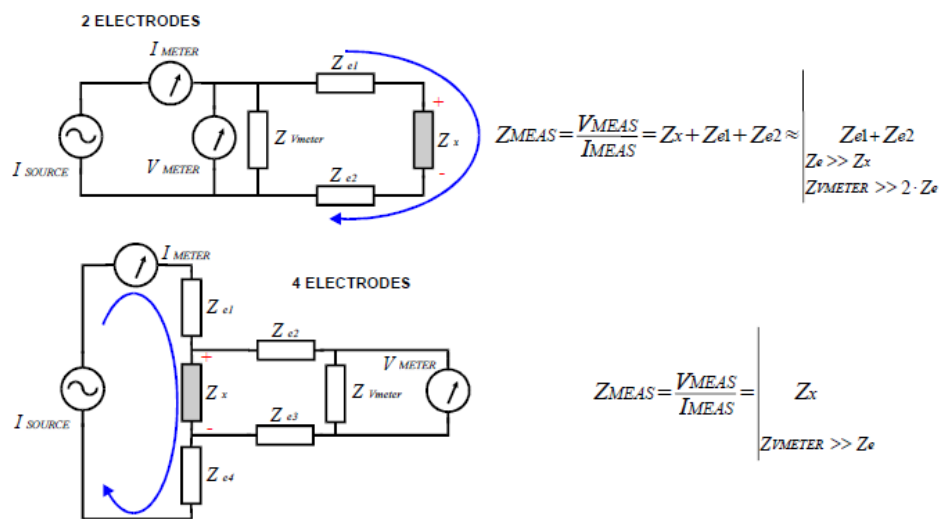


Figure 3.1 Schematic representation of the bipolar and the tetrapolar impedance measurements methodsⁱ.

3.2 Design

3.2.1 The design of the probe

The design of the SU-8 based microprobe for the monitoring of living tissues is based on the silicon probe first designed by Prof. José Millán, Dr. Mark Warren and Dr. Philippe Godignon for the same aim⁵. The design is the result of knowledge of the classical plunge probes and some intuitive ideas developed in CNM (Centro Nacional de Microelectrónica, Barcelona). The plunge probe successfully used by the Dr. Cinca team consists of four platinum needle-shaped electrodes (7,5 mm long, 0.4 mm diameter) mounted in a linear array on an insulating substrate separated by an inter-electrode distance of 2.5 mm⁶. The outer electrodes are employed to inject AC current into the tissue while resulting potential is differentially measured across the inner electrodes⁷ and consequently the impedance is obtained, figure 3.2 a). This classical configuration can be flexibly adapted to many experimental

studies by simply changing the dimensions, but there are some practical drawbacks that restrict its use⁸: a) the fabrication process results in large tolerances because of the critical positioning and alignment of the electrodes, b) the damage caused to the tissue is considerable since each probe causes four punctures, c) the presence of a conductive layer (e.g. blood) on top of the tissue under study shunts the electrodes and seriously disturbs the measurements⁹ and d) the strong dependence of apparent resistance on insertion depth makes crucial the probe fixation to the tissue¹⁰. Because of these facts, bioimpedance *in vivo* studies have been mostly limited to moderate size animals. Only few studies have been carried out by the use of different impedance probes, and showed important practical limitations¹¹.

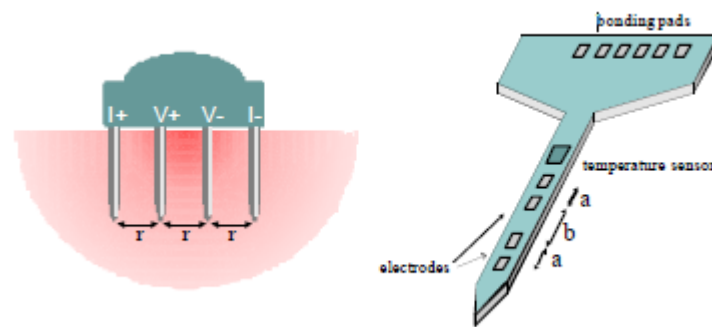


Figure 3.2 a) Classical four electrode-plunge probe and b) planar configuration of the probe

In order to overcome the limitations presented by the plunge electrodes, a planar configuration was proposed by CNM researchers. The planar configuration consists of locating four aligned electrodes in a single probe as shown in figure 3.2 b) so that damage is reduced to a single puncture. Moreover, additional modifications were implemented to improve the functionality of the device^{12, i}:

- The probe must be inserted perpendicular to the tissue and, especially in some specific cases such as the heart, that implies a limitation to the probe length because of the myocardium thickness (<1cm). Thus, taking into account the fact that the electrodes need to be at some distance from the tissue surface, the length of the array was reduced from 7.5 mm to 4 mm.
- The separation distance between the inner electrodes (voltage electrodes) was increased in order to increase the voltage drop and improve the signal to noise ratio.
- The fact that the electrodes are square shaped implies that the electric fields are larger around the vertexes (non-uniform fields) and that non-linear effects of the tissue or the electrode-electrolyte interface impedance will be manifested more easily. These undesired effects could

be minimized by employing circular electrodes but in that case, the available electrode area would be reduced for a given probe width.

- The track areas were designed in order to minimize the resistance from the electrodes to the bonding pads. Furthermore, the tracks for the two inner electrodes (voltage measuring electrodes) were designed in such way that they have equal resistance values.
- The dimensions of the bonding pads were increased from 100 x 100 μm up to 300 x 300 μm in order to be able to use non-standard bonding techniques such as conductive adhesives.
- The chosen electrode material was platinum because of its biocompatibility and its low electrode-electrolyte interface impedance compared to other materials such as stainless steel or silver⁹.

3.2.2 The location of the electrodes

This section analyzes the contribution of the electrode array geometry to the impedance probe performance. The main objective is to show the consequences of choosing a non-constant inter-electrode separation distance, figure 3.3. The analysis is performed considering an array of flat electrodes on a flat surface.

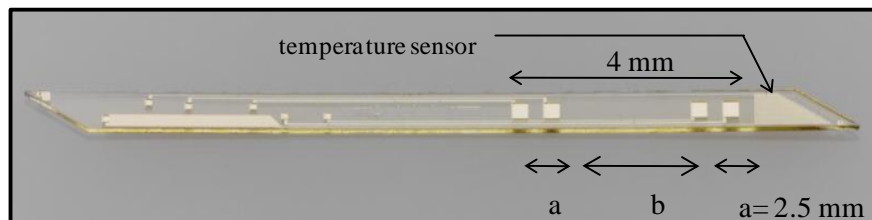


Figure 3.3 The position of the electrodes along the SU-8 probe

In the case of a constant inter-electrode separation distance (IESD) structure, there are some reasons to minimize the spacing between the electrodes¹:

- 1) Signal to noise ratio enhancement. Specifically, it is desirable to increase the voltage drop between the inner electrodes for a given sample and a limited current. The relation between the voltage drop (V), the injected current (I), the sample resistivity (ρ) and the IESD (r) in an isotropic and uniform medium is⁹:

$$V = k \cdot \frac{\rho}{r} \cdot I \quad (1)$$

where k is $(4\pi)^{-1}$ in the case that the medium is finite and $(2\pi)^{-1}$ in the case that the medium is semi-infinite, that is, the electrode array is applied on the flat surface of a medium which is surrounded by another medium with an infinite resistivity such as air. The equivalent expression for an infinite medium when the distance between inner electrodes is b and the total array length is $2a+b$ is straightforward obtained:

$$V = \frac{1}{4\pi} \cdot \rho \cdot \frac{b}{a \cdot (a + b)} \cdot I \quad (2)$$

Therefore, if the distance between the inner and outer electrodes, a , is reduced while the array length is constant, the voltage difference will be increased and the signal-to-noise ratio will be improved.

- 2) Spatial resolution improvement. Robillard and Poussart determined that the impedance measurements are not disturbed by medium transitions at distances beyond $3 \times \text{IESD}^{13}$.
- 3) Probe size reduction and, consequently, tissue damage minimization.

On the other hand, there are also some good reasons not to minimize the spacing¹:

- i) Homogeneity. In order to minimize the scatter of measured values due to the heterogeneity of the living tissues¹⁴. If electrodes are too close, the measured impedances will depend on the position of the probe in relation to the cell matrix. Because of that, an IESD considerably larger than the maximum cellular size is advisable (0.2 mm in the case of the skeletal muscle).
- ii) Blood shunting phenomenon minimization. The presence of a thin layer of blood or serum on the array surface can be the most serious drawback of planar configurations because such a disturbing layer can 'shield' the sample from the probe by short-circuiting the electrodes. Steendijk et al. have modeled the influence of these layers and have determined that a layer with a IESD/10 thickness and a resistivity below one tenth of the sample resistivity causes an impedance module error higher than the 20%¹⁰. If the presence of such a layer cannot be avoided, this error can only be reduced by increasing the IESD/layer thickness ratio.
- iii) Electrode area enlargement in order to reduce their interface impedance.
- iv) Parasitic capacitances reduction.

The case of non-constant IESD had not been studied before and a priori it was not known what was the effect of reducing the distance between inner and outer electrodes. CNM researchers made some trials to justify the design proposal. Using the image method it was analytically found that locating the inner electrodes closer to the outer electrodes was beneficial in terms of spatial resolution. Also, experimental results were implemented to confirm the analytical results. It was observed that the experimental values fit quite nicely the predicted values by the model. It was concluded that the constant IESD configuration was less influenced by the disturbing layer than the non-constant IESD configuration. Although the effect of the disturbing layer was of great relevance, it was found that it rarely appeared unless a blood vessel was damaged. Therefore, it was decided to reduce the distances between the inner and outer electrodes.

Apart from the impedance electrodes, a temperature sensor was added to the probe as can be observed in figure 3.3. Some ischemia events are usually accompanied by temperature changes. The temperature plays an important role in the ionic conductance: the viscosity of the solvent decreases as the temperature rises, increasing ion mobility and, consequently, decreasing resistivity. There exists a linear relation between temperature and ionic conductance that lies roughly around 2%/°C. Thus, it is possible to mathematically compensate the temperature dependence or, at least, to minimize it by using a temperature sensor (the conductivity-temperature coefficient is not fixed and should be determined for each kind of tissue)^{15,i}.

All the deductions made for already tested silicon probes were used to design SU-8 based probes. Besides all the dimensions aforementioned, the thickness of the probe was set at 160 μm due to the adequate mechanical behavior of the probe in order to penetrate in organs such as kidney or liver, without causing significant trauma.

3.3 Fabrication

3.3.1 First fabrication procedure

A 4 inch, 700 μm thick PyrexTM wafer was used as a substrate onto which a KaptonTM film of 150 μm thickness was adhesively bonded¹⁶, figure 3.4 I). KaptonTM was used because of its low adhesion to SU-8, allowing the release of the devices from the substrate when their fabrication finishes. At the same time, most of the deposition and etching processes were possible without delamination problems. Once the KaptonTM film was fixed to the substrate, a 70 μm thick SU-8 layer was spin coated and soft baked (SB), heating the wafer up to 65°C for 10 minutes and up to 95°C for 30 minutes. Then, a 400 mJ/cm^2 dose of UV was applied by standard photolithography followed by a post bake (PB), heating the wafer up to 65°C for 2 minutes and up to 95°C for 4 minutes, figure 3.4 II). By means of the

photolithography process the shape of the probe was defined whereas the area that surrounds the probe was not exposed. Afterwards, chromium (Cr, 50 nm) and gold (Au, 150 nm) sputtering was carried out at a low temperature, figure 3.4 III). Then, a positive resin was processed and both metals were patterned by selective wet chemical etching. As a result, the un-exposed area was protected by chromium and gold in order to protect it from being crosslinked in subsequent processes, figure 3.4 IV). Then, titanium (Ti, 50 nm) and platinum (Pt, 150 nm) were sputtered and patterned by the lift off technique, figure 3.4 V) and VI). In this way, metallic electrodes were implemented along the probe, figure 3.4 VII). As a next step, a 20 μm thick SU-8 passivation layer which covers the metallic tracks was spun and soft baked, heating the wafer up to 65°C for 2 minutes and up to 95°C for 7 minutes, figure 3.4 VIII). After a 140 mJ/cm^2 UV dosage and the PB procedure, the passivation layer was developed. At this state, chromium and gold areas were wet etched and all the un-exposed area that was underneath was developed, figure 3.4 IX). Finally the probes were manually released from the Kapton™ film, figure 3.4 X) and XI). In figures 3.5 a) ,b) ,c), and d) the appearance of the probe is observed at different steps of the fabrication procedure.

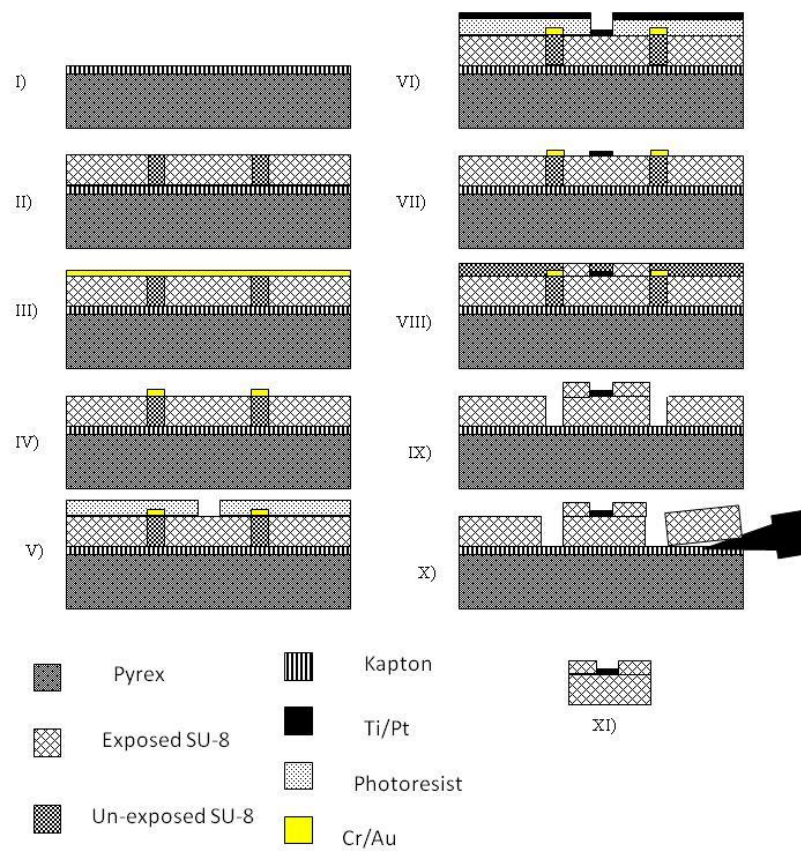


Figure 3.4 Schematic drawing of the fabrication procedure sequence

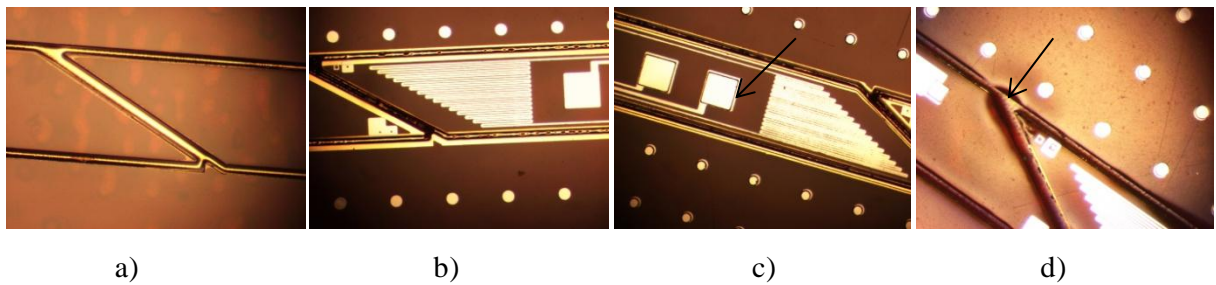


Figure 3.5 a) Cr and Au wet etching to define the probe shape, b) Ti/Pt electrodes patterned by lift off, c) SU-8 passivation layer (arrow) and d) Cr, Au and un-exposed SU-8 removal from the edges of the probe (arrow).

3.3.2 Problems and solutions related to the first fabrication procedure

Main problems related to the first fabrication procedure were detected after initial experimental trials in rat's kidney. Our colleagues from CNM observed during clinical trials that the probes were not robust enough to penetrate the outside layer of the kidney and that they tended to break during the insertion. In addition, the platinum electrodes peeled off during the platinization processes (explained in section 3.5.2) as seen in figure 3.6 a), and, finally, the passivation layer showed delamination problems while manipulating the probe, as can be observed in figure 3.6 b).



Figure 3.6 a) Broken electrodes after a platinization procedure and b) the passivation SU-8 layer is removed from the bottom SU-8 layer.

In order to overcome the already mentioned problems, some assumptions were made:

- 1- The total thickness of the probe had to be increased in order to penetrate the tissue while keeping the flexibility of the probe as high as possible.

- 2- The adhesion between the bottom SU-8 layer and the Ti/Pt electrodes had to be improved to withstand the platinization procedure.
- 3- The adhesion between the bottom layer of SU-8 and the passivation layer had to be more robust.

3.3.3 Second fabrication procedure

In the second fabrication procedure some changes were carried out with regard to the first version to solve the aforementioned drawbacks. After the SB of the first SU-8 layer, a second 70 μm thick SU-8 layer was spin coated in order to increase the rigidity of the probe. The same SB conditions were applied on such layer, and an exposure of a 400 mJ/cm^2 dose was given. Next, as an innovative step, oxygen plasma treatment was applied on the SU-8 surface in order to improve the adhesion between the metal and the SU-8. Right after that, chromium and gold sputtering and wet etching processes were performed as in the previous version. Another change in respect of the first version is that a hard bake (HB) process was performed heating the wafer up to 95°C for 10 minutes before the second oxygen plasma treatment. In this way the SU-8 layers were much more polymerized and the adhesion of the Ti/Pt layers on the SU-8 surface improved. Once the electrodes were patterned, the 20 μm thick passivation layer was spun but in this case, instead of 140 mJ/cm^2 , an UV dose of 240 mJ/cm^2 was applied in order to get a better adhesion between the bottom and top SU-8 layers. Chromium and gold wet etchings and the development of the un-exposed SU-8 area were carried out and finally, the probes were peeled off. A picture of a microprobe once the fabrication has finished is shown in figure 3.7.

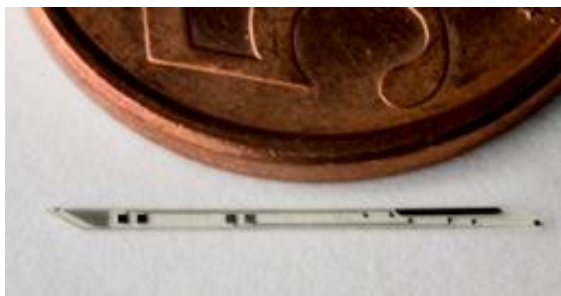


Figure 3.7 A picture of the SU-8 microprobe next to a 5 euro cent coin.

3.3.4 Achievements, problems and solutions related to the second fabrication procedure

The solutions suggested in the second fabrication procedure succeeded in improving the adhesion between the Ti/Pt layers and the SU-8 and, therefore, the platinization process was performed correctly. Also, as the probe was then thicker the insertion into kidney was performed without

breakages. According to the adhesion between the top and bottom SU-8 layers, the increase of the UV dose in the passivation layer kept both layers stuck during experimentation.

3.3.4.1 Metallization on SU-8

One of the goals of the second fabrication procedure, was the improvement of the metal adhesion on SU-8 due to the oxygen plasma treatment. As mentioned in the second chapter, plasma bombard breaks up SU-8 molecules and provides polar functional groups on the surface so that the following chemical bonds, polymer-metal bonding in this case, are stronger. Colleagues from the Microsystem department of Ikerlan S.Coop. had already studied the effect of plasma on the SU-8 surface using the Diener plasma treatment equipment and some useful information was obtained from their work¹⁷. As can be seen in figure 3.8, the contact angle decreases when applying plasma for different PB conditions and power applied in the Diener. The most meaningful result was that in 10 seconds the contact angle decreased to nearly 10 degrees, and then the angle kept almost constant except for the case in which the most aggressive conditions were applied. In addition, the contact angle of a water drop on SU-8 surface was photographed after different plasma treatments. It was observed that 60 W was the minimum power necessary to reduce the contact angle as shown in figure 3.9. In the particular case of the probes, a HB of 10 minutes at 95°C was performed to the SU-8 and then, a plasma treatment with a power of 90W was applied for a minute. These modifications prevent the Ti/Pt electrodes from being peeled off during consecutive experimental trials.

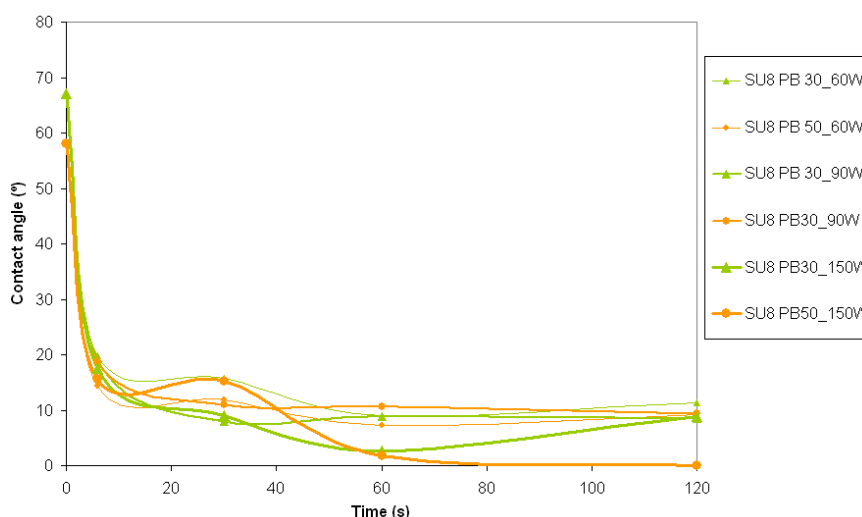


Figure 3.8 Contact angle versus time when applying oxygen plasma to the SU-8 surface

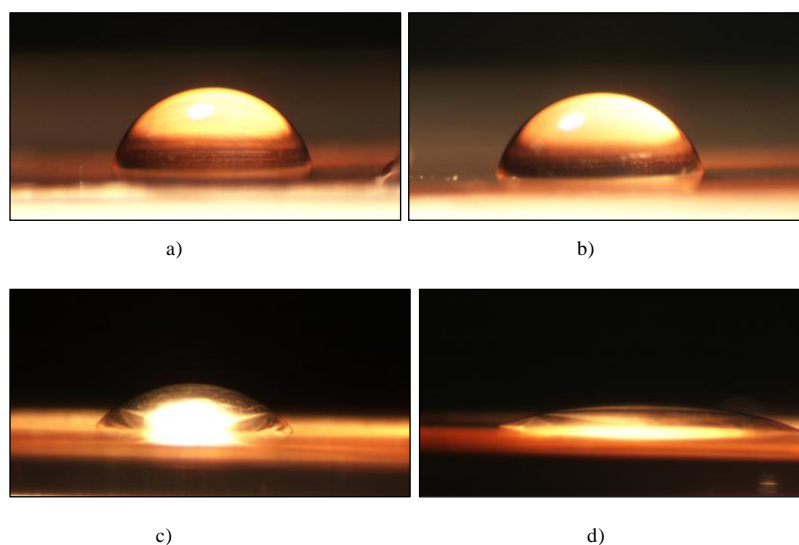


Figure 3.9 Water drop on SU-8 surface after a PB at 95°C for 30 minutes: a) without plasma treatment, b) after 6 seconds at 20W, c) after 6 seconds at 30 W and d) after 6 seconds at 60W

Besides superficial treatments on SU-8, the sputtering parameters were optimized in order to avoid SU-8 cracking and prevent further polymerization of the un-exposed SU-8. Four different metals were chosen: Cr, Au, Ti and Pt. Cr and Au were chosen to protect the un-exposed SU-8 area because both of them can be patterned by very simple and standard clean-room techniques like sputtering and wet etching. In this case, the lift off technique was not suitable because it involves spin coating a sacrificial resin on top of the un-exposed SU-8 area. It was experimentally observed that the mixture of both resins made the patterning of the sacrificial resin difficult. In addition, it was observed that the deposition of 200 nm thick metal layer was necessary in order to keep the un-exposed area protected during the whole fabrication process. Ti and Pt were chosen to create the electrodes. Ti was chosen as an adhesion layer and Pt because of its biocompatibility and low electrode-electrolyte interface impedance⁹. All the metallization sputtering processes were carried out by alternating switch on and switch off steps. In the past, the colleagues of Ikerlan observed that a continuous sputtering process increases the temperature of the sample as can be observed in figure 3.10 for the case of the titanium deposition. The other metals showed similar behavior and it was concluded that this effect damages the SU-8. The sputtering parameters (working power, pressure in the chamber, duration of on and off cycles and amount of cycles) were optimized to obtain the desired film thickness and to keep the temperature in the wafer lower than 50°C, table 3.1. In all the cases the working pressure during sputtering was 10^{-3} mbar.

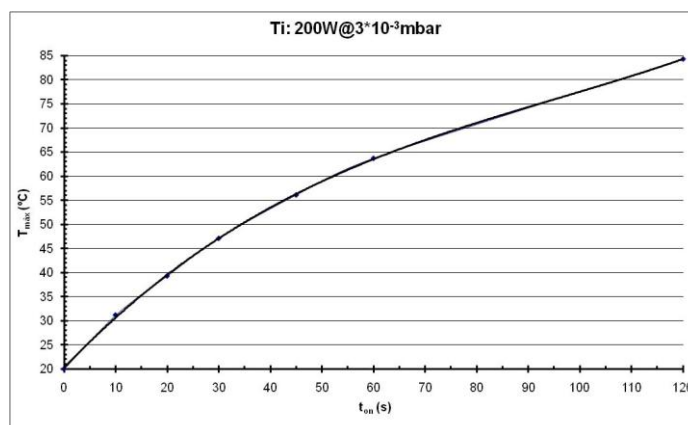


Figure 3.10 The increase of the temperature in the wafer along the time for the Ti continuous sputtering

Table 3.1 Sputtering conditions for Cr, Au, Ti and Pt deposition

		Chromium	Gold	Titanium	Platinum
Thickness (nm)		50	150	50	150
Working power (W)		100	100	200	100
Cycles	ON duration (s)	30	15	15	30
	OFF duration (s)	60	60	30	60
	Amount	12	24	24	28

3.3.4.2 Planarity of the SU-8

Owing to the lack of rigidity, the thickness of the probe was increased adding a 70 μm thick SU-8 layer. Consequently the planarity all over the substrate was worse. In addition, the shrinkage of the patterned SU-8 layers during the PB emphasized this effect. As seen in figure 3.11, the measurements carried out by the confocal revealed that the thickness of the un-exposed SU-8 was approximately 3 μm less than the exposed SU-8 because of the solvent evaporation difference¹⁸. These two reasons entailed a tremendous non-uniformity. Consequently, during the following UV exposure a slight diffraction occurred and as a result, the resolution of the resin patterned on top of the non-uniform area was poor, figure 3.12 a).

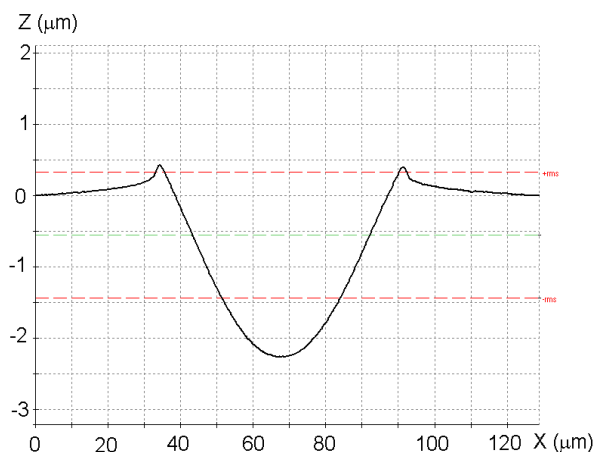


Figure 3.11 Thickness difference between exposed SU-8 and un-exposed SU-8

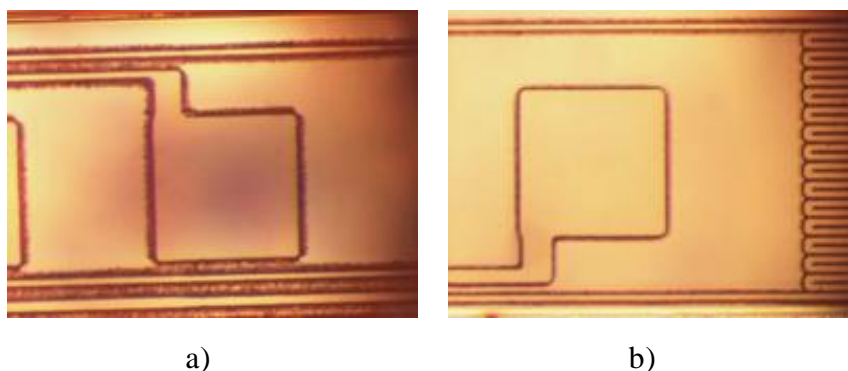


Figure 3.12 a) Poor resolution of the electrodes patterning and b) good resolution of the electrodes patterning.

Firstly, in order to get a better resolution of the sacrificial resin used for the patterning of the electrodes, the SB, the exposure dose and the developing parameters were optimized. 4 μm thick positive resin (SPR 220)¹⁹ was chosen as a sacrificial resin. It was soft baked by infra red light (6 minutes) and a high dose of UV (1000 mJ/cm^2) was applied. In spite of the resolution improvement, it was not precise enough. Therefore, two other changes were made to improve the planarity and, consequently, the resolution of the electrodes: 1) The SB of the second 70 μm thick SU-8 layer was carried out at 95°C for 95 minutes and 2) the PB of both 70 μm thick SU-8 layers was performed in a controlled way after the sputtering of the chromium and gold. It was performed at 50°C for 10 minutes with the aim of minimizing height differences between the two states of the SU-8. As a result of these changes, a good patterning of the sacrificial resin was obtained as seen in figure 3.12 b).

3.3.4.3 Development of the un-exposed SU-8 area

A critical point of the fabrication procedure was the development of the un-exposed area that delimits the probe. This area needs to be fully developed in order to separate the probe from the Kapton™ as a last step. If the edges of the probe are not properly developed, the SU-8 traces remain at the edges and, consequently, the insertion of the device on tissue may be more damaging.

In the second fabrication procedure there were some difficulties on developing the un-exposed SU-8 area because it was partially polymerized, figure 3.13 a). Although this area was supposed to be protected from the UV light, a partial polymerization occurred during several steps of the fabrication procedure. The presence of the UV light in the environment during the first plasma treatment and sputtering process made the crosslinking begin because at that state the un-exposed area was not protected yet. Moreover, the UV light reached the un-exposed area due to the misalignments carried out during the consecutive photolithography processes. Also, the heating processes performed during the SB and PB steps made the SU-8 more and more crosslinked. Therefore, the edges of the probe could not be eliminated in a proper way.

The UV effect during the plasma treatment and the sputtering, was not possible to eliminate. Plasma treatment was essential to get a good adhesion between the SU-8 and the metal. The removal of the SU-8 from the edges was performed avoiding misalignments and by carrying out the development using the ultrasonic bath, figure 3.13 b). As a final step, each probe was released manually from the Kapton™ film using tweezers. In this way a new method was created to obtain complex structures without the need of slow and expensive dicing process which are commonly used in microfabrication procedures.

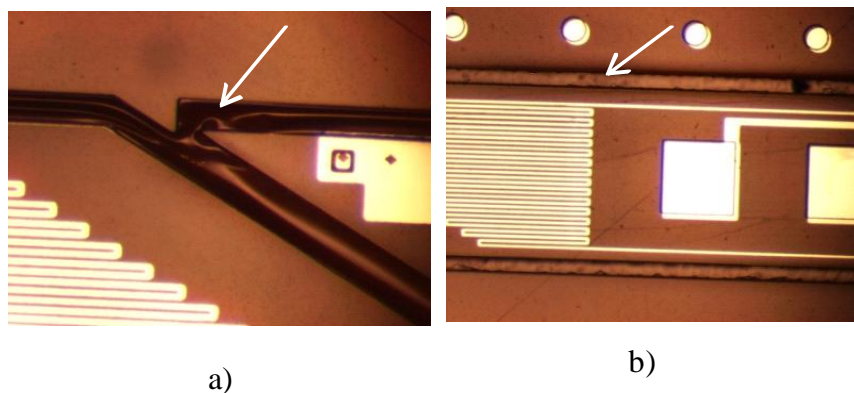


Figure 3.13 a) Although the Cr/Au layers are removed from the edges of the probe the un-exposed SU-8 remains and b) the metals are wet etched and the un-exposed SU-8 is eliminated from the probe edges.

3.4 Packaging

A high yield connection process between the SU-8 microprobe and the macroscopic world is necessary to perform reliable *in vivo* and *in vitro* measurements. In this case a flexible printed circuit (FPC) was chosen for the electrical connection of the probe. It allows an easy handling of the device while decreases the breakage possibility of the device and the damage caused to the tissue.

First, the conductive adhesive (Elecolit 3005 from Panacol-Eosol) was applied onto the contact pads of the probe. Then, the probe was aligned to a flexible printed circuit made of Kapton™ and slightly pressed. Next, the probe and the FPC were heated up to 90°C for half an hour until the adhesive was completely cured. Finally, a zero insertion force connector socket was used for the electrical connection to a rigid printed circuit board (PCB). A picture of a successfully packaged probe can be observed in figure 3.14.

There were no significant problems in the packaging procedure, but since the contact pads were quite small initially, the adhesive overflowed the pads and caused shortcircuiting. In order to avoid this, bigger contact pads (380 x 287 μm) were designed and, as a consequence, the packaging process yield increased.

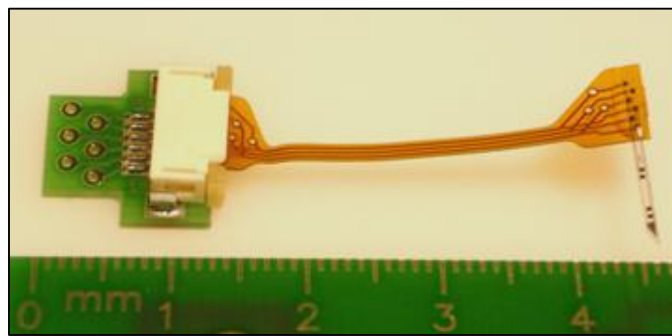


Figure 3.14 A probe fixed to a flexible packaging

3.5 Characterization

3.5.1 Impedance spectroscopy: SU-8 probe vs. Si and SiC probes

In vitro characterization of the probes was performed using commercial impedance analysis systems after the probes were encapsulated. The characterization was based on four-electrode impedance measurements, and involved the use of a front-end 1294 Solartron Analytical added to a SI 1260 system in order to boost its nominal input impedance²⁰.

Impedance readout started once the probes had been immersed in a 0.9% NaCl physiological solution at room temperature. Impedance modulus and phase angle measurements were taken from 10 Hz to 1 MHz in order to estimate the optimum frequency range for the operation of the sensor for all three different structural materials, Si, SiC and SU-8¹⁷. As can be seen in figure 3.15, results for Si probes differ considerably from ideal parameters (constant impedance modulus and a zero phase angle). Contrary to silicon behavior, the electric behavior of SiC and SU-8 microprobes is very similar, although SU-8 measurements are slightly better. The impedance modulus of the Si probe decreases above 1 kHz and this is reflected in the impedance phase angle above 1 kHz. Nevertheless, the characterization of SiC and SU-8 probes shows a constant impedance modulus across almost the whole frequency range. This can be explained by the current leakages that occur across the silicon substrate. Current leakages are present in any conducting substrate and they can be avoided by reducing the conductivity of the material. The comparison of the electrical properties of the three substrates can explain the differences: Si resistivity is 4-40 Ωcm , SiC resistivity is $10^4 \Omega\text{cm}$ (semiconductor substrate) and SU-8 resistivity is $2 \times 10^{17} \Omega\text{cm}$ (insulator substrate). Therefore, there is an effective blockage of the current leakages across the SiC and SU-8 substrates. However, slight differences between SiC and SU-8 can be observed, mainly in the phase where the angle distortion is appreciated. This fact happens at frequencies above 10 kHz for SiC and above 100 kHz for SU-8. The effects of the substrate leakages become less important for frequencies above 100 kHz in comparison with the parasitic capacitance effects of the contact pad interfaces and wires. Therefore, the use of SU-8 substrate eliminates the current leakages, but not parasitic capacitances. For these reasons, any future effort towards the improvement of the microsensor must be focused on the enhancement of the connection process pads and not in the substrate.

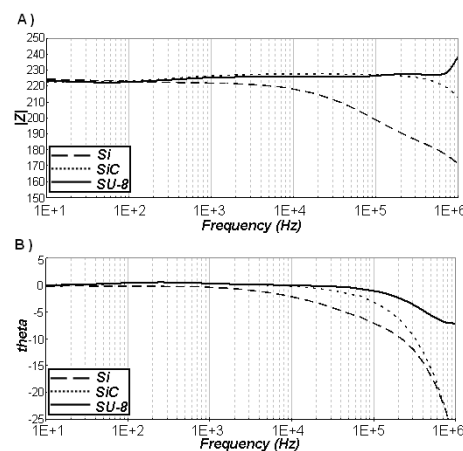
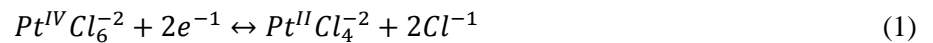


Figure 3.15 *In vitro* impedance recording results for Si, SiC and SU-8 based microprobes modulus (A) and phase (B) immersed in a 0.9.wt.% NaCl solution

3.5.2 Electrochemical deposition of platinum black

It is always desirable to keep the electrode-tissue interface impedance magnitude as low as possible independently of the measurement method (two or four electrodes method). An obvious solution would be to increase the electrode area making them larger. But since the sensor should be as small as possible to minimize damages in living tissue, alternative solutions are required. An alternative for the reduction of electrode-tissue interface impedance is based on the increase of the surface area through the control of the electrode roughness. Getting a rough surface involves increasing the effective area, which is inversely proportional to the resistance of the electrode. A well known method to increase surface roughness at the electrode area is the implantation of the so-called platinization process. This method consists of covering the sensing site with a porous layer of platinum black. This process is performed by immersing the electrode in an electroplating solution and applying a DC current potential across the electrode-solution surface^{9,21}. Thus, sponge-like or dendritic surfaces are obtained. The exchange reactions occurring at the surface result in the deposition of the metal according to the following reactions^{22,23}:



At low frequencies, this method can reduce interface impedance ten or more times²⁴. However, the platinum black surface is fragile and becomes easily detached when the electrode is inserted into the tissue. In this work the technique has been optimized in order to improve the mechanical stability.

As a first step, an initial cleaning of the electrodes surface was performed keeping the probe in ethanol for 3 minutes using the ultrasonic bath. Secondly, the impurities that remained on the electrode surface were eliminated by an "activation process". The aim of the activation process was to remove the possible impurities placed on the electrode surface and, therefore, improve the adhesion between the platinum black and the electrode. In this particular case, a low current was applied. The probe was immersed in distilled water and a current of 100 μ A (the minimum value allowed by the equipment) was applied between each pair of electrodes. Many trials were performed but as can be seen in the figure 3.16 the electrodes broke during the activation process. The activation process was finally rejected.



Figure 3.16. Broken electrodes after the activation process

However, it was observed that the electrodes just cleaned with ethanol were not platinized all over the metal surface in spite of using the optimized parameters of the electroplating process, figure 3.17 a). It was concluded that the black platinum was not adhered on top of the electrodes because some impurities remained on the metal pads. In order to solve this problem, a slight plasma treatment (1 minute at 90W) was applied to the electrodes as an alternative method to the activation process. The impurities were finally removed as seen in figure 3.17 b).

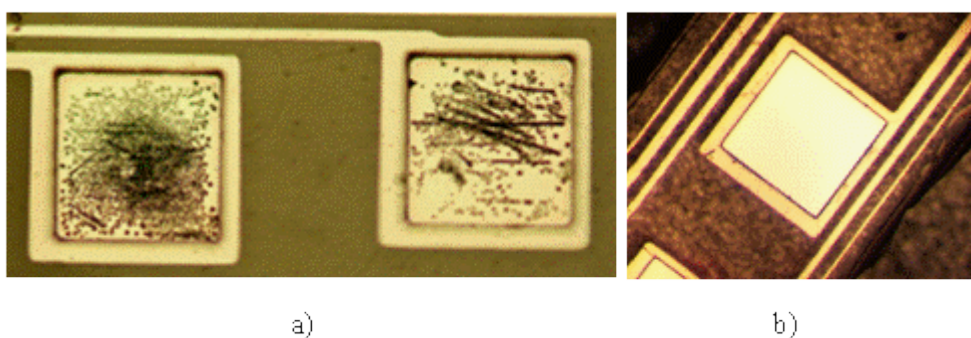


Figure 3.17 a) Electrodes slightly electroplated and b) a clean surface of the electrode

Once the surface of the electrodes was clean, the black platinum electrochemical deposition was carried out. The electrodes were immersed in a solution containing platinum chloride (Hydrochloric acid 0.1M, 2.3% Platinum (IV) chloride and 0.023% Lead (IV) acetate %99). A platinum electrode was then introduced in the solution and 25 μ A were applied between each electrode and the platinum electrode for 60 seconds. Finally, the electrodes were perfectly covered with platinum black, figure 3.18.

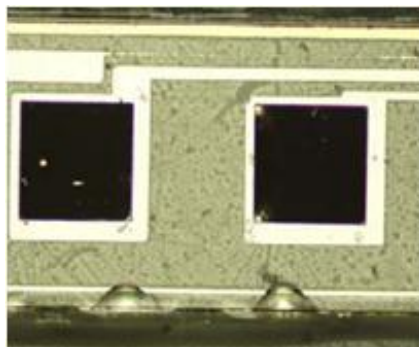


Figure 3.18 Electrodes covered with platinum black

Once the electrodes were electroplated, they were characterized to check whether the impedance of the electrodes had decreased by comparison with their initial state. A commercial impedance analysis system (SI 1260, Solartron Analytical) was used for the measurements. The microprobes were immersed in a physiological saline solution (0.9% NaCl, with a nominal resistivity of $71.3 \Omega\text{cm}$ at 298K) and an impedance spectroscopy was carried out. Independent impedance measurements were conducted for each couple of electrodes, recording the impedance modulus and phase at several discrete frequencies in the 10 Hz to 1 MHz range.

After the platinization of the electrodes, the impedance modulus decreased and became more stable in all the frequency range for both pair of electrodes as seen in figure 3.19. The impedance modulus of the electroplated electrodes was two orders of magnitude lower than that the un-platinized ones at low frequency range ($< 100\text{Hz}$). Although the impedance decreased considerably, these results suggested that at low frequencies the influence of the electrode-electrolyte interface impedance remained and therefore, the useful frequency band was considered over 100 Hz. At high frequencies, the impedance modulus was low for both types of electrode (electroplated and un-electroplated electrodes) as expected. At the same time, the phase tended to zero for the electroplated electrodes. The impedance values were quite similar when plating for 60 seconds and 90 seconds, however, the figure 3.20 shows that the platinum black overflowed the pads of the electrodes when they were electroplated for 90 seconds. Therefore, it was concluded that the best option was an electrodeposition process of 60 seconds.

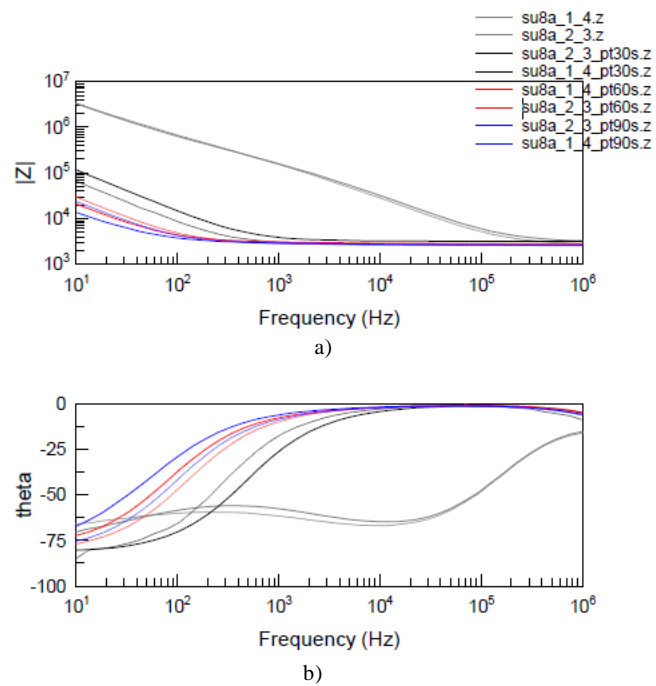


Figure 3.19 *In vitro* impedance recording results of two pairs of electrodes of a SU-8 probe: a) impedance modulus and b) phase measured in a 0.9wt. % NaCl solution.

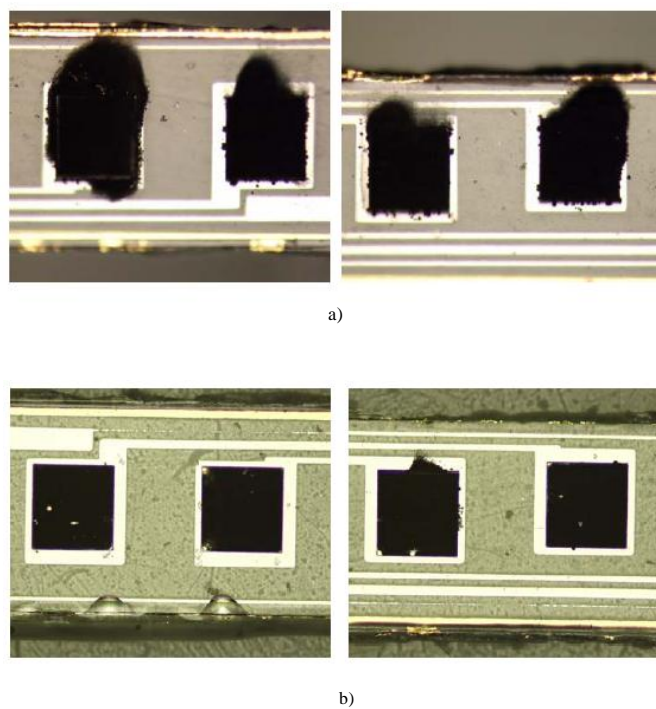


Figure 3.20 a) Electrodes after 90 seconds electroplating procedure and b) after 60 seconds electroplating procedure.

Additionally, the SU-8 microprobes were inserted into a liver bought in the market in order to test the mechanical stability of the platinum black. The objective was to simulate an *in vivo* test and know if the probe could penetrate the organ without breaking. At first, it was not possible to hammer the probe into the liver so the outer layer of the liver was removed. Thus, the insertion was carried out several times without any problem, figure 3.21. Up to ten insertions were made with the same probe and the platinum black was not detached from the surface. After the probes were taken out of the liver, *in vitro* impedance measurements were conducted. The results showed that the impedance values had increased slightly, however, it was an expected effect because of the manipulation. This issue was solved electroplating the probe before every consecutive *in vivo* test when necessary.

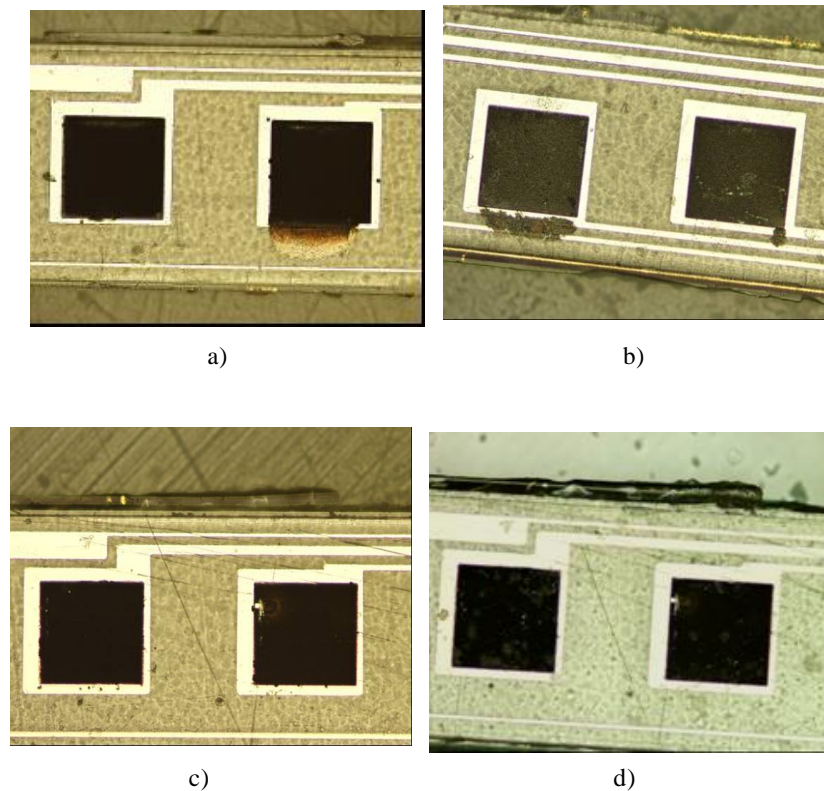


Figure 3.21 a) An electroplated probe before the insertion, b) the same probe after one insertion, c) another electroplated probe before the insertion and d) the same probe after ten consecutive insertions

3.6 Experimental procedures

3.6.1 *In vivo* monitoring of ischemia-reperfusion episode in rat's kidney

Once the electrodes behaviour was studied, the next purpose was to verify the functionality of the probes in a real application such as the monitoring of ischemia-reperfusion episode in rat's kidney. In this study it was tested whether the ischemia-reperfusion episode could be detected by real-time

measurement of electrical impedance employing SU-8 based miniaturized probes. Basically, an increase of electrical impedance was expected as a reliable indicator of anoxic edema due to ischemic cell swelling, which leads to reduced extracellular space, an increase in extracellular resistance, and cell-to-cell uncoupling⁵.

For *in vivo* impedance measurements a customized instrumentation system was used with the corresponding software previously developed to carry out four-electrode measurements²⁵. The impedance measurements were recorded from 100 Hz to 46 kHz applying a current of 100 μ A. The study was performed with male Sprague Dawley rats weighing from 200 to 225 g. The animals were anesthetized with isoflurano (1.5%) and placed in a supine position, with body temperature kept at 36-37°C. All procedures were conducted under the supervision of the IIBB-CSIC Institution's Research commission and followed by European Union guidelines for the handling and care of laboratory animals.

The probe was placed close to the cortico-medullar junction, an area that was found to display the most pronounced effects of ischemia-related injury in ischemia-reperfusion experiments²⁶. In small organs, such as the rat's kidney, the applied electric field covers a relatively high volume and the measurements may be considered representative of homogeneous tissue properties. In this particular case, ischemia was induced by clamping the kidney artery for 45 minutes, after which it was released and blood reperfusion ensued.

Multifrequency bioimpedance was monitored from 100 to 46 kHz as shown in figure 3.22. Measurements with low frequencies (from 100 to 1 kHz) enable the study of the extracellular medium⁵ and the use of high frequencies allows an important contribution of the intracellular medium and the cellular membrane to the measurements. Due to these reasons, the impedance and the phase angle values are lower for high frequencies than those obtained for low frequencies. As can be seen in figure 3.22(A), there is a substantial increase in the impedance module during the 45 minutes ischemic period (from 5th^{minute} till the 50th minute). This was previously attributed^{27,28,29} to the occurrence of a hypoxic edema as a result of cell swelling, which causes an increase of the extracellular resistance. After unclamping the renal artery (50 min reperfusion) the impedance modulus returns almost to its basal value, a fact that can be attributed in this experimental setting to a reversion from a short period of ischemia without substantial structural damage to the tissue. The same behaviour is observed in the phase angle above 1 kHz, figure 3.22 (B). At these frequencies, both the departure from and the sudden return impedance phase angle to its basal levels reflect clearly the period of arterial clamping-induced ischemia. Most importantly, the return of impedance phase angles to their initial levels upon reperfusion contributes to discard cell death and membrane disruption, since such events should not

lead to basal impedance phase values, complementing and confirming the results inferred from impedance modulus read at low frequencies. It was concluded that an organ that suffers a short ischemic period is able to recover the initial impedance values because there has been little damage.

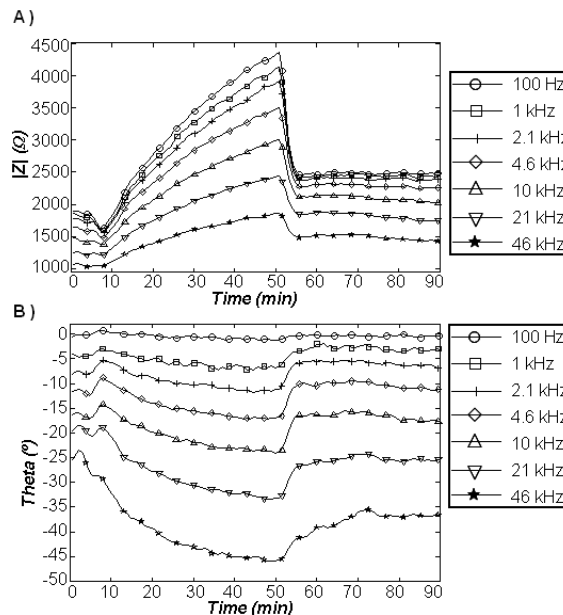


Figure 3.22 Impedance modulus (A) and phase (B) *in vivo* results for SU-8 based impedance probes in rat kidney warm ischemia experiments

3.7 Conclusions

Microprobes for living tissue monitoring were for the first time fabricated using the polymer SU-8 as a structural material. Optimized microfabrication processes such as the sputtering and superficial treatments allowed the integration and perfect adhesion of platinum microelectrodes into the polymer SU-8, making the device suitable for the insertion in living tissues. Moreover, the fabrication of the probes on top of the Kapton™ film and developing the un-exposed SU-8 as a final step avoided the use of slow and expensive dicing processes. Also, platinum black electrochemical deposition was adapted for this application in order to reduce electrode-electrolyte impedance. Finally, it was successfully demonstrated that SU-8 microsensors are capable of monitoring an ischemia-reperfusion episode in rat's kidney.

In this chapter it has been demonstrated that the SU-8 based probes are as functional as silicon based probes for ischemia detection. Additionally, a low-cost fabrication process has been presented. All these conclusions suggest the polymer SU-8 being a suitable structural material for other biomedical applications.

3.8 References

- ¹Foster, K.R., Schwan, H.P. Dielectric properties of tissues and biological materials: a critical review. (1989) *Critical Reviews in Biomedical Engineering*, 17 (1), pp. 25-104
- ²Yamada, T., Hirose, H., Mori, Y., Onitsuka, A., Hayashi, M., Senga, S., Futamura, N., Sakamoto, K.-I., Sago, T., Takagi, H., Yasumura, M., Iwata, H. Dielectric spectrogram for evaluating ischemic microstructural changes of the liver in simple cold preservation (2002) *Surgery Today*, 32 (12), pp. 1058-1063
- ³Schaefer, M., Gross, W., Preuss, M., Ackemann, J., Gebhard, M.M. Monitoring of water content and water distribution in ischemic hearts (2003) *Bioelectrochemistry*, 61 (1-2), pp. 85-92
- ⁴Gersing, E. Impedance spectroscopy on living tissue for determination of the state of organs (1998) *Bioelectrochemistry and Bioenergetics*, 45 (2), pp. 145-149
- ⁵Warren, M. Electrical impedance of normal and ischemic myocardium. Role on the Genesis of ST segment changes and ventricular arrhythmias (1999) *Thesis Universitat Autònoma de Barcelona*
- ⁶Cinca, J., Warren, M., Carreño, A., Tresànceh, M., Armadans, L., Gómez, P., Soler-Soler, J. Changes in myocardial electrical impedance induced by coronary artery occlusion in pigs with and without preconditioning: Correlation with local ST-segment potential and ventricular arrhythmias (1997) *Circulation*, 96 (9), pp. 3079-3086
- ⁷RUSH, S., ABILDSKOV, J.A., McFEER Resistivity of body tissues at low frequencies. (1963) *Circulation research*, 12, pp. 40-50
- ⁸Ivorra, A., Gómez, R., Noguera, N., Villa, R., Sola, A., Palacios, L., Hotter, G., Aguiló, J. Minimally invasive silicon probe for electrical impedance measurements in small animals (2003) *Biosensors and Bioelectronics*, 19 (4), pp. 391-399
- ⁹Steendijk, P., Mur, G., Van der Velde, E.T., Baan, J. The four electrode resistivity technique in anisotropic media: Theoretical analysis and application on myocardial tissue in vivo (1993) *IEEE Transactions on Biomedical Engineering*, 40 (11), pp. 1138-1148
- ¹⁰Tsai, J.-Z., Cao, H., Tungjitkusolmun, S., Woo, E.J., Vorperian, V.R., Webster, J.G. Dependence of apparent resistance of four-electrode probes on insertion depth (2000) *IEEE Transactions on Biomedical Engineering*, 47 (1), pp. 41-48
- ¹¹Raicu, V., Saibara, T., Irimajiri, A. Dielectric properties of rat liver in vivo: A noninvasive approach using an open-ended coaxial probe at audio/radio frequencies (1998) *Bioelectrochemistry and Bioenergetics*, 47 (2), pp. 325-332
- ¹²Ivorra, Antoni. Contributions to the measurement of electrical impedance for living tissue ischemia injury monitoring (2005) *Universitat Politècnica de Catalunya*
- ¹³Robillard, P.N., Poussart, D. Spatial resolution of four electrode array (1979) *IEEE Transactions on Biomedical Engineering*, 26 (8), pp. 465-470

- ¹⁴Roth, B.J. Interpretation of skeleton muscle four-electrode impedance measurements using spatial and temporal frequency-dependent conductivities (1989) *Medical and Biological Engineering and Computing*, 27 (5), pp. 491-495
- ¹⁵Gersing, E. Monitoring temperature-induced changes in tissue during hyperthermia by impedance methods (1999) *Annals of the New York Academy of Sciences*, 873, pp. 13-20
- ¹⁶Tijero, M., Gabriel, G., Caro, J., Altuna, A., Hernández, R., Villa, R., Berganzo, J., Blanco, F.J., Salido, R., Fernández, L.J. SU-8 microprobe with microelectrodes for monitoring electrical impedance in living tissues (2009) *Biosensors and Bioelectronics*, 24 (8), pp. 2410-2416
- ¹⁷Ugarte I., Desarrollo de laboratorios bioquímicos miniaturizados basados en polímeros termoplásticos con componentes termoplásticos y termoendurecibles que integran monolíticamente dispositivos microfluídicos con componentes fluídicos (2007)
- ¹⁸Chung, C.K., Hong, Y.Z. Surface modification of SU8 photoresist for shrinkage improvement in a monolithic MEMS microstructure (2007) *Journal of Micromechanics and Microengineering*, 17 (2), art. no. 004, pp. 207-212
- ¹⁹<http://www.chemplate.com/>
- ²⁰Gersing, E. Measurement of electrical impedance in organs. Measuring equipment for research and clinical applications (1991) *Biomedizinische Technik*, 36 (1-2), pp. 6-11
- ²¹Geddes, L. A., *Electrodes and the measurement of bioelectric events* New York: Wiley-Interscience (1979)
- ²²Feltham, A.M., Spiro, M. Platinized platinum electrodes (1971) *Chemical Reviews*, 71 (2), pp. 177-193
- ²³Harrison, J.A., Thompson, J. The electrodeposition of precious metals; a review of the fundamental electrochemistry (1973) *Electrochimica Acta*, 18 (11), pp. 829-834
- ²⁴Geddes, L.A., *Electrodes and the measurement of bioelectric events* (1972) *Wiley-Interscience/wiley*, New York, pp. 32-35
- ²⁵Gómez, R., Noguera, N., Ivorra, A., Villa, R., Aguiló, J., Millán, J., López, J., Palacios, L., Sola, A., Hotter, G. Instrumentation system for in vivo organ studies (2001) *Proceedings of the International Semiconductor Conference, CAS*, 1, pp. 261-264
- ²⁶Tønnessen, T.I., Kvarstein, G. PCO₂ electrodes at the surface of the kidney detect ischaemia (1996) *Acta Anaesthesiologica Scandinavica*, 40 (5), pp. 510-519
- ²⁷Gómez, R., Ivorra, A., Villa, R., Godignon, P., Millán, J., Erill, I., Solà, A., Hotter, G., Palacios, L. A SiC microdevice for the minimally invasive monitoring of ischemia in living tissues (2006) *Biomedical Microdevices*, 8 (1), pp. 43-49
- ²⁸Flores, J., DiBona, D.R., Beck, C.H., Leaf, A. The role of cell swelling in ischemic renal damage and the protective effect of hypertonic solute (1972) *Journal of Clinical Investigation*, 51 (1), pp. 118-126

²⁹Seoane, F., Lindecrantz, K., Olsson, T., Kjellmer, I., Flisberg, A., Bågenholm, R. Brain electrical impedance at various frequencies: The effect of hypoxia (2004) *Annual International Conference of the IEEE Engineering in Medicine and Biology - Proceedings*, 26 III, pp. 2322-2325

4. FIRST SU-8 MICROPROBE PROTOTYPE FOR NEURAL MONITORIZATION AND DRUG DELIVERY

This chapter deals with the first SU-8 polymer based microprobe prototype developed for the monitoring and drug delivery into neural tissues. The device was mechanically designed to ensure an easy insertion in the brain while minimizing the damage caused to the tissue. A microchannel with multiple outlets was integrated in the device to avoid excessive pressure at the probe tip during liquid delivery, and platinum electrodes were placed close to the outlet ports to monitor the response of the tissue. In order to obtain such device, photolithography, sputtering and bonding techniques were used.

A dedicated packaging was also developed in order to achieve an easy and reliable fluidic and electrical connection to the microprobe. Once the prototype was ready to be tested, delivery capacity was measured introducing the microprobe in agarose gel and sensing the liquid flow (water) through the microchannels as a function of the applied pressure. The electrical behaviour was monitored while introducing the probe in a saline solution. Moreover, *ex vivo* and *in vivo* tests were carried out on rat's brain. Post mortem tests showed the diffusion of the blue methylene in the prefrontal cortex and finally, *in vivo* trials concluded that the lesion evoked the SU-8 probes in the brain was lower than the one caused by standard rigid probes.

Contents

4. FIRST SU-8 MICROPROBE PROTOTYPE FOR NEURAL MONITORIZATION AND DRUG DELIVERY	58
4.1 DESIGN	59
4.2 FABRICATION.....	60
4.2.1 Fabrication procedure.....	60
4.2.2 Problems and solutions related to the fabrication procedure.....	62
4.3 PACKAGING	64
4.4 CHARACTERIZATION	65
4.4.1 Fluid delivery characterization.....	65
4.4.2 Impedance monitoring while delivering in the agarose gel.....	66
4.5 EXPERIMENTAL PROCEDURES	67
4.5.1 Mechanical and fluidic capability evaluation of the SU-8 probes by means of ex vivo tests	67
4.5.2 Evaluation of the damage evoked by the SU-8 probes by means of in vivo tests....	68
4.6 CONCLUSIONS.....	70
4.7 REFERENCES.....	71

4.1 Design

The design of the probe was focussed toward a micro scale device where multiple sensing sites and a fluidic channel should be integrated. Therefore, the design of the microprobe was divided into three different zones as can be observed in figure 4.1 a)¹. The widest area, $5 \times 5 \text{ mm}^2$, was designed to achieve a proper electric and fluidic encapsulation of the probe. Then, an 8 mm long path was created to progressively reduce the probe size. The part of the probe which is inserted in the tissue was designed to be 3 mm long in order to reach the neural zones of interest, while the width and thickness were chosen to be $400 \text{ }\mu\text{m}$ and $220 \text{ }\mu\text{m}$ respectively. Silicon-based microprobes can be comparably smaller², with typical dimensions in the order of $100 \text{ }\mu\text{m}$ wide and $20 \text{ }\mu\text{m}$ thick, but the aim of this design was to ensure the mechanical stability of the probe in the experimental applications. The insertion of the probe to a depth of up to 3 mm was believed to allow the infusion of fluids to superior neuronal areas of rodents, such as the cerebral cortex, in animal models of experimental neuroscience. The width and length of the microfluidic channel integrated in the microprobe was set at $50 \text{ }\mu\text{m}$ and 16 mm respectively. In order to reduce blocking effects during the probe insertion, five different outlet ports were implemented at the probe tip. Finally, six different electrodes with a size of $50 \times 50 \text{ }\mu\text{m}^2$ were placed close to the probe tip (the distances between electrodes are shown in figure 4.1 b)). Such electrodes were meant to be used not only as sensors for neuron activity but also to monitor the neuron response to a specific drug delivered by the probe.

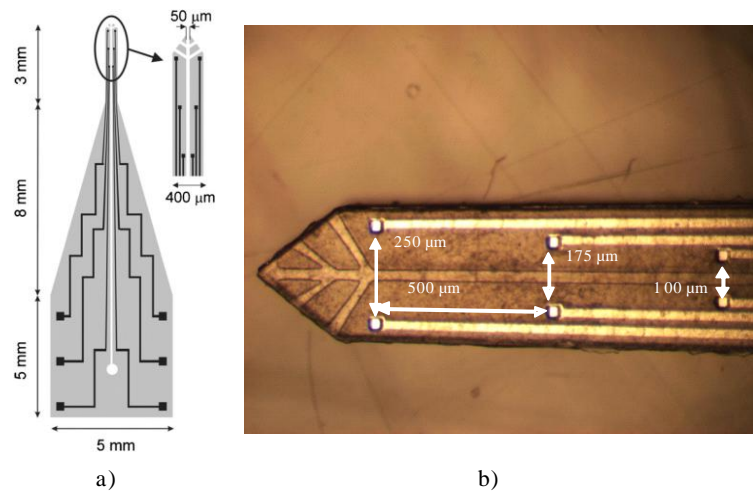


Figure 4.1 a) Schematic drawing of a SU-8 based microprobe and b) the close-up picture of a microprobe tip showing the electrode configuration

4.2 Fabrication

4.2.1 Fabrication procedure

The fabrication of the probes began with a temporary bonding of a thin Kapton™ film (125 μm) on top of a Pyrex substrate, figure 4.2 I)³. As mentioned in the previous chapter, Kapton™ was used because of its low adhesion to SU-8, allowing the release of the devices from the substrate when their fabrication was completed. Once the Kapton™ film was fixed to the substrate, a 70 μm thick SU-8 layer was deposited on top of it. The wafer was heated up to 65°C for 10 minutes and up to 95°C for 30 minutes to perform the soft bake. Then, another 70 μm thick SU-8 layer was spin coated and it was soft baked at 95°C for 90 minutes. It should be noted that these parameters were thoughtfully studied in order to obtain a flat SU-8 surface and could pattern the electrodes on top of it. Once the wafer cooled down, an exposure dose of 400J/cm² was given using a mask which defined the shape of the microprobe, figure 4.2 II). After the exposure, oxygen plasma treatment was applied on the SU-8 surface to improve the adhesion between the SU-8 and the metal. The metallization was performed by sputtering; thus, 50 nm of chromium and 150 nm of gold were deposited, figure 4.2 III). This process was performed alternating switch off and switch on steps in order to keep the temperature below 50°C and avoid cracking and further crosslinking of the un-exposed SU-8. After the sputtering, a slight post bake was performed at 50°C. This step was necessary for the alignment of the next lithography process, however, the duration was controlled for each case in order to prevent the already mentioned crosslinking. Chromium and gold were patterned using standard photolithography and wet chemical etching, figure 4.2 IV). As a result, the un-exposed SU-8 was protected by the chromium and gold layers from being crosslinked during the subsequent fabrication processes. As a next step, once oxygen plasma treatment was applied, 50 nm of titanium and 150 nm of platinum were deposited by

sputtering and patterned by a lift-off technique, figure 4.2 V) and VI). In this way, the electrodes were implemented on top of a patterned 180 μm thick structure, figure 4.2 VII). Then, the 20 μm thick SU-8 passivation layer, which defined the walls of the channel and covered the metallic tracks, was spun and patterned by standard photolithography, figure 4.2 VIII). At this point, chromium and gold were etched and all the un-exposed SU-8 was developed, figure 4.2 IX). The innovation of this fabrication procedure started when another Pyrex wafer with a Kapton™ film laminated on top was used for the creation of the microchannels. A new 20 μm thick layer of SU-8 was processed on top of the Kapton™ film in order to define the cover of the microchannels, figure 4.2 X). This layer included the holes to allow the electrical contact to electrodes and the fluidic connection to the microchannel. Once the processing of the two different substrates finished, they were ready to be bonded together to define a microchannel structure. First, the wafers were properly aligned and transferred to the bonding chamber. Misalignment between both wafers previous to the bonding was found to be in the order of 5 μm or less, since both wafers were transparent. Therefore, a proper alignment with an error much smaller than any of the probe dimensions was always achievable. Then, the chamber was evacuated to 10^{-3} mbar to remove air gaps between both wafers. Afterwards, the wafers were brought into contact, and temperature and pressure were applied, figure 4.2 XI)^{1,4,5}. Since the cover layer had been processed by photolithography, inlet and outlet ports were already defined. Finally, devices were manually released from the Kapton™ film, figure 4.2 XII). A picture of a complete microprobe can be observed in figure 4.3 a) and figure 4.3 b) shows a SEM picture of a microprobe tip.

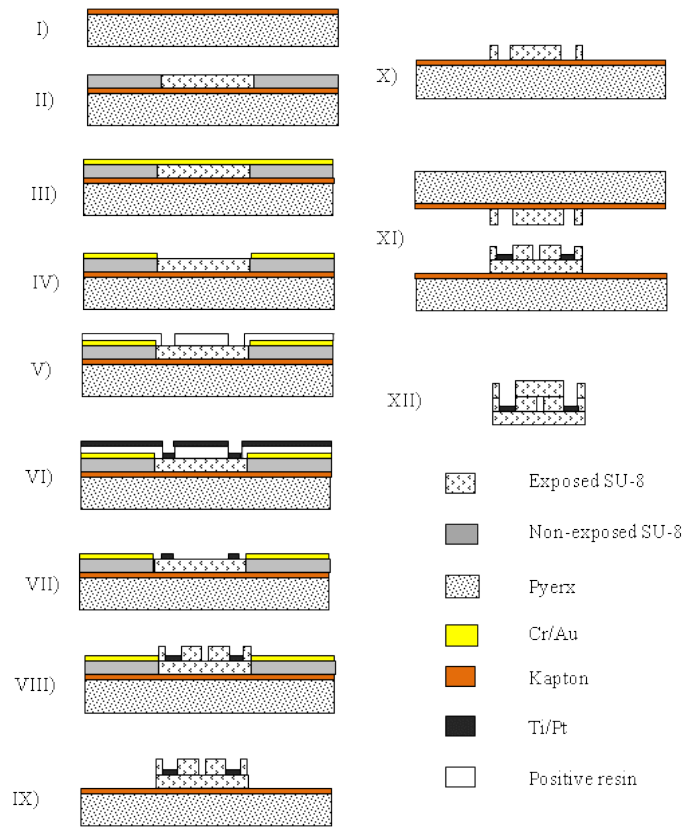


Figure 4.2 Schematic drawing of the fabrication procedure sequence

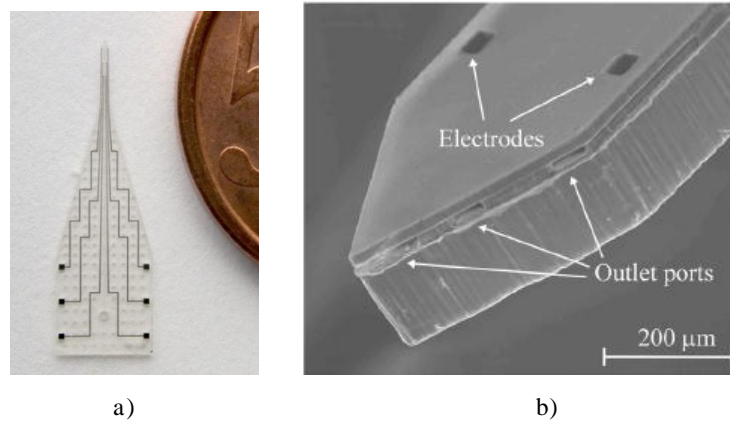


Figure 4.3 a) The top view picture of a finished microprobe next to a 5 euro cents coin and b) a SEM picture of a probe tip showing outlet ports.

4.2.2 Problems and solutions related to the fabrication procedure

4.2.2.1 Optimization of the bonding process

Creating a microchanell consists of getting a perfect adhesion between the floor, walls and cover. Moreover, any deformation have to be avoided in order to obtain a well-defined cavity. For such reasons, optimum bonding condition of temperature and pressure have to be found. In addition, the fabrication conditions of the sidewall and cover SU-8 layers need to be studied. As mentioned in the

state of art, both layers of SU-8 have to be partially crosslinked so that during the bonding process the chemical bonds that were initially free are then used to bond the two different SU-8 layers^{6,7,8}. In the first attempt to get a channel, the sidewall and the cover of the channel, which were 20 μm thick, were processed at 95°C and with a 140 mJ/cm^2 exposure dose. The first bonding attempt was carried out at 1 bar and 95°C. Once the bonding process finished and the Kapton™ film was removed, a low bonding yield was observed by a simple inspection using an optical microscope. At first, it was believed that the walls and the cover were not properly bonded. Then, a transversal cut was made on a probe and it was checked in the SEM to confirm the hypothesis. As seen in figure 4.4 a), the channel was perfectly created but there was a gap between the structural SU-8 layers and the passivation layer. Once the problem was identified, the UV exposure dose of the passivation layer was increased to improve its adhesion to the structural layer. This fact affected negatively to the bonding process because the passivation layer was too crosslinked in order to bond the cover layer. Several tests were performed applying different bonding pressure values from 1 bar up to 3 bar. Also, temperature was varied. Finally, the best results were obtained when both SU-8 layers were soft baked at 65°C and post baked at 50°C. The optimum UV exposure dose given to the sidewall layer was 200 mJ/cm^2 and the dose for the cover was 140 mJ/cm^2 . The bonding process was carried out at 3 bar and at 50°C. Thus, a good adhesion between all the SU-8 layers and a well-defined channel was achieved as shown in figure 4.4 b) .

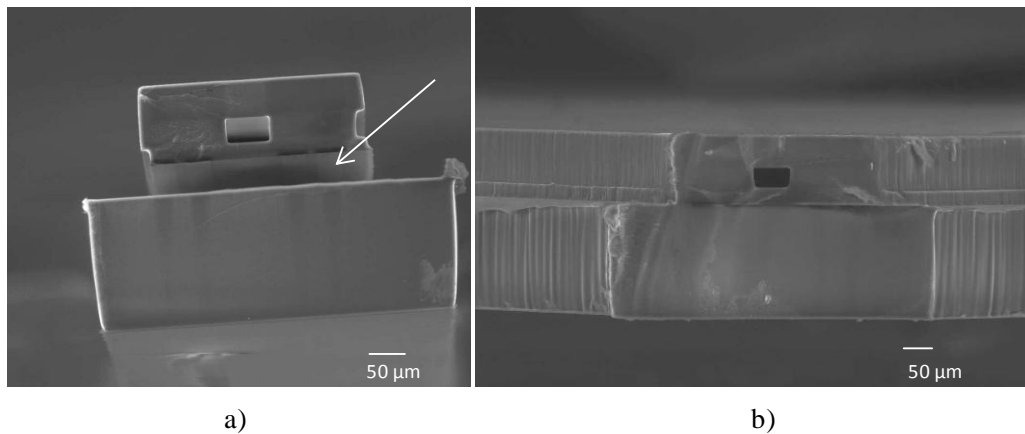


Figure 4.4 SEM pictures for the inspection of the microchannel: a) separation gap between the structural and passivation SU-8 layers (arrow) and b) a well-defined microchannel

4.2.2.2 Profile of the microprobe

The fabrication process described in the previous section solved the adhesion problems, however, microprobes with traces of SU-8 at the edges were obtained once they were peeled off from the Kapton™, figure 4.5 a). These traces were believed to be a drawback for the penetration of the probe into neural tissue because it was expected to cause an extra damage during the experimental trials. The

reasons of such an issue were the consecutive misalignments and as a result, the crosslinking of the probe edges. Briefly, there were slight misalignments during the photolithography processes and as a result the UV radiation reached areas that were not supposed to be exposed. Consequently, traces of SU-8 remained at the edges because they were partially crosslinked and were impossible to remove by standard development. Moreover, this issue got worse because an extra heating process was performed during the bonding. This caused the edges to become more crosslinked. As a consequence, the development was even more complicated. In order to eliminate the traces from the edges and obtain a smoother surface, the microprobes required an extra immersion on SU-8 developer once released from the substrate using an ultrasonic bath for 4-5 minutes. Thus, microprobes with a smooth and well-defined shape were obtained, figure 4.5 b).

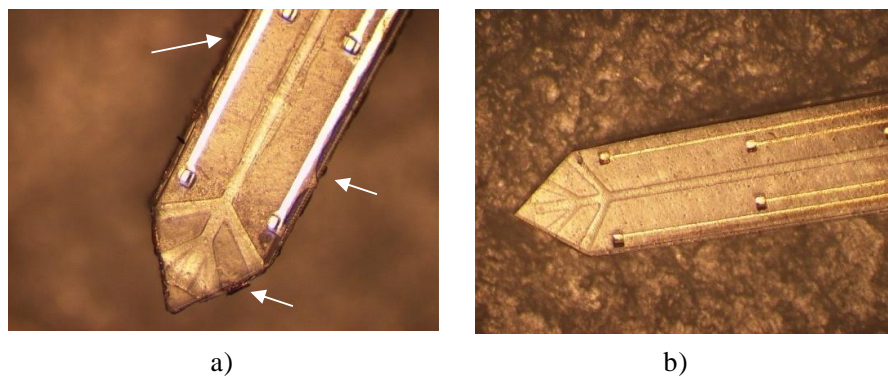


Figure 4.5 Microprobes appearance after the fabrication is completed: a) the non-developed SU-8 remains at the edges when the probe is developed in a conventional bath and b) there are no traces of SU-8 at the edges when the probe is developed by ultrasonics

4.3 Packaging

A special package was designed and fabricated in order to perform the characterization of the microprobes and obtain preliminary data from *in vitro* and short *in vivo* tests. In a brief view, the package consists of a deep red structure with the fluidic connection in the back side and electrical connections in the top side, figure 4.6 a). The dimensions of the main structure were set at 25 x 20 x 5 mm and it was fabricated by stereolithography technique. Stereolithography is the most widely used rapid prototyping technology. It can produce highly accurate and detailed polymer parts. It uses low-power and a high focused UV laser to trace out successive cross-sections of a three-dimensional object in a vat of liquid photosensitive polymer, figure 4.6 b). As the laser traces the layer, the polymer solidifies and the excess areas are left as liquid. When a layer is completed, a leveling blade is moved across the surface to smooth it before depositing the next layer. The platform is lowered by a distance equal to the layer thickness and a subsequent layer is formed on top of the previously completed layers. This process of tracing and smoothing is repeated until the build is complete. Once complete,

the part is elevated above the vat and drained. Excess polymer is swabbed or rinsed away from the surfaces. In many cases, a final cure is given by placing the part in a UV oven. After the final cure, supports are cut off the part and surfaces are polished, sanded or otherwise finished. Once the main piece is fabricated other components are fixed to complete the packaging. Figure 4.6 c) shows a schematic overview of the packaging developed for the housing of the probes. The fluidic connection between the outside world and the microprobe was performed by a channel placed in the top capsule. The use of cylindrical-shaped gaskets guaranteed a perfect sealing without leakage for pressures up to 4 bar. Finally, the 50 μm wide channel present in the microprobe allowed the fluidic delivery at the probe tip. The electric connection was made using spring contact pins installed in the top capsule. In order to prevent any undesired displacement, the bottom capsule included a pattern to fit the microprobe base. Once the probe was placed on the bottom packaging piece, two fixed slides were used to align both capsules, and four screws ensured a proper contact. In this way, electric and fluidic connections and mechanical fixation of the probe were automatically performed once the four screws had been fixed.

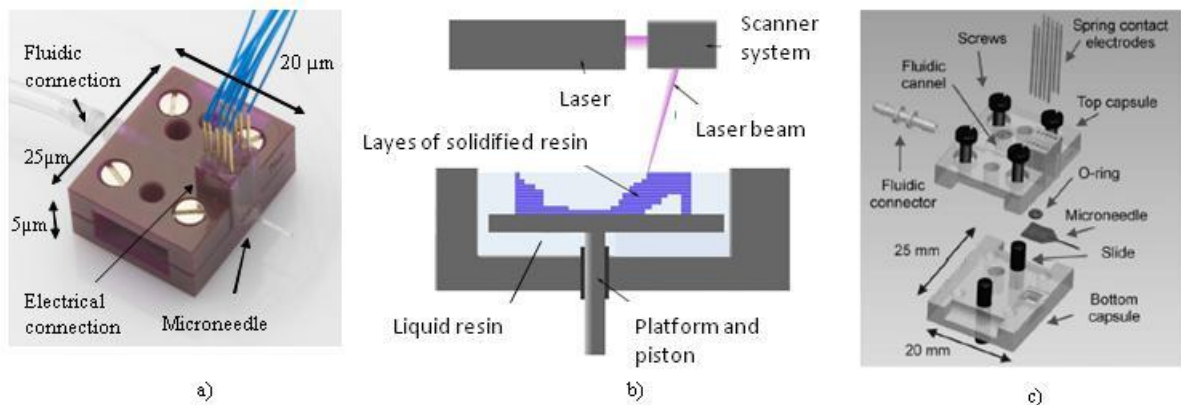


Figure 4.6 a) A picture of an encapsulated microprobe, b) schematic picture of the stereolithography technique and c) package drawing scheme

4.4 Characterization

4.4.1 Fluid delivery characterization

The flow rate as a function of applied pressure was measured for the SU-8 microprobes when they were immersed in two different environments: open air, figure 4.7 a), and agarose gel (0.6% weight/volume (w/v)). The agarose gel was selected since it mimics the pressure-driven flow in the brain tissue⁹. Both, brain tissue and agarose gel can be considered poroelastic materials. Although overall the brain is inhomogeneous and anisotropic in its composition, localized regions of grey matter can be largely homogeneous and isotropic like agarose gel. Furthermore, the homogeneity and isotropy of agarose gel makes it the most basic test bed with which to investigate CED¹⁰. The fluidic

setup for the characterization of the probes was composed of an EFD 1400 fluid dispensing system (<http://www.efd-inc.com/>), which was used to apply controlled pressure on the microprobe. Such system was directly connected to an ASL1600-10 mass flow sensor from Sensirion (<http://www.sensirion.com/>) in order to measure the flow. Finally, the fluidic circuit ended with the connection to the microprobe using the packaging described in section 4.3. As can be observed from figure 4.7 b), a linear relation between flow rate and pressure was obtained. As expected, higher fluidic resistance is observed when the probe was inserted in agarose. During this fluidic characterization, the SU-8 microprobes showed enough rigidity to penetrate the agarose gel without observing any deformation, and no rupture occurred after several trials.

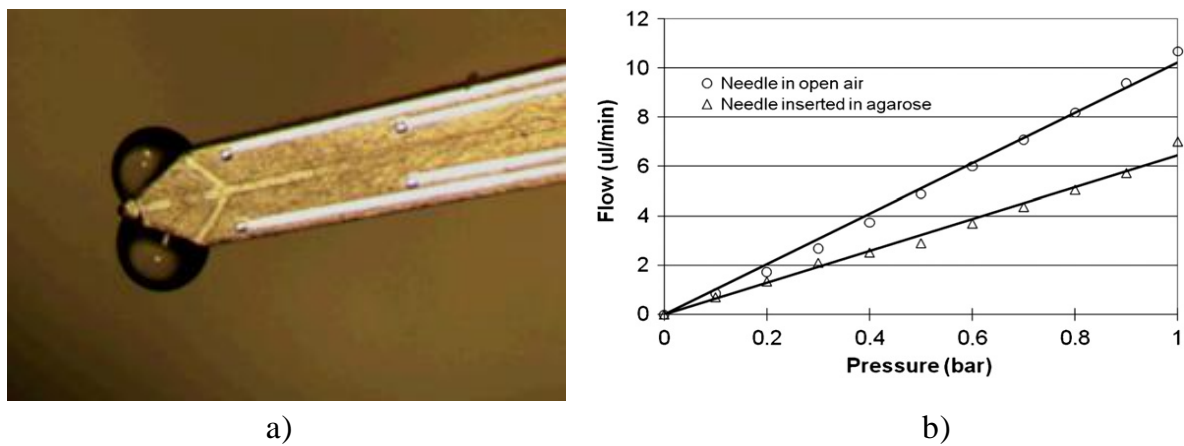


Figure 4.7 a) Water getting out from the lateral outputs and b) fluidic characterization of a microprobe in open air and inserted in agarose (0.6 % w/v)

4.4.2 Impedance monitoring while delivering in the agarose gel

In order to validate the electrodes placed at the probe tip, impedance measurements between two of them (the ones placed closest to the tip) were performed using an HP4284A LCR meter while delivering a saline solution (0.9% of NaCl) in the agarose gel (0.6% w/v). As reported in section 4.1, the electrodes had an area of $50 \times 50 \mu\text{m}^2$, and were separated by $250 \mu\text{m}$ from each other while the shortest distance to the outlet ports was $100 \mu\text{m}$. Impedance measurement results obtained at 1 MHz are presented in figure 4.8. As can be observed, a very stable impedance value was obtained when the microprobe was in open air (0–36 s). When the microprobe was introduced in the agarose gel, a sudden small decrease in impedance was observed (36 s). The impedance value between the electrodes was also found very stable when immersed in the agarose gel (36–75 s). After applying a $2 \mu\text{l}/\text{min}$ flow of a saline solution to the microprobe (75 s), a slow decay in impedance was observed (75–129 s) until a new stable value was reached (129 s). In this way, the absorption of the saline solution by the agarose gel was measured.

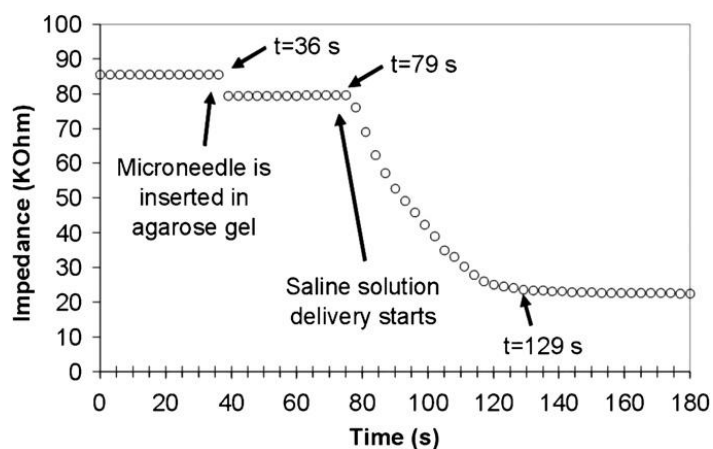


Figure 4.8 Monitoring of a SU-8 based microprobe by means of impedance measurements: $t=36$, the microprobe was inserted in the agarose gel (0.6% w/v), $t=79$ s, the saline solution delivery started with a flow rate of 2 $\mu\text{l}/\text{min}$.

4.5 Experimental procedures

4.5.1 Mechanical and fluidic capability evaluation of the SU-8 probes by means of ex vivo tests

A post-mortem experiment with a rat brain was done in order to analyze the probe's mechanical and microfluidic viability¹. Adult male Wistar rats (body weight 300–350 g) were obtained from the animal housing facilities of the School of Medicine (Universitat de Barcelona). They were kept on a 12h/12h day and night cycle, and housed with free access to food and water. Animals were manipulated according to the European legislation (86/609/EEC). All the efforts were made to minimize the number of animals used, and their suffering and procedures were approved by the Ethic Committee of the Universitat de Barcelona, under supervision of the Generalitat de Catalunya. The rats were anesthetized and decapitated. The brains were quickly removed and placed in an ice-cold glass dish to perform the experiment. Even though it is flexible, the SU-8 based microprobe was easily inserted into the parietal cortex in a perpendicular plane. To test the device as a drug delivery system, a 0.5% (w/v) solution of methylene blue in distilled water was used, which was injected at a fluid rate of about 0.5 $\mu\text{l}/\text{min}$. The solution was inserted by a microprobe installed in a stereotaxic instrument. A standard microinjection protocol was followed, i.e. after completion of the infusion, the probe was left in place for an additional 3 min to allow passive diffusion and to prevent the spread of the excitotoxin up the probe track upon removal; then, the probe was slowly retracted. As can be observed in figure 4.9 a), the solution was injected progressively without any relevant flow peaks. At the end of the insertion, a negative flow is observed around 90 s, meaning that some of the solution was retracted from the tissue through the microprobe. This is probably due to an excess of flow rate applied, which could have not been completely absorbed. The brains were frozen after the delivery with powdered

dry ice for further histological analysis. 20 μm coronal slices were obtained by microtomy at the level of the injection in order to analyze the probe placement and the blue of methylene dispersion in the brain, figure 4.9 b). This analysis showed that probe penetration depth was up to 3 mm, which means that the fluid solution was delivered to the V and VI layers of the cerebral cortex. The analysis also showed good probe performances with a dispersion of methylene blue in the internal layers of cerebral cortex and corpus callosum disruption as shown in figure 4.9 c).

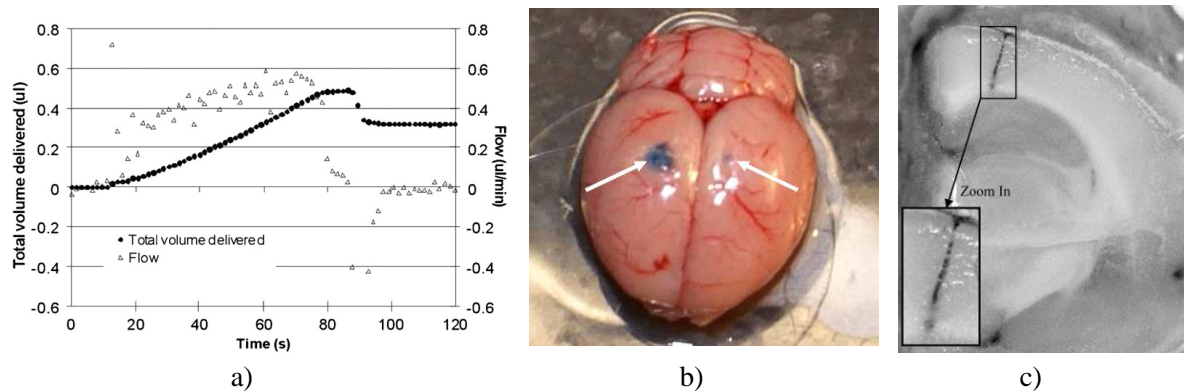


Figure 4.9 a) Flow and total volume of methylene blue delivered into the rat's brain by the first SU-8 probe prototype, b) external view of the brain after methylene blue delivery in both hemispheres. c) Blue staining in the prefrontal cortex clearly shows the methylene blue injection and diffusion with a corpus callosum disruption (arrow)

4.5.2 Evaluation of the damage evoked by the SU-8 probes by means of in vivo tests

During stereotaxic procedures, a small relative movement between the brain and the skull is possible and may result in small undetectable brain damage. Also, an accidental movement of the probe during the procedure cannot be discarded. In this test, it was tested whether the flexibility of an SU-8 probe constitutes an advantage comparing with other probes made from any rigid material. It was evaluated the mechanical damage produced by the SU-8 probe in a rat's brain during its insertion, and a comparison with a stereotaxic standard probe was performed. Under equithesin anesthesia (a mixture of chloral hydrate and sodium pentobarbital; 0.3 ml/100 g body weight, intraperitoneally), rats were placed in a stereotaxic instrument (David Kopf, Carnegie Medicin, Sweden) with the incisor bar set at -3.3 mm. After opening of the head skin with a scalpel, the skull was drilled and the dura mater broken. Probes were then introduced in the rat's dorsal hippocampus. The stereotaxic coordinates were 3.3 mm caudal to bregma, 2.2 mm lateral to bregma and 2.9 mm ventral from dura mater, according to the Atlas of Paxinos and Watson¹¹. The SU-8 microprobe was inserted into the right hemisphere, and stereotaxic standard probe (0.28 mm external diameter) was inserted into the left one. The probes were moved ± 1 mm caudal from the initial point (in the perpendicular plane with respect to the probe direction), and then slowly retracted. Twenty-four hours later, the rats were anesthetized and

sacrificed. The brains were removed, frozen with powdered dry ice and stored at -80 °C. Adjacent coronal 14 µm sections from the whole hippocampus were obtained from all brains and mounted on slides. Standard Nissl staining was performed to evaluate the neuronal loss and the morphometry of cerebral cortex and hippocampus. Microglial cells were identified by histochemical procedures using Isolectin B4 (IB4), a Griffonia Simplicifolia extract that binds to microglial galactose-containing glycoconjugates. IB4 is used conjugated with biotin, and detected by the biotin-avidin-peroxidase method. Briefly, sections were incubated overnight at 4 °C with IB4 (Sigma, St Louis, MO) diluted 1:25 in normal goat serum, that is, 1:100 volume/volume (v/v) in 0.01 M PBS; pH 7.4. After incubation with ExtrAvidin (1:250; Sigma, St Louis, MO), sections were developed in a 0.05 M Tris solution containing 0.03% (w/v) diaminobenzidine (DAB) and 0.006% v/v H₂O₂. Nissl staining was used to assess neuronal injury in terms of area of neuronal loss evidenced by a lack of staining, figures 4.10 (i) and (ii). No significant neuronal loss was detected in the dorsal hippocampus after the movement of the probes. Still, this mechanical movement showed a small area of cellular loss in the case of SU-8 probe insertion evidenced in the cerebral cortex as a small area of reduction of staining figure 4.10 (ii). However, this area of decreased staining was much larger for the case of the insertion made by the standard probe, figure 4.10 (i). IB4 histochemistry was performed in order to stain the area of inflammation mediated by a microglial reaction, which was evidenced as an increasing of staining. IB4 histochemistry evidenced a larger area of inflammation associated with microglial reactivity in response to the standard probe movement, figure 4.10 (iii), when compared with the SU-8 one, figure 4.10 (iv). Thus, it can be summarized that due to its flexibility, the tissular injury caused by the SU-8 probe was lower than the one caused by standard probes currently used in stereotaxia procedures.

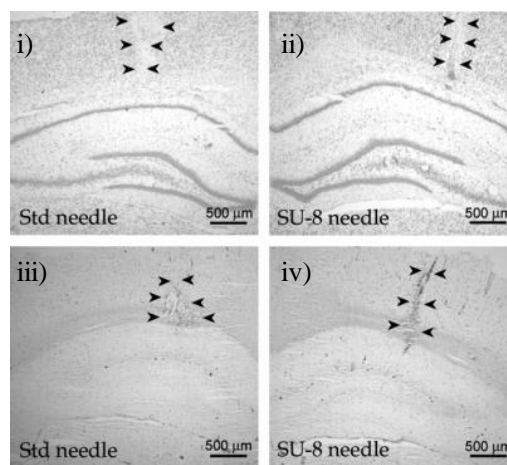


Figure 4.10 Cresyl-violet staining of the brain sections: i) stereotaxic standard probe injection and ii) SU-8 probe. IB4 histochemistry showed the area of microglial reaction associated with the lesion: iii) standard probe injection and iv) SU-8 probe. The areas of lesion and microglial reaction are delimited by arrow heads.

4.6 Conclusions

As a first conclusion, it can be considered the design of the microprobe being suitable because both, the electrodes and the microchannel, were successfully integrated into the SU-8 device. Bonding process had to be optimized because at first the SU-8 layers were delaminated. The combination of appropriate SU-8 layers crosslinking state and, pressure and temperature optimized values was the key to create a well-defined channel. Working at low temperature and specific pressure (50 °C and 3 bar) avoided the deformation of the walls. A dedicated package was also designed and fabricated to allow a robust fluidic and electrical connection. *Ex vivo* and *in vivo* tests showed the viability of the SU-8 based first microprobe prototype. In general terms, it was observed an optimal electric and fluidic functionality of the probe. As an additional promising feature, it was demonstrated by means of *in vivo* tests a decrease in the damage evoked into the brain compared with conventional probes. This fact made us continue developing the technology of the SU-8 and microfabrication techniques to obtain functional microprobes for several applications in the neuroscience field.

4.7 References

- ¹Fernández, L.J., Altuna, A., Tijero, M., Gabriel, G., Villa, R., Rodríguez, M.J., Batlle, M., Vilares, R., Berganzo, J., Blanco, F.J. Study of functional viability of SU-8-based microprobes for neural applications (2009) *Journal of Micromechanics and Microengineering*, 19 (2), art. no. 025007
- ²Papageorgiou, D.P., Shore, S.E., Bledsoe Jr., S.C., Wise, K.D. A shuttered neural probe with on-chip flowmeters for chronic in vivo drug delivery (2006) *Journal of Microelectromechanical Systems*, 15 (4), pp. 1025-1033
- ³Agirregabiria, M., Blanco, F.J., Berganzo, J., Arroyo, M.T., Fullaondo, A., Mayora, K., Ruano-López, J.M. Fabrication of SU-8 multilayer microstructures based on successive CMOS compatible adhesive bonding and releasing steps (2005) *Lab on a Chip - Miniaturisation for Chemistry and Biology*, 5 (5), pp. 545-552
- ⁴Arroyo, M.T., Fernández, L.J., Agirregabiria, M., Ibáñez, N., Aurrekoetxea, J., Blanco, F.J. Novel all-polymer microfluidic devices monolithically integrated within metallic electrodes for SDS-CGE of proteins (2007) *Journal of Micromechanics and Microengineering*, 17 (7), art. no. 011, pp. 1289-1298
- ⁵Blanco, F.J., Agirregabiria, M., Garcia, J., Berganzo, J., Tijero, M., Arroyo, M.T., Ruano, J.M., Aramburu, I., Mayora, K. Novel three-dimensional embedded SU-8 microchannels fabricated using a low temperature full wafer adhesive bonding (2004) *Journal of Micromechanics and Microengineering*, 14 (7), pp. 1047-1056
- ⁶Blanco, F.J., Agirregabiria, M., Garcia, J., Berganzo, J., Tijero, M., Arroyo, M.T., Ruano, J.M., Aramburu, I., Mayora, K. Novel three-dimensional embedded SU-8 microchannels fabricated using a low temperature full wafer adhesive bonding (2004) *Journal of Micromechanics and Microengineering*, 14 (7), pp. 1047-1056
- ⁷Arroyo, M.T., Fernández, L.J., Agirregabiria, M., Ibáñez, N., Aurrekoetxea, J., Blanco, F.J. Novel all-polymer microfluidic devices monolithically integrated within metallic electrodes for SDS-CGE of proteins (2007) *Journal of Micromechanics and Microengineering*, 17 (7), art. no. 011, pp. 1289-1298
- ⁸Agirregabiria, M., Blanco, F.J., Berganzo, J., Arroyo, M.T., Fullaondo, A., Mayora, K., Ruano-López, J.M. Fabrication of SU-8 multilayer microstructures based on successive CMOS compatible adhesive bonding and releasing steps (2005) *Lab on a Chip - Miniaturisation for Chemistry and Biology*, 5 (5), pp. 545-552
- ⁹Hall, W.A., Rustamzadeh, E., Asher, A.L. Convection-enhanced delivery in clinical trials. (2003) *Neurosurgical focus [electronic resource]*, 14 (2),

¹⁰Dawe B. and Erickson T. Convection-enhanced delivery into agarose gel brain tissue phantoms (2008)

Journal of young investigators, 18 (6)

¹¹Paxinos G and Watson C *The rat brain in stereotaxic coordinates-The New Coronal Set*

(Amsterdam: Elsevier) 2004

5. SECOND SU-8 MICROPROBE PROTOTYPE FOR NEURAL ACTIVITY RECORDING

This chapter presents the development of a new generation of SU-8 probes for neural activity recording. The distinctive features of the design are the dimensions of the probe and the configuration of the sensing site. Few centimeters long and near a hundred of micrometers wide probes were designed in order to reduce tissue damage during experimentation. Moreover, a tetrode-like sensing configuration was selected to discriminate independently firing neurons. Three fabrication procedures were developed modifying the microfabrication techniques each time. Finally, a flat, robust and highly functional microprobe was obtained. The most critical parameter was the gap introduced by the thickness of the passivation layer. As it is well known, a close contact between the electrode and the tissue is essential to record action potentials with accuracy. Hence, a microprobe with the electrodes at the probe surface level was developed. In order to test the capability of the probe, a dedicated printed circuit board (PCB) was designed and fabricated for its proper encapsulation. Once the probe was fixed to the PCB the electrical behavior of the tetrode was tested by impedance spectroscopy; thus, making a prediction of further measurements in neural tissue. In addition, some attempts of platinum black and carbon nanotubes deposition were carried out to reduce electrode-electrolyte impedance and, consequently, improve the sensing capability of the electrodes. Finally, extracellular spontaneous signals were recorded from rat's hippocampus by means of *in vitro* and *in vivo* experimental procedures. Technological advances represented in each consecutive probe demonstrated each time action potentials with higher peak-to-peak amplitudes and a lower noise level. Moreover, different amplitude and shape of action potentials recorded from all the four recording sites suggested improved capability of the tetrode to distinguish different neuronal sources.

Contents

5. SECOND SU-8 MICROPROBE PROTOTYPE FOR NEURAL ACTIVITY RECORDING	73
5.1 BACKGROUND	74
5.1.1 Neuron- electrode interface	74
5.1.2 In vitro and in vivo neural recording procedures	76
5.2 DESIGN	78
5.3 FABRICATION	79
5.3.1 First fabrication procedure: 20 μm embedded electrodes	79
5.3.2 Achievements, problems and solutions related to the first fabrication procedure....	81
5.3.3 Experimental limitations related to the first fabrication procedure	83
5.3.4 Second fabrication procedure:electrodes 2-3 μm embedded into a layered probe ...	89
5.3.5 New concepts on the fabrication sequence.....	91
5.3.6 Third fabrication procedure: electrodes at the probe surface level.....	92
5.3.7 Achievements related to the third fabrication procedure	94
5.3.8 Resume of the most relevant features of the first, second and third fabrication procedures	96
5.4 PACKAGING	97
5.5 CHARACTERIZATION OF THE SENSING SITES	97
5.5.1 Impedance spectroscopy.....	97
5.5.2 Platinum black electrochemical deposition	99
5.5.3 Single walled carbon nanotubes (SWNTs) coating.....	100
5.6 EXPERIMENTAL PROCEDURES: EXTRACELLULAR NEURAL ACTIVITY RECORDING.....	102
5.6.1 In vitro tests.....	102
5.6.2 In vivo tests	104
5.7 CONCLUSIONS	105
5.8 REFERENCES.....	107

5.1 Background

5.1.1 Neuron- electrode interface

The recording of extracellular action potentials generated by isolated neurons within groups of cell assemblies is one of the principal techniques for studying the central nervous system. This technique has provided much information about neural architecture and the functional relationship associated with the sensory and motor areas of the brain. Progress in understanding neural signal processing has been impaired significantly by the lack of adequate electrodes and instrumentation for multichannel data acquisition¹.

The efficacy of any electrical device for the stimulation or recording of the neural tissue is ultimately determined by the quality of neuron-electrode interface. Although the material of the device is being optimized with materials such as polymers, the final contact between the brain tissue and the amplifiers is still a metal surface in all the cases. When metal microelectrodes are immersed in a conducting medium, then electrochemical reactions occur at the interface between the solid microelectrodes and the electrolyte². The circuit model for the metal-electrolyte interface has already

been developed, including the interfacial capacitance (C_i), the charge transfer resistance (R_t), the diffusion-related Warburg elements (R_w and C_w) and the solution resistance (R_s)^{3,4}. Although parameters in the model are related to some physical properties, they can be scaled with frequency and electrode area. The impedances scaling with the frequency (f), the surface area (A_s) and the geometric area (A_G) are in equations (1) to (4), where k is a constant determined by the electrochemistry and ion mobility. Also, these impedances are schematically represented in figure 5.1.

$$|Z_{C_i}| = \frac{k}{fA_s} \quad (4)$$

$$|Z_{R_t}| = \frac{k}{fA_s} \quad (5)$$

$$|Z_{W}| = \frac{k}{A_s\sqrt{f}} \quad (6)$$

$$|Z_{R_s}| = \frac{k}{\sqrt{A_G}\sqrt{f}} \quad (7)$$

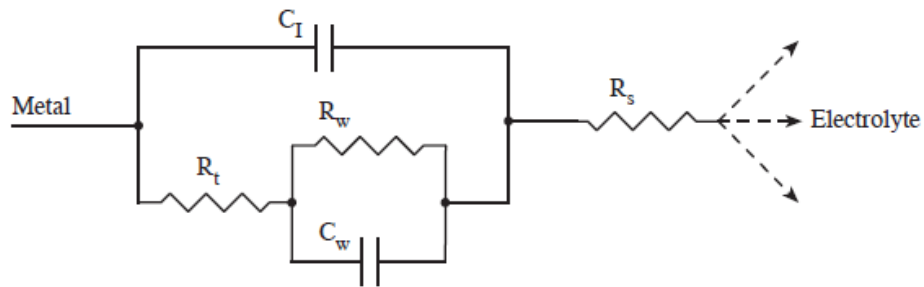


Figure 5.1 Circuit model for the metal-electrolyte interface including the interfacial capacitance (C_i), charge transfer resistance (R_t), diffusion-related Warburg elements (R_w and C_w), and the solution resistance (R_s).

The ability to record action potentials from individual neurons is mainly dependent on a trade off between the area of the recording site, and the impedance between the neuron and the electrode, often referred to as the trade off between selectivity and sensitivity^{4,5,6}. A recording site with small geometric area is required to isolate action potential of an individual neuron from more distant neural sources. Unfortunately, decreasing the geometric area of a recording site causes an increase in the impedance of the recording site. Also, the electrode area acts like a low-value capacitor in series with the electrical resistance of the immediately surrounding. As a result, a high-impedance value is obtained which is associated with noise.

As with most circuit elements, there is an intrinsic noise related to the metal-electrolyte interface. This noise has been empirically shown to be thermal⁷, following the standard Johnson noise equation for the rms voltage noise resistor:

$$V_{rms\ noise} = \sqrt{4kTR_N\Delta f} \quad (8)$$

Where k is Boltzmann's constant ($1.38 \times 10^{-23} \text{ J/K}$), T is the absolute temperature in Kelvin, R_N is the real part of the electrode impedance in ohms, and Δf is the bandwidth of interest.

High source impedance is also associated with a propensity to pick up extraneous noise by inductive and capacitive coupling of signals from other electromagnetic sources⁸. When noise is superimposed on the bioelectric potentials (on the order of microvolts), it confounds their interpretation, particularly in the common application of discriminating similar waveforms generated by action potentials from several different neurons near a given microelectrode tip. Improvements in amplifier technology have greatly reduced the noise that their electronics add to the input signal⁹, so that noise associated with the microelectrode itself is often the limiting factor in the overall signal-to-noise ratio, figure 5.2.

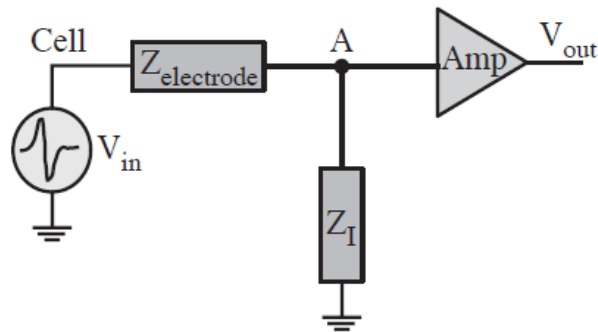


Figure 5.2 Common circuits for recording electrical activity (action potentials) from living cells. The action potential (V_{in}) signal is attenuated by the voltage divider created by the electrode impedance ($Z_{electrode}$) and the amplifier circuit input impedance (Z_I). Thus, reduction of $Z_{electrode}$ results in less signal loss.

5.1.2 *In vitro* and *in vivo* neural recording procedures

There are several methods used in animal studies to understand the electrical function of neurons in the central nervous system. In this section *in vitro* and *in vivo* testing procedures are explained because both of them have been used in order to test the functionality of the SU-8 probes developed in this chapter.

MacIlwain first discovered that if a brain is rapidly removed from the skull and rapidly cooled, a slice of brain tissue could survive for many hours in the proper organ culture environment *in vitro*¹⁰. The process starts with a rapid removal of the brain from the skull and placed in ice-cold saline or cerebrospinal fluid (ACSF) saturated with carbogen (95% O_2 , 5% CO_2) gas. Using either vibrating microtome or tissue chopper, a thin (usually 100-400 μm) slice of fresh brain is cut through the area of interest. This slice is rapidly placed in cold carbongenated ACSF and transferred to a slice recording chamber containing ACSF. Recording is usually performed after 1-2 hr of incubation to allow recovery from the impact of the surgery. The chambers have the ability to continuously perfuse the

slice with fresh ACSF and to add drugs to the ACSF perfusate at known concentrations. The two most common *in vitro* techniques are:

- (i) Submerged slices: the tissue is fully submerged in the bath with continuous superfusion
- (ii) “Interface” slices: the bath fluid extends just to the upper surface of the tissue

During the experiments, the temperature is maintained in the physiological range (37 C). Such conditions keep the brain-slice viable for neuron survival, induce normal neuronal activity and allow excellent electrophysiological recordings for 12 hours or more. Figure 5.3 shows a real *in vitro* test using the microprobes developed in this chapter. In our case the “interface” technique was used.

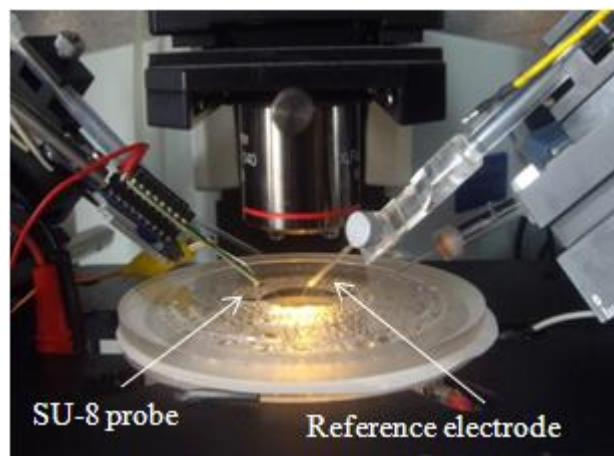


Figure 5.3 *In vitro* testing using SU-8 microprobes

Additionally, brain regions or neurons in their intact state with its normal complement of inputs and targets in their milieu of circulating hormones and factors can be studied by means of *in vivo* studies. The cells being studied usually have not been severed or damaged as can happen in the case of slice studies. Furthermore, the neurons have developed normally in the intact organism, in contrast to the culture preparation. These considerations lead additional credibility and fewer caveats to results concerning neuronal activity *in vivo*.

In vivo experimental procedures are usually performed as follows. First, the animal is anesthetized, most commonly with a barbiture, urethane, chloralose or halothane. The animal is then placed in a stereotaxic instrument which places the skull in the exact position and orientation with respect to submillimeter scale in three dimensions on the instrument. By positioning the microelectrode tip at desired coordinate along these scales determined by reference to a stereotaxic atlas of the brain of that species, any site within the brain can be found and cellular activity recorded. In extracellular recordings, the tip of the microelectrode is positioned immediately adjacent to, but outside of, a neuron. When in close proximity to the neuron, current fields generated by action potentials in that cell are ideally detected. The advantage of *in vivo* electrophysiology compared to the *in vitro* methods is

obviously due to the more intact preparation *in vivo*. Figure 5.4 shows a real *in vivo* test using the probes developed in this chapter.



Figure 5.4 *In vivo* testing using SU-8 microprobes

5.2 Design

The design of the microprobe was divided into three different sections such as the insertion area, body and connection head as shown in figure 5.5 a)¹¹. The insertion area was designed 180 μm long since the tip needs to be inserted into the tissue to a depth of about 100-150 μm . In order to ensure a good penetration, a sharp tip was designed, figure 5.5b). In addition, the insertion area thickness was fixed at 30 μm to minimize the damage caused to the tissue, and also to avoid a dragging effect on the tissue slice during the experimental application. In order to measure the activity from small neuronal ensembles, which is the main objective of this application, the electrode diameter was set at 20 μm , quite comparable to a neuron size. The electrodes were configured as a tetrode, figure 5.5 b); thus, an 80 μm wide probe was designed in order to fit the electrodes at the tip. The tetrode configuration was chosen because it is considered to contribute to neurons discrimination¹². In many situations, two different neurons generate action potentials having very similar shapes in the recorded waveform. When four recording electrodes are used, pairs of cells are less likely to be equidistant from all the electrodes. Under the assumption that the extracellular space is electrically homogeneous, four electrodes provide the minimal number necessary to identify the spatial position of a source based only on the relative spike amplitudes on different electrodes. Among other dimensions, the width of the microprobe body was designed to increase from 80 μm to 1 mm gradually along its length, the thickness being kept at 100 μm to make the probe mechanically stronger. In order to test different probe sizes in the experimental applications, 2 and 3 cm body lengths were designed. Finally, the connection head dimensions (6.4 mm long, 3.8 mm wide and 100 μm thick) were established in order to make the probe easy to handle and package. This is the area where the external contact pads were

located. There were four 1.7 mm long and 0.6 mm wide contact pads. These dimensions were fixed to guarantee an easy connection of the probe to the PCB.

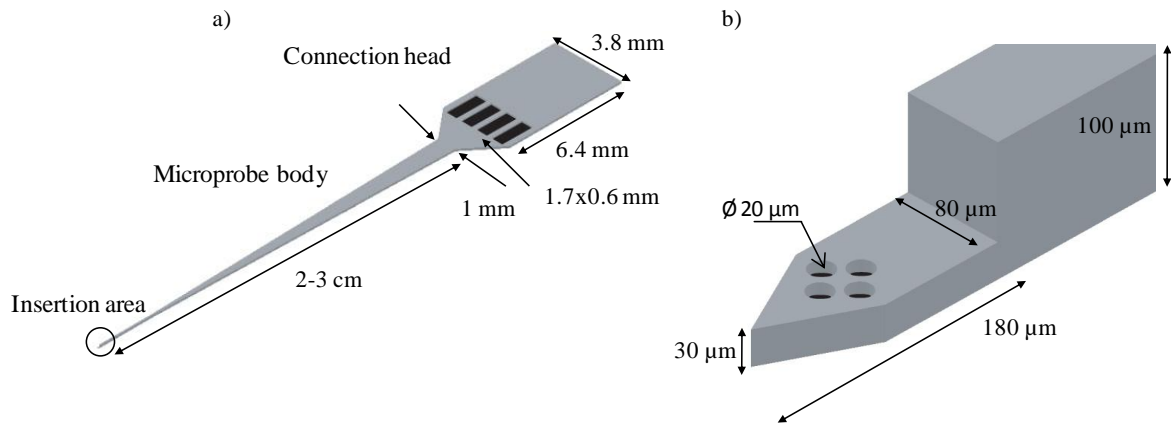


Figure 5.5 a) Schematic drawing of the microprobe and b) schematic drawing of the tip

5.3 Fabrication

Three fabrication procedures are explained in the following sections. The three of them are based on the initial design but as long as drawbacks in the experimental tests appeared the fabrication procedures were optimized. Finally, advances made in the fabrication techniques and the exhaustive inspections of the experimental results were the key to create the ideal SU-8 microprobe.

5.3.1 First fabrication procedure: 20 μm embedded electrodes

The fabrication of the microprobe started with an aluminum deposition on a silicon wafer by sputtering, as shown in figure 5.6 I)¹¹. This is the sacrificial layer that replaces the Kapton™ film used in previous fabrication procedures to release the probes from the substrate. A chemical release was used instead of the mechanical release in order to avoid damages in the probes. On the aluminum, a 10 μm thick SU-8 layer was spun and soft baked, heated up to 65 °C for 2 minutes and up to 95 °C for 7 minutes. Then, a UV dose of a 140 mJ/cm² was given by standard photolithography, and finally a post bake for 2 minutes at 65 °C and 4 minutes at 95 °C was applied. Once the shape of the probe was defined, figure 5.6 II), chromium (50 nm) and gold (150 nm) layers were deposited by sputtering, figure 5.6 III). In order to define the electrodes, the resin S1818 was patterned, figure 5.6 IV). This layer was used as a mask for gold and chromium patterning by wet chemical etching, figure 5.6 V). Then, the resin covering the electrodes was removed with methanol, figure 5.6 VI), and a 20 μm thick SU-8 passivation layer was spin coated to cover the metallic tracks and open the sensing areas, figure 5.6 VII). It was soft baked heating up to 65°C for 2 minutes and up to 95°C for 7 minutes, a 140 mJ/cm² dose was given and it was post baked heating up 65°C for 2 minutes and up to 95°C for 4

minutes. On top of that, a 70 μm thick SU-8 layer was processed in order to increase the thickness of the probe at its “body” area, and obtain a robust device. The wafer was heated up to 65 $^{\circ}\text{C}$ for 10 minutes and up to 95 $^{\circ}\text{C}$ for 30 minutes as a soft bake, figure 5.6 VII). Next, an UV dose of a 140 mJ/cm^2 was applied and a post bake of 2 minutes at 65 $^{\circ}\text{C}$ and 4 minutes at 95 $^{\circ}\text{C}$ was performed. Once the last two SU-8 layers were developed, figure 5.6 VIII), the microprobes were released from the silicon wafer by introducing the wafer in a phosphoric acid solution, figure 5.6 IX). The phosphoric acid etched the aluminum and the probes were separated from the wafer. Just after that, each probe was individually rinsed with water and isopropanol. A SEM picture of the tip of a typical microprobe and microprobes with different lengths can be observed in figure 5.7 a) and b) respectively.

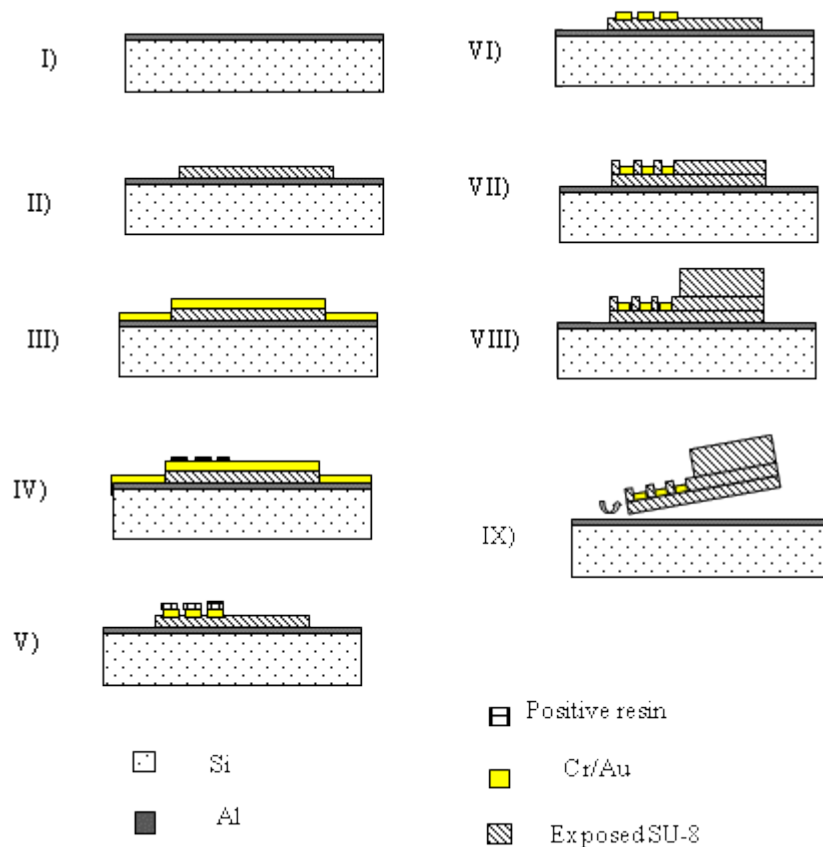


Figure 5.6 Schematic drawing of the first fabrication procedure sequence

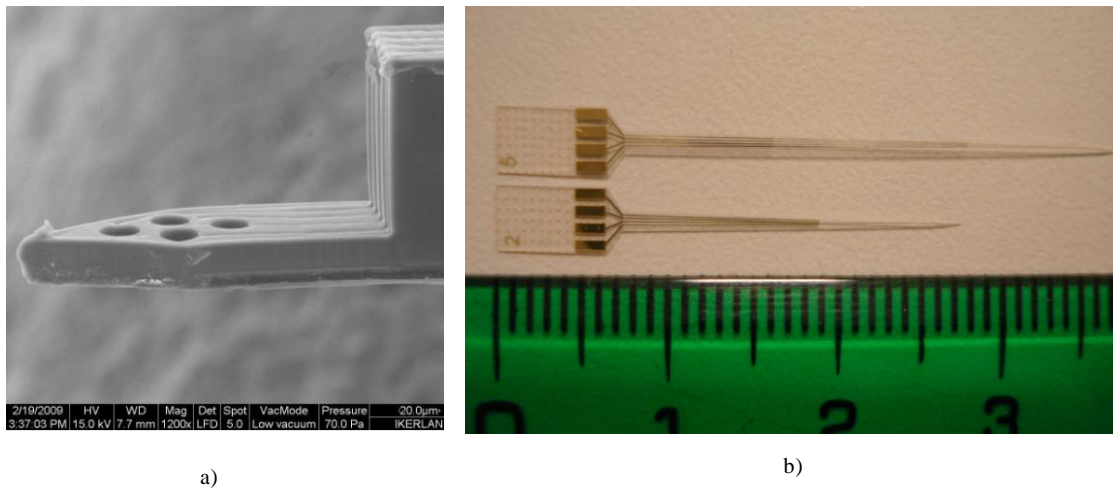


Figure 5.7 a) A SEM picture of the SU-8 microprobe tip with the electrodes 20 μm embedded and b) microprobes of different lengths

5.3.2 Achievements, problems and solutions related to the first fabrication procedure

The dimensions of the current probe were considerably smaller comparing to the dimensions of the probe described in Chapter 4. Therefore, many fabrication processes were modified in order to obtain thinner and narrower devices.

5.3.2.1 Electrodes patterning

The patterning of the electrodes turned out to be a critical step because narrow figures had to be defined. The photolithography process of the structural resin was optimized to create 3.5 μm wide tracks (the narrowest dimension required) on top of a discontinuous 10 μm thick SU-8 layer. As explained in the previous section, the electrodes were patterned on top of a developed SU-8 layer. There were two types of irregularity: a slight increase of height at the edges of each probe (figure 5.6 III)) and the typical edge bead in the wafer¹³. These two facts made difficult the patterning of the sacrificial resin. Moreover, the conventional wet etching process was slightly modified in order to avoid underetching.

The photoresin S1818 was chosen to pattern the electrodes because it was already reported its potential as a structural material¹⁴. The thickness of the S1818 resulted in 1.8 μm once it was spin coated. It was considered low enough in order to obtain a high resolution of the patterning. First, some experiments were carried out varying the soft bake conditions and the exposure dose given to the S1818. It is believed that increasing the duration of the SB at a certain temperature, improves the resolution of the patterning. The soft bakes were performed on a hot plate at 90°C (between 5 and 30 minutes) or applying infra red light (between 3 and 6 minutes), and the exposure dose was varied between 200 and 600 mJ/cm^2 . As shown in figure 5.8 a), the narrowest lines were not properly defined. As an additional step, a primer was used before the S1818 being spin coated. The use of the

primer improved the definition of the most critical figures. Finally, the primer and the resin were soft baked for 20 minutes at 90°C on the hot plate and 600 mJ/cm² UV dose was given. In this way, well-defined tracks were obtained as seen in figure 5.8 b).

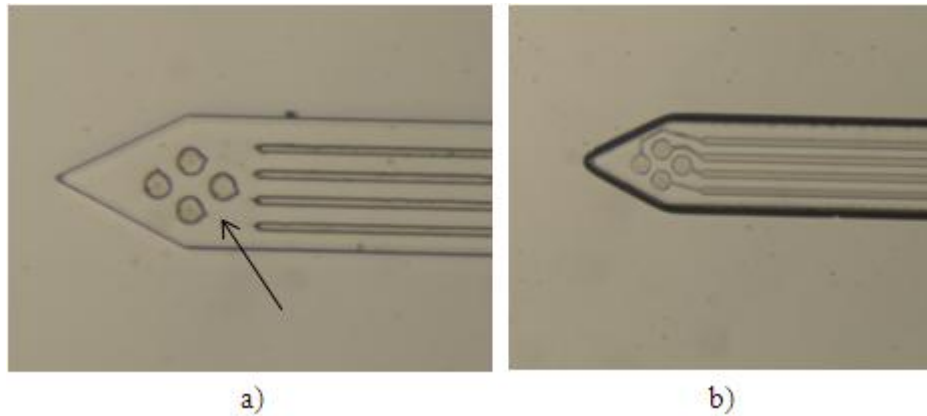


Figure 5.8 a) Poor resolution of the resin S1818 (arrow) and b) good resolution of the resin S1818.

However, rests of the resin remain at the edges of the probe due to the irregularity of the surface

However, although a suitable patterning was obtained using S1818, the wet chemical etching step was critical because of the underetching issue. The composition of the etchants was the following one: chromium etchant was based on a nitric acid and ceric ammonium nitrate mixture (commercial product) and the gold etchant was a homemade mixture of iodine (5%), potassium iodide (10%) and deionized water (85%). At first, both wet etchings were carried out immersing the wafer in the etchants for 15 seconds and rinsing the wafer as many times as necessary until the metallic patterning appeared. In this way, there was gold underetching as seen in figure 5.9 a). Shorter etching cycles were tested and the concentration of the etchant was varied but did not work. Finally, the gold etching process was carried out in a spinner controlling the revolutions and the duration of the process. The gold etchant was spun at 3500 r.p.m. for 30 seconds and, as a result, the underetching was avoided, figure 5.9 b).

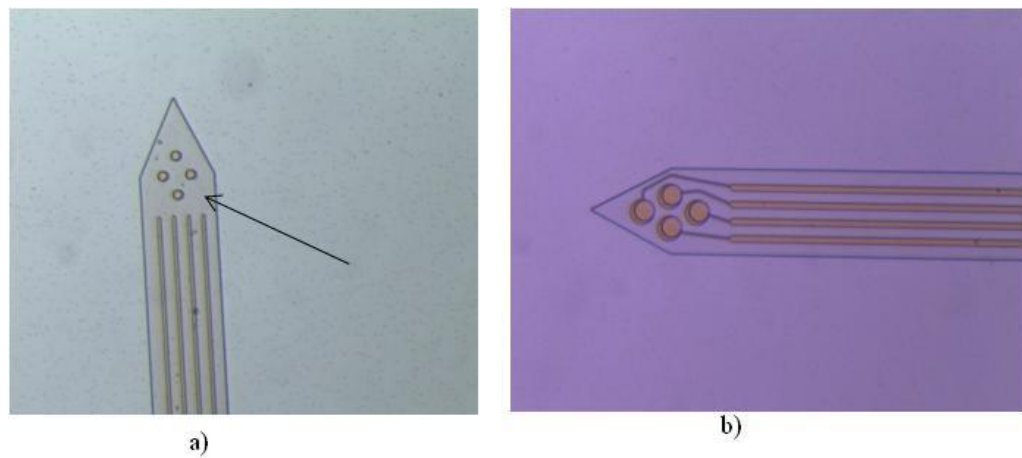


Figure 5.9 a) The underetching of 3.5 μm thick structures (arrow) following the conventional wet etching process and b) well-defined metallic tracks after etching the gold in the spinner.

5.3.2.2 Release process

Another challenge was to separate such a long, narrow and thin device from the wafer. The probes described in Chapter 4 were processed on a Kapton™ film, hence, they were easily peeled off from the substrate. Nevertheless, the mechanical release was not viable in this case because the probes tended to break during their detachment. A chemical release was chosen to replace the mechanical method. Phosphoric acid solution was used to etch the aluminium film and thus, liberate the devices. In this way, the probes were released on their own, without applying any external force. Additionally, the phosphoric solution did not damage the SU-8, chromium or gold present on the probe.

5.3.3 Experimental limitations related to the first fabrication procedure

Once the probes were fabricated and encapsulated (explained in section 5.4), several coatings were performed on top of the electrodes in order to improve their sensing capability (more information in section 5.5.3). Just after that, the probes were *in vitro* tested in brain slices and first limitations with reference to the design and fabrication procedure emerged.

5.3.3.1 Passivation layer thickness

There was a gap of 20 μm between the electrodes and outside determined by the thickness of the passivation layer. This thickness resulted to be too high and two limitations were detected. The first one is related to the *in vitro* experimental results obtained with these probes. They were inserted in brain slices and it was concluded that the neuronal tissue was too far from the sensing area in order to have a good electrode-neuron contact. As a result, action potentials with high amplitudes were not detected (explained in section 5.6.1). The second limitation was associated with the single wall nanotubes (SWNTs) coating (more detailed explanation in section 5.5.3). Basically, during the

SWNTs coating there were two problems. Firstly, the SWNTs did not reach the bottom of the pad during the coating and, therefore, there was no contact between the electrode and the nanotubes, figure 5.10 a). Secondly, once the nanotubes were placed on the bottom of the pad, figure 5.10 b), a gap between the tissue and the sensing area was created and, consequently, the electrode-tissue contact was poor too. In order to solve these problems, it was decided to decrease the thickness of the passivation layer. Three attempts were realized changing the formulation of the SU-8 and the spin coating recipe, resumed in Table 2.1. As a result a 2-3 μm thick SU-8 passivation layer was finally obtained.

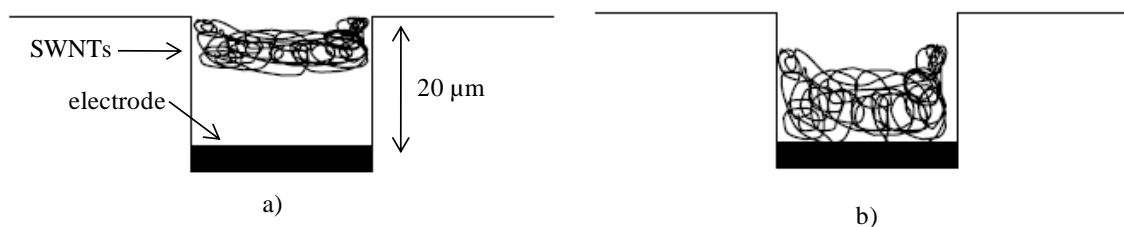


Figure 5.10 Explanatory drawing of SWNTs deposition on top of an electrode: a) a gap is formed between the SWNTs and the electrode and b) there is a gap between the SWNTs and the tissue

Table 2.1 Several attempts for the optimization of the passivation layer

Attempt	SU-8 formulation	Consecutive spin rate steps	Thickness (μm)
1 st	50	30s at 200 r.p.m. 10s at 600 r.p.m. 60s at 5000 r.p.m.	20
2 nd	50	30s at 200 r.p.m. 10s at 600 r.p.m. 60s at 10.000 r.p.m.	10
3 rd	5	30s at 200 r.p.m. 10s at 600 r.p.m. 60s at 10.000 r.p.m.	2-3

5.3.3.2 Restrictions related to 70 μm thick SU-8 layer

As aforementioned, after the fabrication of the passivation layer, a 70 μm thick SU-8 layer was processed in order to make the probe more robust. This layer was placed 180 μm from the tip of the device as shown in figure 5.5 b). Nevertheless, this layer limited the deposition of SWNTs. Briefly,

the mixture of SWNTs was poured over the probe, and the sensing areas that were limited by the passivation layer were filled. Then, the SWNTs that were located out of the sensing areas were removed with a wipe (more detailed information in section 5.5.3). However, the 70 μm thick step did not allow us to manipulate the nanotubes with precision. As a result, just the electrode that was located in the furthest position from the 70 μm high step was coated as shown in figure 5.11. In addition, the SWNTs remained trapped on the surface of the tip, out of the sensing areas.

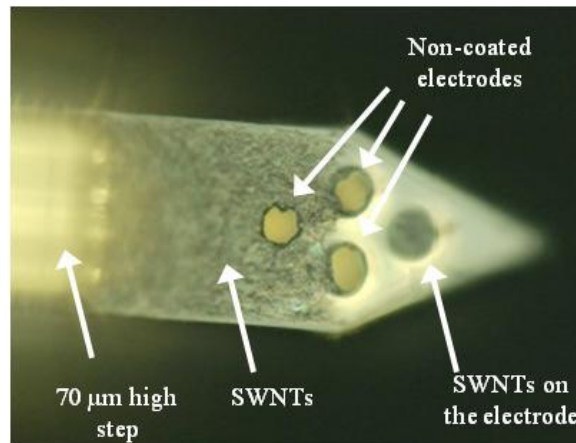


Figure 5.11 Just the electrode that is located near the tip was coated with SWNTs. Moreover, the SWNTs remained trapped on the tip surface out of the sensing areas.

Several attempts were made to reduce the 70 μm thick SU-8 layer. In the first attempt, four 20 μm thick SU-8 layers were processed instead of one of 70 μm . A probe with a layered shape was fabricated as shown in figure 5.12. The four 20 μm thick layers were individually spin coated, exposed and post baked. In this way, a 20 μm high step was located near the electrodes instead of a 70 μm step. By means of this modification, the robustness of the probe was maintained.

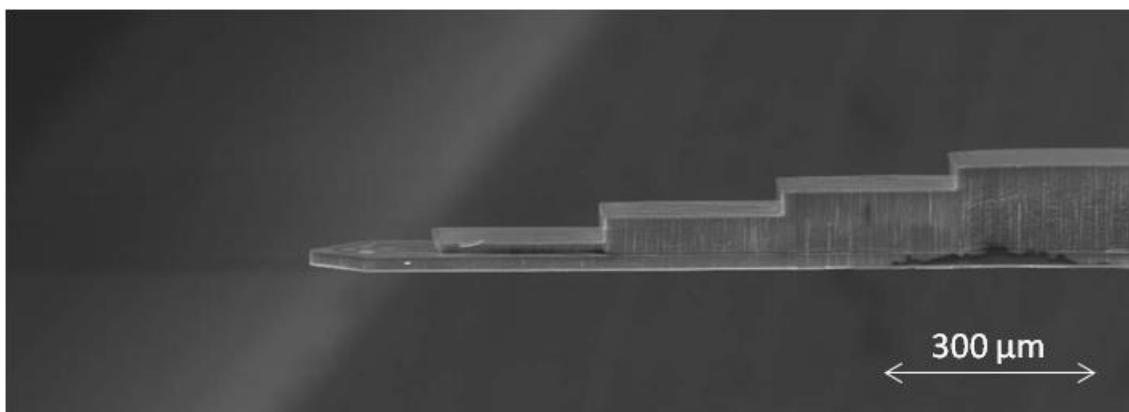


Figure 5.12 A layered SU-8 probe

5.3.3.3 Planarity of the probe

The modification made in the fabrication procedure to avoid the presence of a 70 μm thick layer near the electrodes provided an additional drawback. The probes curved upwards with a prominent angle once they were released from the wafer, figure 5.13 i). The reason for such a curvature was that there were many UV exposure processes and heating steps during the fabrication procedure. The SU-8 layers located at the bottom were much more polymerized than the ones of the top. It is believed the cross linking density gradient being the reason of such curvature¹⁵. In order to solve this problem, two 20 μm thick layers and a 40 μm thick layer were processed instead. By means of this configuration one soft bake, one UV dose and one post bake were avoided. Soft bake and post bake temperature was set at 95°C for all the layers. Although the curvature of the probe decreased, it was still too stressed as seen in figure 5.13 ii). In the third attempt, the temperature of the baking processes was decreased to 65°C. These trials were also vain attempts. Finally, the location of the 70 μm thick SU-8 layer was changed. It was located 500 μm from the tip of the probe, figure 5.14. Thus, there were no problems during the SWNTs coating and the probe was flat enough. In spite of being a solution, a more robust probe was required because the insertion area tended to break.



Figure 5.13 The curvature of: i) Four 20 μm thick SU-8 layers processed using the masks based on the first design, ii) two 20 μm thick SU-8 layers and a layer of 40 μm processed using the masks based on the first design, and iii) four 20 μm thick SU-8 layers patterned using the masks with the novel design.

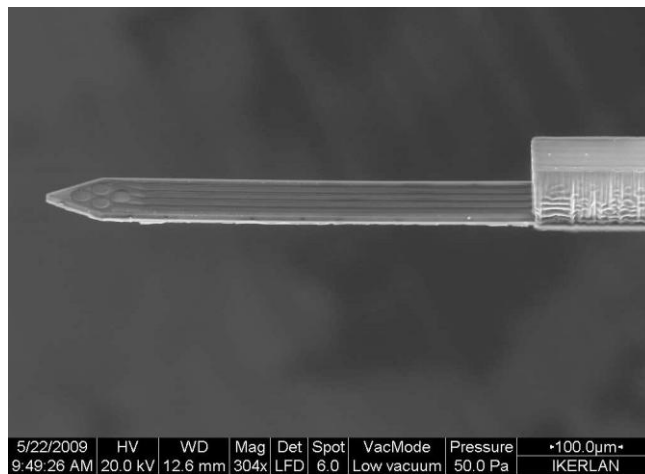


Figure 5.14 SEM picture of a modified probe where the 70 μm thick SU-8 layer was placed 500 μm from the tip

At that state, the fabrication of such a long and narrow SU-8 device became challenging. Many fabrication parameters were modified until it was thought to decrease the exposure dose given to each layer of the probe. The design of the masks used to pattern the last four SU-8 layers resulted decisive to achieve a planar device. At first, the four SU-8 layers were patterned using the mask's configuration shown in figure 5.15 a). In all those trials, a large area of the probe was repeatedly exposed to UV light. As a result, those layers processed first had a higher degree of polymerization with respect to layers placed on top of them due to the accumulation of UV radiation, SB and PB steps. Such polymerization difference between the layers created a stress gradient along the thickness direction of the probe, causing the curvature. In order to solve this problem, new masks were designed to build the probe under a new strategy. Using the new configuration, in each exposure step just a small area of the probe was lightened as shown in figure 5.15 b). In this way, all different layers were exposed just once at all different areas of the probe. Additionally, all the heating processes were performed at 65°C. As a result, although the tip of the probe was slightly curved downwards, it was considered that the probes were flat enough in order to encapsulate and use them in experimental tests, figure 5.13 iii).

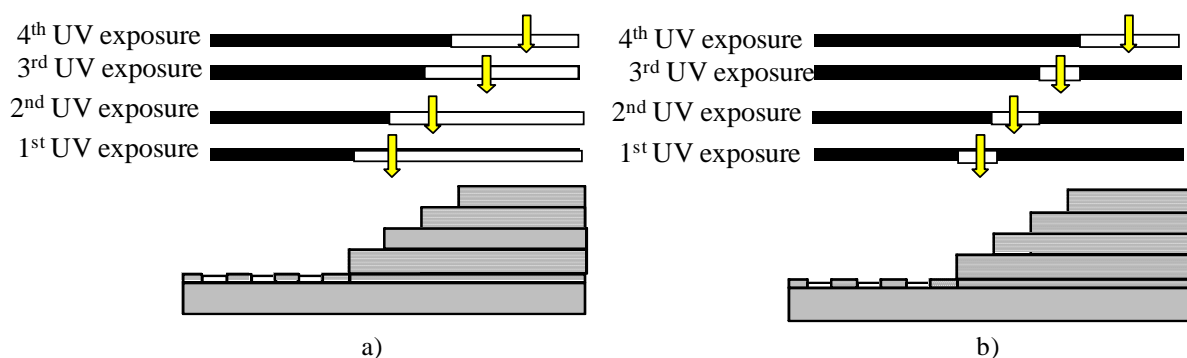


Figure 5.15 Schematic drawing of: a) consecutive UV exposures using the first masks' design with which curved probes were obtained and b) consecutive UV exposures using the masks based on the novel design with which flat probes were obtained

5.3.3.4 Electrochemical etching: a fast release method

A fast method was required to release the probes from the substrate because the chemical etching lasted up to 5 or 6 days due to the underetching of the probes. As an alternative, the electrochemical etching of the aluminum was chosen. The set up was formed by a cell filled with a NaCl 2M solution and a potentiostat. The wafer was introduced in the cell and connected to the voltage source. Opposite to the wafer covered with aluminum and probes, another wafer covered with a platinum film was placed. This wafer worked as a counter electrode. A voltage of 0.8 V was applied between both wafers and all the probes were successfully separated in 4 hours approximately. As a typical behavior of the aluminum in aqueous solutions, corrosion pits were formed until the entire cross-sectional area of the metal was finally dissolved and the probes released. Figure 5.16 shows the set up used for the release of the probes.



Figure 5.16 A picture of the electrochemical etching set up used for the release of the SU-8 probes

5.3.3.5 Conclusions related to the first fabrication procedure

Firstly, the thickness of the passivation layer was decreased modifying the spin rate and replacing the SU-8 50 by SU-8 5 until a 2-3 μm thick passivation layer was obtained. Secondly, the 70 μm thick SU-8 layer was replaced by four 20 μm thick layers patterned using a new mask configuration. In this way the electrodes did not have any obstacle close to them. Thirdly, the probes were released by electrochemical etching as an alternative to the Kapton™ film use in order to avoid breaking the probes. All these modifications devised to improve the functionality of the probe and resulted in the creation of the second fabrication procedure.

5.3.4 Second fabrication procedure: electrodes 2-3 μm embedded into a layered probe

In the same way as in the first fabrication procedure, the initial step was the deposition of an aluminum film by sputtering on a silicon wafer, figure 5.17 I). The innovation started when a 20 μm thick SU-8 layer was spun onto the aluminum film. This layer was soft baked heating the wafer up to 65°C for 2 minutes and up to 95°C for 7 minutes. Then, the shape of the probe was patterned by photolithography when a 140 mJ/cm^2 was given and after that, the SU-8 layer was developed as shown in figure 5.17 II). The area where the SU-8 had been removed was filled with a sacrificial resin in order to keep the wafer completely flat, figure 5.17 III). An 8 μm thick SPR was processed by photolithography. This step was crucial to obtain a good patterning of the narrowest metallic tracks on top of the structural SU-8 layer. Next, chromium (50 nm) and gold (150 nm) films were deposited by sputtering, figure 5.17 IV). In order to pattern the electrodes, the resin S1818 was processed, figure 5.17 V), and chromium and gold wet etchings were carried out, figure 5.17 VI). Once the electrodes were patterned, all the S1818 and SPR were removed and it was ensured that the sensing area did not have any impurity on top. The innovative step consisted of spinning a SU-8 (SU-8 5 formulation) layer at high revolutions so that a 2-3 μm thick passivation layer was created as already reported in section 5.3.3.1. It was soft baked heating the wafer up to 65°C for 20 minutes. Then, an exposure dose of 140 mJ/cm^2 was given and the post bake was performed at 65°C for 7 minutes, figure 5.17 VII). Next, four 20 μm thick SU-8 layers were processed in order to get a robust and an easy handling device using the new masks' configuration as explained in section 5.3.3.3, figure 5.17 VIII). Each layer was soft baked heating the wafer up to 65°C for 40 minutes, exposed to 140 mJ/cm^2 and post baked at 65°C for 7 minutes. All these heating steps were carried out at such a low temperature because it is believed that processing at lower temperature decreases the stress of the SU-8¹⁶. In the first SU-8 layer just the tip of the probe was exposed and in the consecutive three layers different parts of the probe were exposed along its length. In this way a layered shape was obtained. At this state, all the SU-8 layers were developed and the probes were separated from the wafer. The electrochemical etching of the aluminum was used as already dealt in section 5.3.3.1, figure 5.17 IX). As a last step,

each probe was rinsed with water and isopropanol. SEM pictures of a typical microprobe and the tip of a probe are observed in figure 5.18 a) and b) respectively. Once the electrodes were separated from the substrate, rinsed and dried, the thicknesses of the SU-8 layers were measured by the profilometer, figure 5.19 a). It was verified that the electrodes were 2-3 μm embedded into the probe, figure 5.19 b).

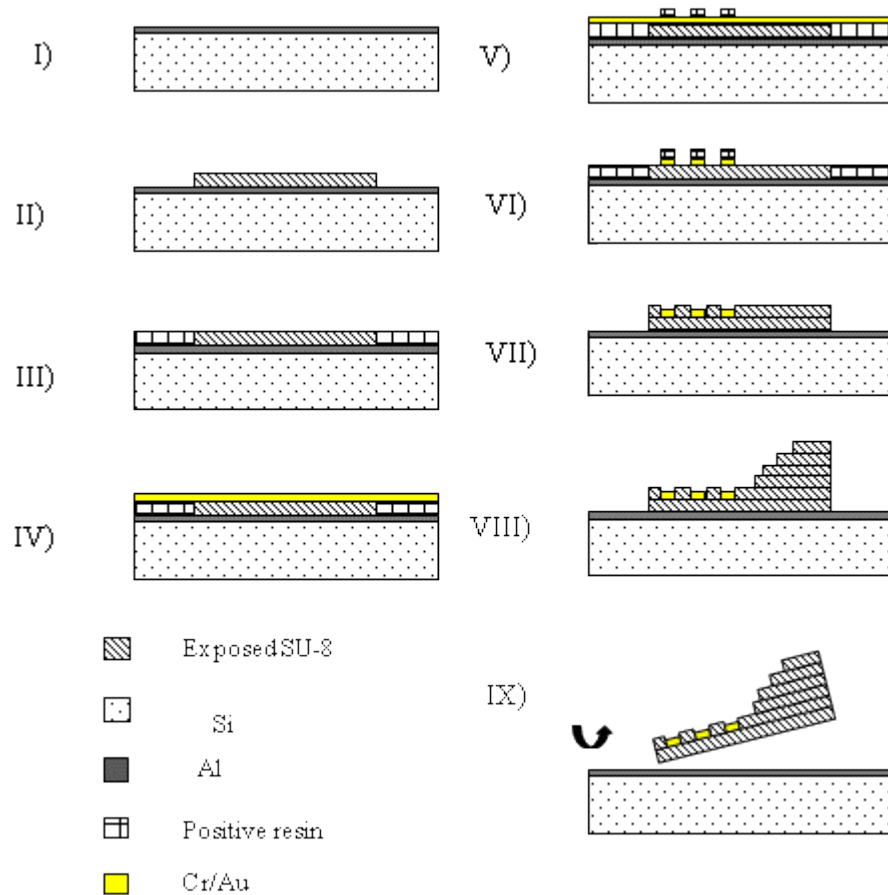


Figure 5.17 Schematic drawing of the second fabrication procedure sequence

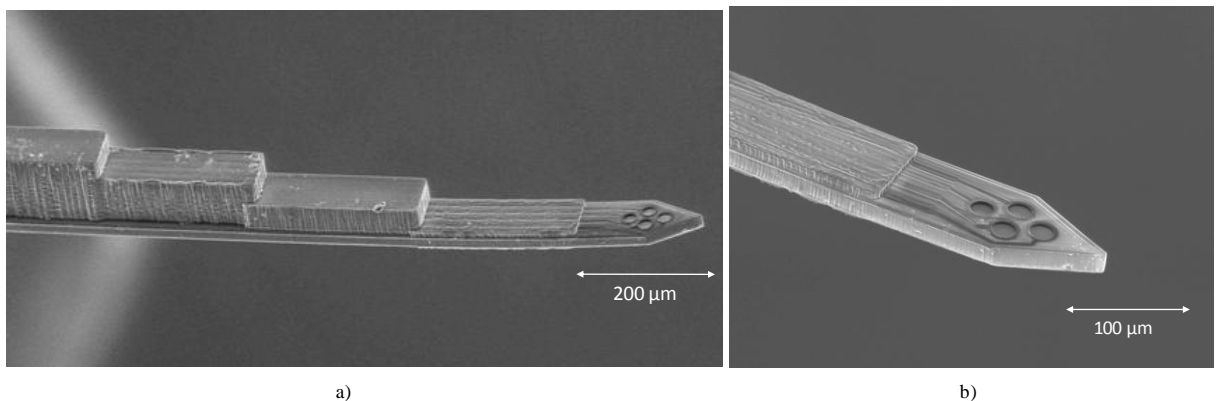


Figure 5.18 SEM pictures of: a) a layered SU-8 microprobe and b) the tip of the probe

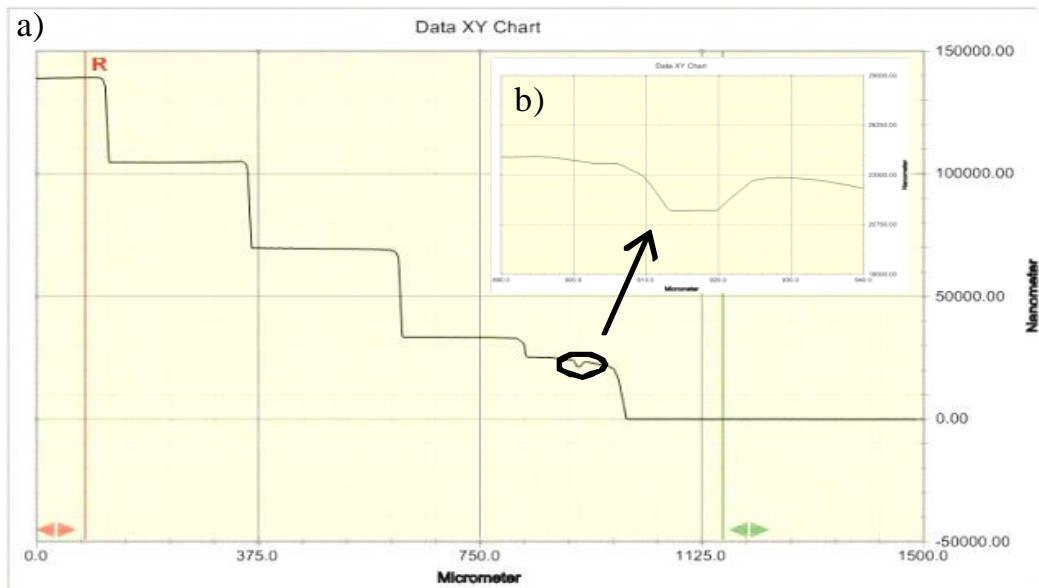


Figure 5.19 Profilometer measurements of: a) a layered microprobe shape and b) the electrode gap

A satisfactory microprobe was achieved based on the second fabrication procedure. It was a flat and a robust device and the electrodes were located very close to the outside. At this state, more experimental recordings were carried out in rat's hippocampus and the measurements suggested a relevant improvement. Nevertheless, even a closer contact of the electrode-neuron was required in order to measure from spikes with higher peak-to-peak amplitudes (explained in section 5.6.1). Consequently, the scheme of the fabrication processes was changed.

5.3.5 New concepts on the fabrication sequence

In the first and second fabrication procedure a typical scheme was followed. First, the floor which defines the shape of the probe was patterned. Then, the microelectrodes were placed on top of this layer and, finally, the metallic tracks were covered with the so-called passivation layer, leaving the sensing sites opened. The thickness of the passivation layer thus determined the gap between the electrode and the tissue, figure 5.20 a).

In order to integrate electrodes at the probe surface level, a novel fabrication procedure was designed. Contrary to the conventional fabrication sequence, the passivation layer was now processed first. The shape of the probe was defined and the sensing sites were opened. On top of this layer, the electrodes were patterned in such a way that the sensing sites were filled with the metal. Finally, all the surface was covered with a continuous SU-8 layer. In this way, once the probes were released from the substrate, the electrodes were placed at the probe surface level, figure 5.20 b). Furthermore, the four 20 μm thick SU-8 layers were located on the opposite site of the electrodes in order to decrease the

invasive effect in the recording area. All these modifications devised to improve the recording capability of the probe and resulted in the third fabrication procedure.

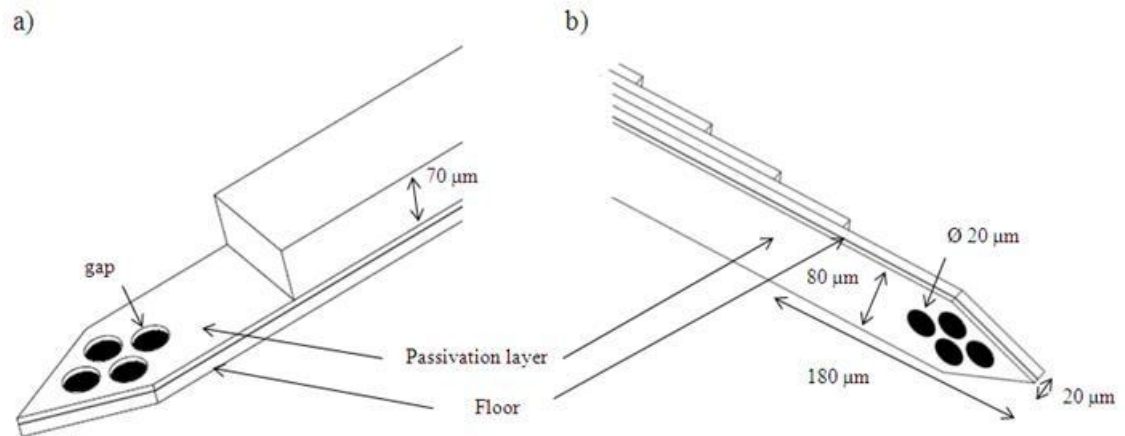


Figure 5.20 Schematic drawing of: a) the initial design and b) a layered microprobe with the electrodes at the probe surface level.

5.3.6 Third fabrication procedure: electrodes at the probe surface level

The variations respect the first and second fabrication procedure started once the aluminum was deposited on the silicon wafer by sputtering, figure 5.21 I). The wafer was heated up and maintained at 200°C for one hour. In this way, a good adhesion between the aluminum and the SU-8 was achieved. After the wafer was cooled down, a 2-3 μm thick SU-8 (SU-8 5) layer was spin coated and soft baked. The wafer was heated up to 65°C for 2 minutes and up to 95°C for 4 minutes. Then, an UV exposure of a 140 mJ/cm² was given using the mask which defines the passivation layer. Contrary to the previous fabrication procedures, the layer that opens the sensing area was processed first. After the exposure, the wafer was heated up to 65°C for 2 minutes and up to 95°C for 4 minutes as a post baking process. Once this layer was developed, figure 5.21 II), the sputtering of the chromium (50 nm) and gold (150 nm) was performed, figure 5.21 III). In order to pattern the electrodes, a resin was patterned and the wet chemical etchings were carried out, figure 5.21 IV). Just after that, a 20 μm thick SU-8 layer was spin coated and soft baked. The wafer was heated up to 65°C for 20 minutes and an UV dose of a 140 mJ/cm² was given. Then, a post bake was performed heating the wafer up to 65°C for 7 minutes. By means of this layer, all the metallic tracks were covered figure 5.21 V). Then, four 20 μm thick layers of SU-8 were spin coated, exposed and post baked. Each of them were heated up to 65°C

for 20 minutes as a soft bake, exposed to 140 mJ/cm^2 and heated up to 65°C for 7 minutes as a post bake. Next, the five layers were developed, figure 5.21 VI). Finally, the probes were released from the substrate by the electrochemical etching of the aluminum, figure 5.21 VII), and rinsed with water and isopropanol. At this state, the electrodes had the chromium surface in contact with the outside and the objective was to get gold made electrodes. As a last step, chromium wet etching was performed and thus, electrodes made of gold were obtained, figure 5.21 VIII). SEM pictures show the layered microprobe and the tip, figure 5.22 a) and b).

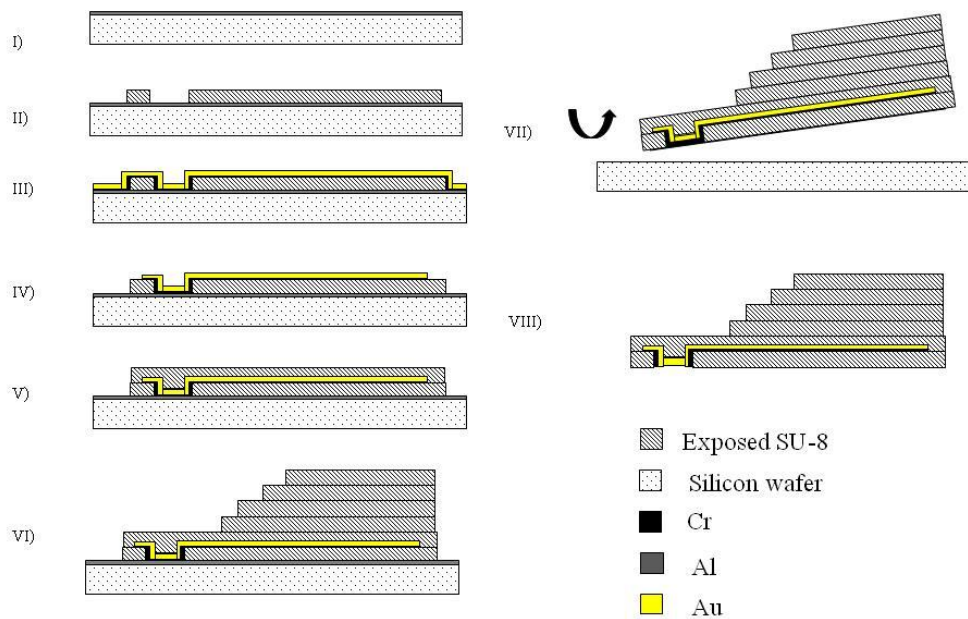


Figure 5.21 Schematic drawing of the third fabrication procedure sequence

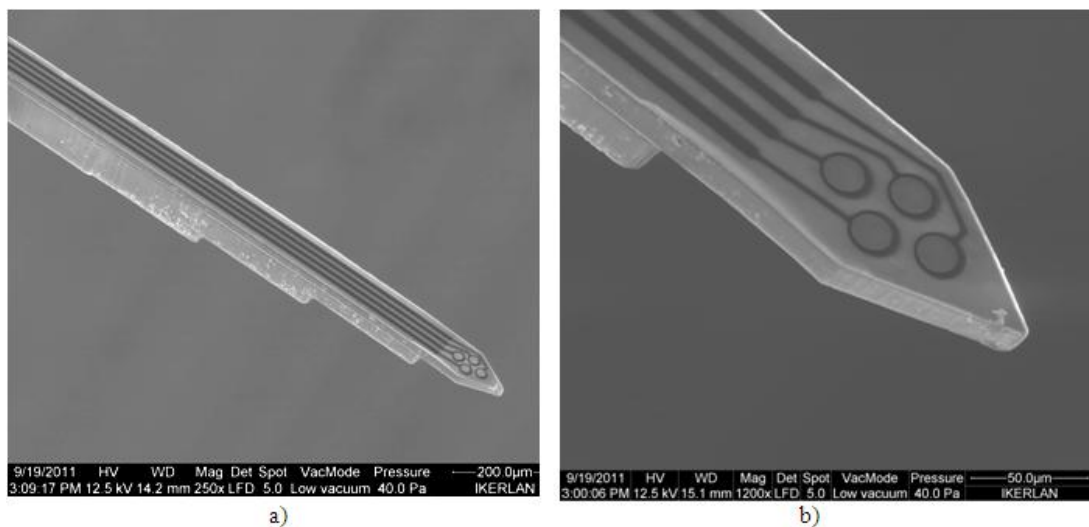


Figure 5.22 SEM pictures: a) A layered SU-8 probe with the electrodes at the probe surface level and b) the tip of the probe

5.3.7 Achievements related to the third fabrication procedure

5.3.7.1 Adhesion between the aluminum and the SU-8

In the first and second fabrication procedures there were no problems associated with the adhesion between the SU-8 and the sputtered aluminum layer. However, in the third fabrication procedure a layer of SU-8 from the so called “5” formulation was processed on top of the aluminum instead “50” and adhesion problems emerged.

The SU-8 resin is composed of three components: an EPON resin, an organic solvent and a photoinitiator. The quantity of the solvent determines the viscosity and consequently the thickness of the spin coated layer. The viscosity of the SU-8 “50” is 12250 cSt, and 290 cSt for the case of the SU-8 “5” as reported by MicroChem¹⁷. Therefore, the SU-8 5 was chosen to get a thinner layer to help with the achievement of a good electric contact between the metal deposited on top of the SU-8 and the metal placed at the sensing areas. Sputtering on top of a thin layer was essential to ensure that the entire wafer was covered. Nevertheless, adhesion problems between the aluminum and the SU-8 were detected during the fabrication process. The probe was detached from the substrate before the fabrication of the probes was completed as can be observed in figure 5.23. When the adhesion problem arose for the first time using this strategy, it was believed that the different composition of the photoresist was the cause. As a possible solution, a dehydration step (one hour at 200 °C) was added to the fabrication procedure before the SU-8 5 was spin coated. As a result, the adhesion between the SU-8 5 and the aluminum was found to be strong enough to keep the probes attached to the substrate until their release step.

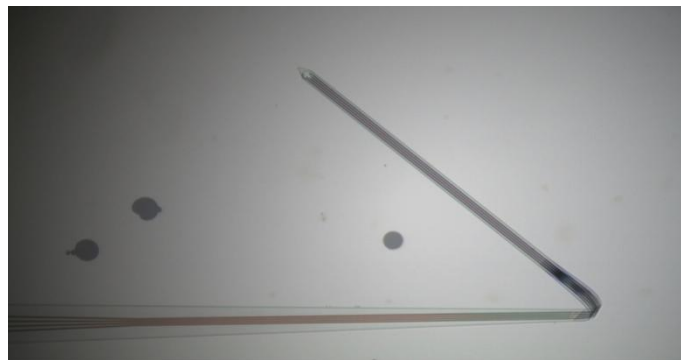


Figure 5.23 A part of the probe is removed from the aluminium layer just after the patterning of the electrodes

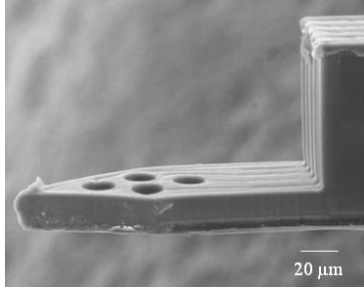
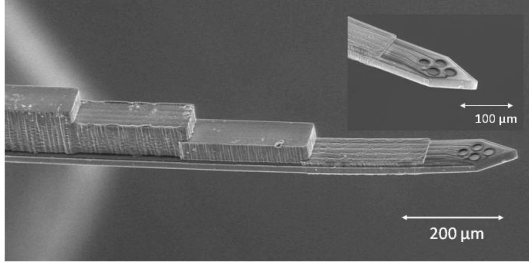
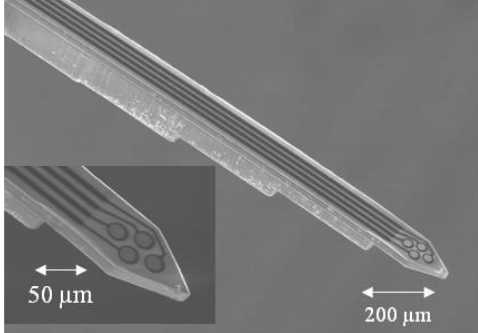
5.3.7.2 Electrodes at the probe surface level and without impurities

In an effort to locate the electrodes at probe surface level and free of impurities thoroughly studied steps were followed. The resin SU-8 5 was used to define the passivation layer on top of the aluminum foil, because as mentioned the previous sections it is less viscous than the SU-8 50 and therefore, a thinner layer can be obtained. For that, the SU-8 5 was spin coated at 10.000 r.p.m. and thus, a 1.5 μm

thick layer was obtained. When this layer was developed the pads that limit the sensing areas were opened and approximately 200 nm thick metallic layer was placed on top by means of the sputtering method. The step coverage of the sputtering process was high enough in order to cover the flat surface and also the 1.5 μm walls of the pads. In this way, when the fabrication of the probes finished and the aluminum was removed, the metallic area remained at the SU-8 5 bottom surface level. Chromium that is used as an adhesion layer was etched and as a result, gold made electrodes were obtained. Additionally, electrodes without impurities were obtained following this method. Briefly, many methods commonly used to pattern the metal and cover the metallic tracks involve the use of resins that finally have to be removed from the surface of the sensing area. Consequently, resins remain on the electrodes and this fact affects their sensing behavior. In this case, the gold surface that is in contact with the outside was perfectly clean because it did not make contact with any resin during the fabrication procedure.

5.3.8 Resume of the most relevant features of the first, second and third fabrication procedures

Table 2.2 Most relevant characteristics of the first, second and third fabrication procedures

Fabrication procedure	Design & fabrication features	Improvements and limitations	SEM picture
First	<ul style="list-style-type: none"> - Passivation layer: 20 μm thick - Additional layer: 70 μm thick - Release method: aluminum chemical etching 	<ul style="list-style-type: none"> ✓ Exclusively SU-8 made microprobe for neural activity recording is fabricated for the first time. ✗ Electrode-tissue interface is too high (20 μm) ✗ Mechanical limitations emerge due to the 70 μm thick layer 	
Second	<ul style="list-style-type: none"> - Passivation layer: 2-3 μm thick - Additional layer: layered body - Release method: aluminum electrochemical etching 	<ul style="list-style-type: none"> ✓ Electrode-tissue interface is decreased down to 2-3 μm ✓ Mechanical problems are overcome ✓ Fast release method is used 	
Third	<ul style="list-style-type: none"> - Passivation layer: none - Additional layer: layered body - Release method: aluminum electrochemical etching 	<ul style="list-style-type: none"> ✓ Electrodes are located at the probe surface level ✓ Electrodes without impurities are fabricated ✓ Huge advances in recording capability are expected 	

5.4 Packaging

A PCB with multiple electrical connections was designed and fabricated to allow the data acquisition during the experimental tests, figure 5.24 a) ¹¹. The PCB had 16 connections available but in this case just four of them were used for the tetrode version. The encapsulation process consisted of fixing the probe to a commercial PCB following a standard procedure. First a conductive adhesive (Elecolit 3005 from Panasol-Eosol) was applied in each pad of the probe and the PCB. Then, the probe was aligned and pressed against the PCB. Next, the probe and the PCB ensemble were heated up to 60°C for half an hour until the adhesive was completely cured. Once it cooled down, Loctite 3430 was deposited in the edges of the probe to fix it mechanically onto the PCB. After 12 hours, the microprobes were introduced in a saline solution to verify the electrical connections. In figure 5.24 b) the probe and PCB ensemble fixed to the recording equipment can be observed.

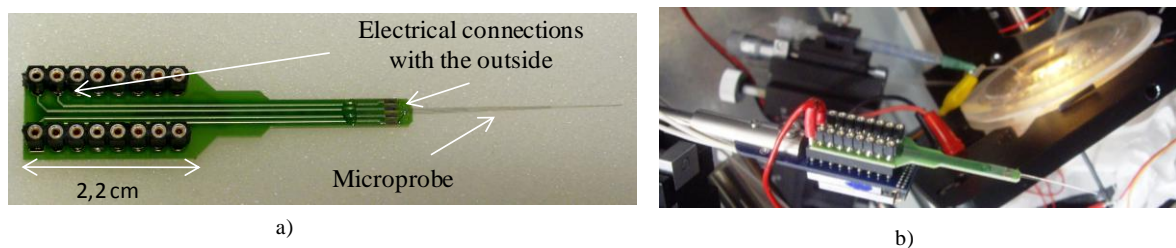


Figure 5.24 a) A packaged microprobe and b) the packaged probe attached to the recording equipment.

5.5 Characterization of the sensing sites

5.5.1 Impedance spectroscopy

Impedance measurements were conducted in order to characterize the electrode-electrolyte interface and predict the sensing behavior of the electrodes. The electrode-electrolyte interface impedance behavior can be approximated by an equivalent circuit. It is composed by the parallel combination of the charge transfer resistance (RCT) and a capacitance (CPE – nonfaradaic pseudocapacitance). The CPE component is the best approach for modeling the double layer behavior. These are also connected in series with the spreading resistance (Rs-solution resistance) which models the spreading current from the conductive solution into the electrode. However, in this application the RCT can be neglected because there is no charge transfer between the electrode and the solution. Two-electrode impedance measurements were conducted using a commercial impedance analysis system (SI 1260, Solartron Analytical), in order to characterize the electrode-electrolyte interface impedance compared with a platinum reference electrode (Radiometer Analytical). Impedance

modulus and phase were recorded at several discrete frequencies in the 10 Hz to 1 MHz range. During characterization, the microprobes were immersed in physiological saline solution (0.9 wt. % NaCl, with a nominal resistivity of 71.3 Ω -cm at 298 K) and impedance spectroscopy was carried out.

Impedance spectroscopy results from the three different versions of probes (based on the first, second and third fabrication procedures) are shown in figure 5.25. Average measurements and standard deviation from 6 probes (24= electrode) of each version were obtained. All the results show great dependence on the frequency which corresponds to a typical capacitive behavior of the electrode double layer, figure 5.25. Due to the small size of these electrodes (20 μ m) the measured capacitance is very low, so only the capacitive part of the equivalent circuit described before can be observed in the measured frequency range. As can be observed the impedance phase shift is higher than -90° , this fact can be explained by the surface roughness of the electrode. In the equivalent circuit this behaviour is modeled by the CPE instead of the pure capacitance component, which is ideally used for perfectly smooth electrodes.

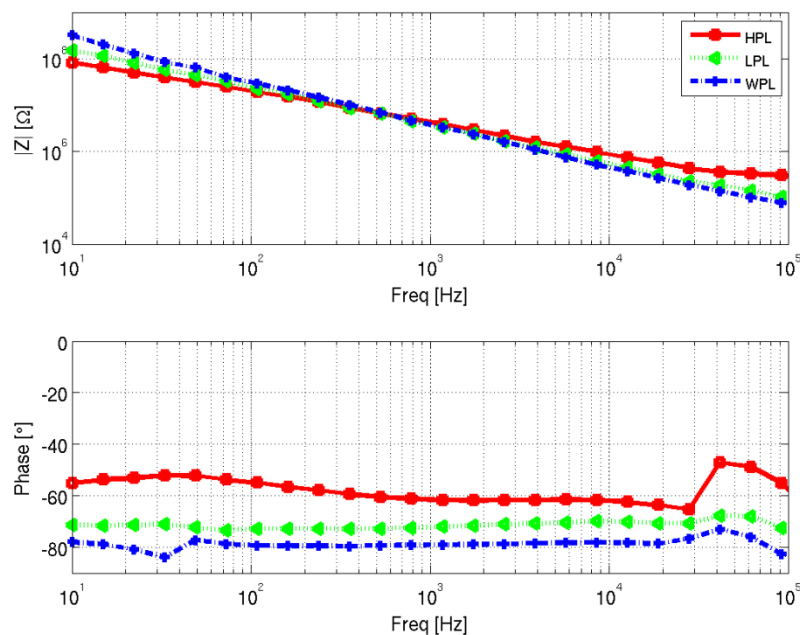


Figure 5.25 Impedance modulus and the phase shift for the three types of probe. Red line: 20 μ m electrode gap (HPL: high passivation layer), green line: 2-3 μ m electrodes gap (LPL: low passivation layer) and blue line: electrodes at probe surface level (WPL: without passivation layer)

Additionally, a deeper characterization of the electrodes was carried once the fabrication procedure was fully optimized. Strikingly, impedance characterization confirmed that the third fabrication design resulted on large impedance homogeneity. Hence, for every probe tested we

found similar impedance values ($\pm 0.75 \text{ M}\Omega$) in all the four recording sites. This can be observed in figure 5.26 where the impedance modulus values at 1 KHz for the four electrodes of each probe is represented. The boxplot representation shows the mean value and the dispersion of the measurements grouped by quartiles. Dispersion of impedance values between probes can be explained by wafer-scale fabrication limitations. It is believed that the area of the electrodes may change between probes due to slight misalignments over the wafer. Also, the roughness of the metal could be different depending on the position of the probe in the wafer. The homogeneity impedance values allow us to select the probes according to the application requirements. For the purpose of neuronal application tested here, tetodes with impedance in the range of $0.5\text{-}3 \text{ M}\Omega$ were chosen.

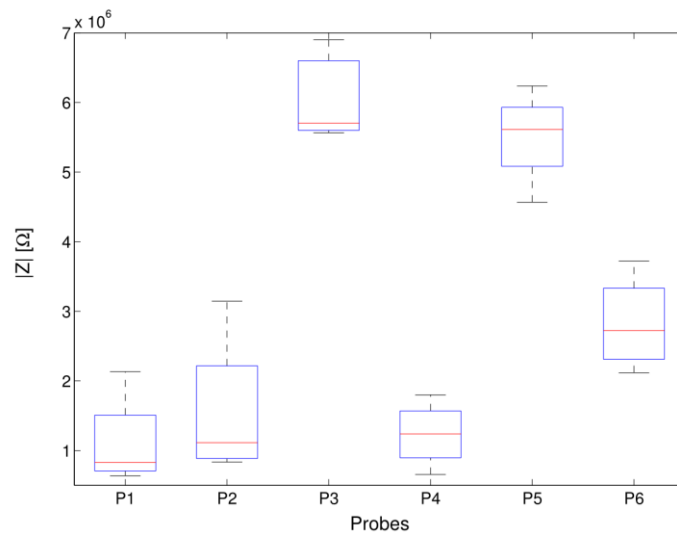


Figure 5.26 Impedance modulus measured at 1 KHz for each probe (electrodes placed at the probe surface level). The box plot representation shows the mean value, the dispersion of the measurements grouped by quartiles (boxes and bars) for the four electrodes of each probe.

5.5.2 Platinum black electrochemical deposition

The platinization of the SU-8 probes was carried out by our colleagues from CNM (Centro Nacional de Microelectrónica, Barcelona) following the recipe already reported in Chapter 3. Before and after the platinization procedure, the electrodes were undergone to an impedance spectroscopy in order to know the effect of the platinum black coating in the impedance values. First impedance values were obtained before the platinization and they were represented by black lines in figure 5.27. At 1 KHz, the impedance was in the order of $10^7 \Omega$, quite superior to the impedance reported by commercial probes, which are around $1 \text{ M}\Omega$. Once the tetrode was electroplated at 500 nA for 60 and 90 seconds, the impedance decreased (blue lines), and impedance values in the order of $10^5 \Omega$ were obtained for the

four electrodes. Moreover, the four electrodes reached almost the same value at 1 KHz and this fact suggested a homogeneous sensing behavior of the tetrode. Nevertheless, 24 hours after the coating, the impedance values of each electrode increased as shown with red lines. The electrodes were replatinized and it was observed that the impedances returned to their lowest value. Although at first attempts the impedance values varied, it is believed that the tendency was to block the values at low values.

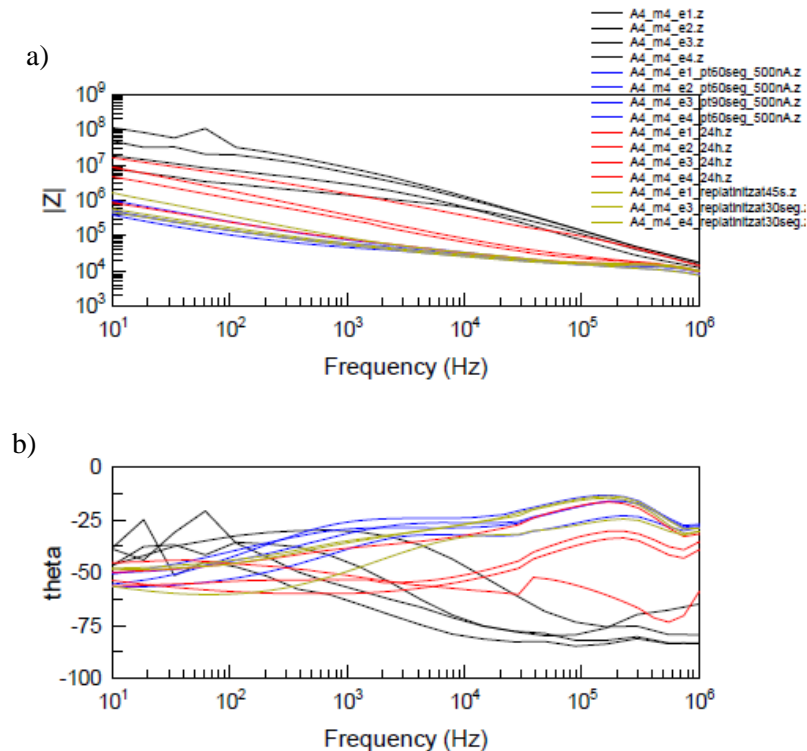


Figure 5.27 A representative behavior of impedance modulus a) and the phase shift b) of the tetrode 2-3 μm embedded before the platinization process (black lines), just after the platinization (blue lines), 24 hours after the platinization (red lines) and after a second platinization process (yellow lines).

5.5.3 Single walled carbon nanotubes (SWNTs) coating

Carbon nanotubes (CNTs) have many qualities that make them desirable as a material for use in neurobiological applications¹⁸. They are electrically conductive, biocompatible, small and flexible, yet are very strong, and can be functionalized with different molecules, properties that may be useful in basic and applied neuroscience. The combination of high conductivity, strength and flexibility is highly desirable for any neural interface, therefore, the possible usefulness of CNTs in neural stimulation and recording has been proposed by several authors^{19,20,21,22,23}.

In this work, high purity SWNTs purchased from Sigma Aldrich were used²⁴. A simple and easy procedure was carried out to cover the sensing sites with carbon nanotubes, figure 5.28. Briefly, 10mg of pure SWNT were dispersed in 10 ml of dimethyl formamide (DMF) under ultrasonic agitation

resulting in a 1 mg/ml black suspension. A drop of the resulting solution, typically 5 μ l, was placed onto the surface of the electrodes and left to dry at 90–100 °C. Finally, the device was rinsed with distilled water and thoroughly wiped with wet cleanroom wipers to ensure that the carbon nanotubes stayed only in the electrode area.

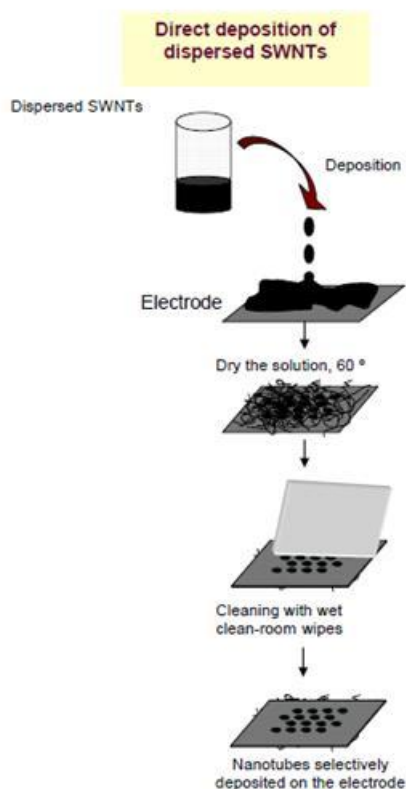


Figure 5.28 Single walled nanotubes deposition schematic procedure

In order to study the contribution of the SWNTs to the sensing behaviour of the tetrode, initial approaches were carried out. It should be noted that the surfaces of the electrodes were fully covered but the coating was not uniform as shown in figure 5.29 a). It can be observed that the electrode number 1 has less nanotubes than the electrode number 4, figure 5.29 b). Furthermore, it was estimated that there were 2 or 3 μ m between the coated surface and the outside. This technology was not further studied because it required an extra effort to optimize the deposition of the CNTs. However, these initial tests confirmed us that the technology of SWNTs is compatible with the technology developed in this thesis. Nevertheless, additional test would be carried out to see the real potential of this technique.

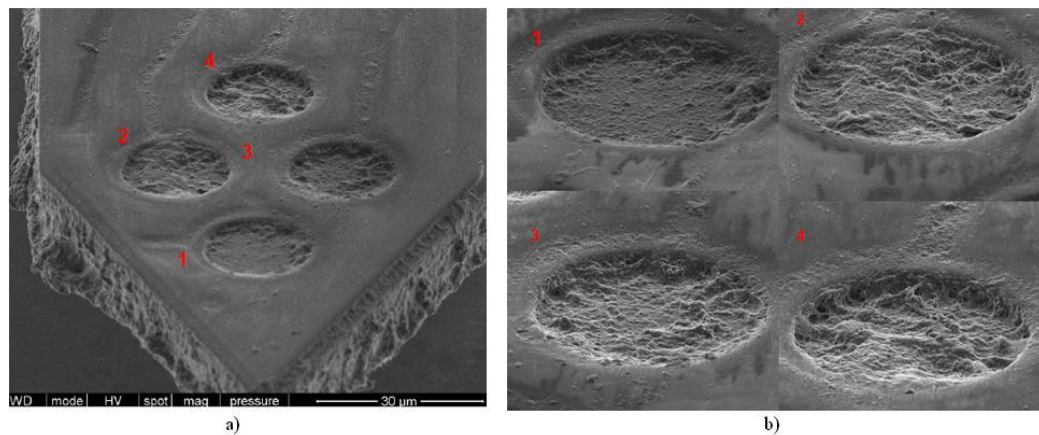


Figure 5.29 SEM pictures of: a) a tip of a probe where the tetrode is covered with SWNTs and b) the magnified view of each electrode

5.6 Experimental procedures: extracellular neural activity recording

5.6.1 *In vitro* tests

Initially, functional viability of the SU-8 based microprobes was tested *in vitro*¹¹. Recording capability of the electrodes and the mechanical behavior of the probe were checked using hippocampal slices. The experimental procedure was carried out as follows. Horizontal slices were prepared from normal adult rats and kept in interface conditions using standard bathing solutions²⁵. Recordings were obtained from the CA3 region of the hippocampus and several slices were tested at 32°C. The microprobe tip was gently inserted to a depth of about 150 μm into a 400 μm thick hippocampal slice and spontaneous signals were recorded in the band of 10 Hz to 10 KHz.

First attempts were performed using probes with sites embedded 20 μm into the probe. As shown in figure 5.30, signals demonstrated the typical shape of extracellularly recorded action potentials superimposed on noise. The noise level was in the range of 22 to 30 μV rms (mean 27.3 μV rms, n=8 electrodes from 2 probes), which mostly accounted for the thermal noise from the electrodes (10 μV rms) and the setup noise that is about 12 μV rms. Detectable action potentials had peak-to-peak amplitudes up to 200-250 μV, quite comparable to those recorded with conventional tetrodes²⁶. However, large spikes (>300 μV rms) were not observed with these probes; probably, due to the poor electrode-neuron interface caused by the presence of a 20 μm passivation gap between the electrode and the tissue. From a mechanical point of view, the probes were perfectly inserted into the neural tissue. They did not show any buckling or dragging in the event of penetration.

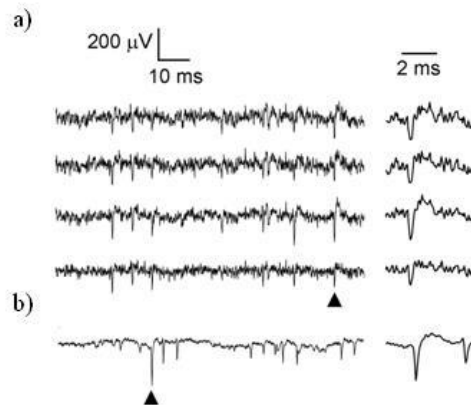


Figure 5.30 Extracellular spontaneous signals recorded *in vitro* using the SU-8 based microprobes with recording sites embedded 20 μm (a) and a conventional low impedance electrode, $\sim 400\text{ K}\Omega$ (b).

Both recordings were obtained from the same slice. Action potentials from several neurons were distinguishable with both probes. The different noise level is attributable to difference in electrode shape and impedance. Arrowheads point to one of such action potentials recorded in all four electrodes of the SU-8 probe, which is expanded at right. Spike waveforms, duration and amplitude are all consistent with signal emerging from single neuron, as recorded with conventional electrodes.

These first tests suggested that the critical point was the gap of the interface. Next, the same *in vitro* approaches were performed using the 2-3 μm embedded electrodes in order to verify the thoughts. Results are shown in figure 5.31. It was observed that while reducing the electrode gap resulted in lower noise levels (figure 5.31 b versus figure 5.31 a), recording quality was still poor as compared with standard silicon probes (figure 5.31d). Only small action potentials were visible above a still large background noise. Interestingly, it was observed that filling the gap with platinum black electroplating resulted in large improvement of both the signal-to-noise ratio and the ability to record larger amplitude spikes (figure 5.31 c). This suggested that even with reduced gaps of less than 3 μm the electrode-neuron interface was severely compromised and that new designs were required in order to improve the electrical behaviour of the probe.

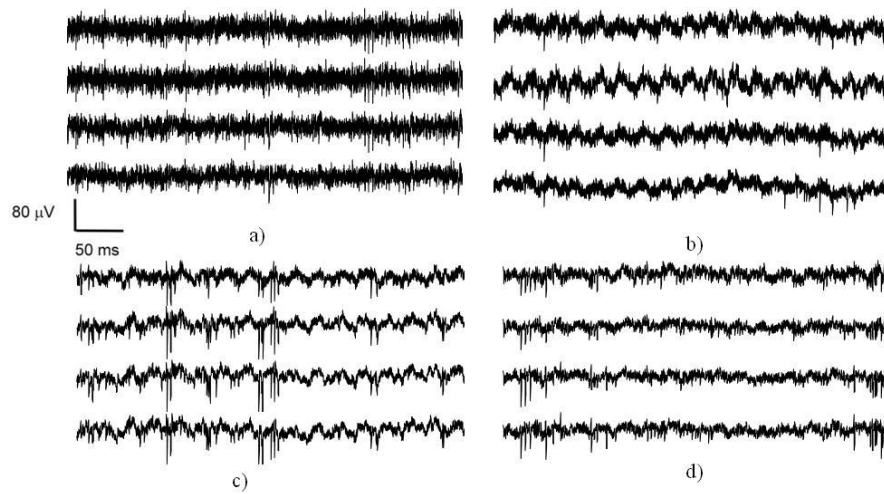


Figure 5.31 Extracellular spontaneous signals recorded *in vitro* using: a) SU-8 microprobes based on the first fabrication procedure (electrode gap 20 μm) b) SU-8 microprobes based on the second fabrication procedure (electrode gap 2-3 μm), c) SU-8 microprobes based on the second fabrication procedure with electroplated electrodes and d) standard silicon based microprobes. Some of the individual spikes are truncated in C due to their large amplitude of $> 200 \mu\text{V}$.

5.6.2 *In vivo* tests

Next, the electrodes placed at the probe surface level were tested. Due to promising preliminary characterization *in vivo* testing method was chosen since the major goal was to be able to use these probes for depth recording applications. The novel probes were tested using the anesthetized rat preparation²⁷. Briefly, the probes targeted the CA1 cell layer of the dorsal hippocampus (2.2 mm deep from the brain surface) of urethane anesthetized rats. The *cisterna magna* was opened and the cerebrospinal fluid was drained to decrease pulsation of the brain and to favour stability. The probe was gently inserted into the brain and advanced using a hydraulic micro-manipulator under stereotaxic control. Extracellular signals were preamplified (4 \times gain) and recorded with a multi-channel AC amplifier (Multichannel Systems, Germany), further amplified by 100, filtered by analog means at 1 Hz to 5 kHz, and sampled at 20 kHz/channel with 12 bit precision. Noise level was in the range of 15 to 40 μV , mostly depending on the impedance of the recording site.

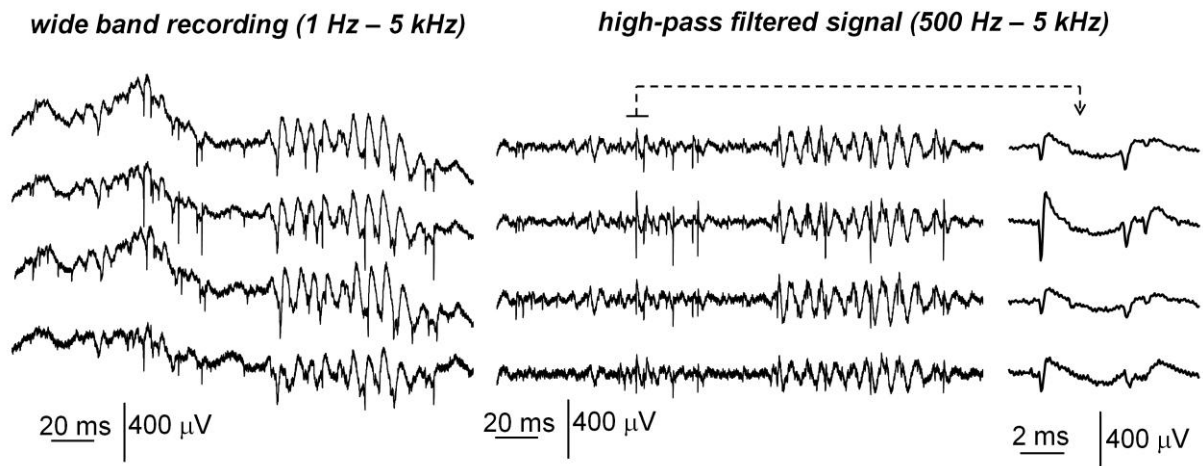


Figure 5.32 a) Representative wide band depth recordings of local field potentials and action potentials from the CA1 layer of the dorsal hippocampus in an anesthetized rat. b) Action potentials (spikes) were typically analyzed after high-pass filtering the original signals. They were evident as large and fast fluctuations. Examples of three of these spikes are shown in c). Their different amplitude and shape in all the four recording sites of the tetrode suggest different neuronal sources.

Action potentials (spikes) and local field potentials (oscillations) were captured by the tetrodes immediately upon penetration of the CA1 cell layer (figure 5.32 a), similar to conventional silicon-based tetrodes²². Signals were typically high-pass filtered offline to look for the firing contribution of different neurons (figure 5.32 b). The peak-to-peak amplitude of action potentials ranged from noise level to up to 400-500 μV , well above the amplitudes reported using the previous two designs. This suggests good neuron-electrode interface favouring recording from proximal cells. Firing from multiple single cells was also clearly observed, in the form of spikes with different amplitudes and shapes (figure 5.32 c). Thus, the importance of the electrode-tissue interface was verified. Finally, the ability for isolation purposes compared with the previous designs was proved.

5.7 Conclusions

Three SU-8 based microprobe versions were successfully fabricated and encapsulated for neural testing. A tetrode configuration was fixed at the tip of the probe in all the versions, however, the gap created between the electrode and the outside was reduced in each consecutive fabrication procedure. Finally, the electrodes were located at the probe surface level following an advanced fabrication procedure. The resin SU-8 5 was used which is less viscous than the SU-8 50 for such an achievement. Sputtering on top of a 1.5 μm passivation SU-8 layer and releasing the probes by electrochemical

etching were the most relevant steps to reduce the interface gap entirely. Moreover, modifying the design of the masks and thus, lightening the SU-8 areas just once, flat probes were obtained. Briefly, the study and development of the SU-8 polymer and microfabrication techniques were the point of getting each time a superior microprobe. This technological advance has been for the first time used on depth neural activity recording. Individual action potentials with peak-to-peak amplitudes of up to 400-500 μ V over the noise were measured *in vivo* on the dorsal hippocampus of experimental rats. Moreover, different amplitude and shape of action potentials recorded from all the four recording sites suggested improved capability of the tetrode to distinguish from different neuronal sources. Next attempts will be focused on integrating other functions to the probe such as delivery capability in order to advance towards a better understanding of the neuronal behaviour.

5.8 References

- ¹Drake, K.L., Wise, K.D., Farraye, J., Anderson, D.J., BeMent, S.L. Performance of planar multisite microprobes in recording extracellular single-unit intracortical activity (1988) *IEEE Transactions on Biomedical Engineering*, 35 (9), pp. 719-732
- ²Paik, S.-J., Park, Y., Cho, D.-I.D. Roughened polysilicon for low impedance microelectrodes in neural probes (2003) *Journal of Micromechanics and Microengineering*, 13 (3), pp. 373-379
- ³Robinson, D.A., The electrical properties of metal microelectrodes (1968) *Proceedings of the IEEE*, 56 (6), pp.1065-1071
- ⁴Kovacs G T A, Introduction to the theory, design, and modeling of thin-film microelectrodes for neural interfaces (1994) *Enabling Technologies for Cultured Neural Networks*, D A Stenger and T McKenna (London: Academic), pp. 121–65
- ⁵Ludwig, K.A., Uram, J.D., Yang, J., Martin, D.C., Kipke, D.R. Chronic neural recordings using silicon microelectrode arrays electrochemically deposited with a poly(3,4-ethylenedioxythiophene) (PEDOT) film (2006) *Journal of Neural Engineering*, 3 (1), pp. 59-70
- ⁶Schmidt E. and Humphrey D. R., Extracellular single-unit recording methods (1990) *Neurophysiol. Tech.* (Clifton, NJ: Humana Press), pp. 1–64
- ⁷Gesteland, R.C., Howland, B. Bridge for measuring the impedance of metal microelectrodes (1959) *Review of Scientific Instruments*, 30 (4), pp. 262-264
- ⁸Loeb, G.E., Peck, R.A., Martyniuk, J. Toward the ultimate metal microelectrode (1995) *Journal of Neuroscience Methods*, 63 (1-2), pp. 175-183
- ⁹Szabo, I., Marczynski, T.J. A low-noise preamplifier for multisite recording of brain multi-unit activity in freely moving animals (1993) *Journal of Neuroscience Methods*, 47 (1-2), pp. 33-38
- ¹⁰ www.acnp.org/g4/GN401000005/CH005.html
- ¹¹ Altuna, A., Gabriel, G., De La Prida, L.M., Tijero, M., Guimerá, A., Berganzo, J., Salido, R., Villa, R., Fernández, L.J. SU-8-based microneedles for in vitro neural applications (2010) *Journal of Micromechanics and Microengineering*, 20 (6), art. no. 064014
- ¹² Harris, K.D., Henze, D.A., Csicsvari, J., Hirase, H., Buzsáki, G. Accuracy of tetrode spike separation as determined by simultaneous intracellular and extracellular measurements (2000) *Journal of Neurophysiology*, 84 (1), pp. 401-414
- ¹³Blanco, F.J., Agirregabiria, M., Garcia, J., Berganzo, J., Tijero, M., Arroyo, M.T., Ruano, J.M., Aramburu, I., Mayora, K. Novel three-dimensional embedded SU-8 microchannels fabricated using a low temperature full wafer adhesive bonding (2004) *Journal of Micromechanics and Microengineering*, 14 (7), pp. 1047-1056

- ¹⁴Agirregabiria, M., Blanco, F.J., Berganzo, J., Fullaondo, A., Zubiaga, A.M., Mayora, K., Ruano-López, J.M. SDS-CGE of proteins in microchannels made of SU-8 films (2006) *Electrophoresis*, 27 (18), pp. 3627-3634
- ¹⁵Sameoto, D., Tsang, S.-H., Foulds, I.G., Lee, S.-W., Parameswaran, M. Control of the out-of-plane curvature in SU-8 compliant microstructures by exposure dose and baking times (2007) *Journal of Micromechanics and Microengineering*, 17 (5), art. no. 032, pp. 1093-1098
- ¹⁶Anhoj, T.A., Jorgensen, A.M., Zauner, D.A., Hübner, J. The effect of soft bake temperature on the polymerization of SU-8 photoresist (2006) *Journal of Micromechanics and Microengineering*, 16 (9), art. no. 009, pp. 1819-1824
- ¹⁷<http://www.microchem.com/#>
- ¹⁸Malarkey, E.B., Parpura, V. Applications of carbon nanotubes in neurobiology (2007) *Neurodegenerative Diseases*, 4 (4), pp. 292-299
- ¹⁹Wei, W., Sethuraman, A., Jin, C., Monteiro-Riviere, N.A., Narayan, R.J. Biological properties of carbon nanotubes (2007) *Journal of Nanoscience and Nanotechnology*, 7 (4-5), pp. 1284-1297
- ²⁰Lovat, V., Pantarotto, D., Lagostena, L., Cacciari, B., Grandolfo, M., Righi, M., Spalluto, G., Prato, M., Ballerini, L. Carbon nanotube substrates boost neuronal electrical signaling (2005) *Nano Letters*, 5 (6), pp. 1107-1110
- ²¹Wang, K., Fishman, H.A., Dai, H., Harris, J.S. Neural stimulation with a carbon nanotube microelectrode array (2006) *Nano Letters*, 6 (9), pp. 2043-2048
- ²²Yu, Z., McKnight, T.E., Ericson, M.N., Melechko, A.V., Simpson, M.L., Morrison III, B. Vertically aligned carbon nanofiber arrays record electrophysiological signals from hippocampal slices (2007) *Nano Letters*, 7 (8), pp. 2188-2195
- ²³Gabriel, G., Gómez, R., Bongard, M., Benito, N., Fernández, E., Villa, R. Easily made single-walled carbon nanotube surface microelectrodes for neuronal applications (2009) *Biosensors and Bioelectronics*, 24 (7), pp. 1942-1948
- ²⁴<http://www.sigmaaldrich.com/spain.html>
- ²⁵Menendez De La Prida, L., Huberfeld, G., Cohen, I., Miles, R. Threshold behavior in the initiation of hippocampal population bursts (2006) *Neuron*, 49 (1), pp. 131-142
- ²⁶Csicsvari, J., Henze, D.A., Jamieson, B., Harris, K.D., Sirota, A., Barthó, P., Wise, K.D., Buzsáki, G. Massively parallel recording of unit and local field potentials with silicon-based electrodes (2003) *Journal of Neurophysiology*, 90 (2), pp. 1314-1323
- ²⁷Ibarz, J.M., Foffani, G., Cid, E., Inostroza, M., De La Prida, L.M. Emergent dynamics of fast ripples in the epileptic hippocampus (2010) *Journal of Neuroscience*, 30 (48), pp. 16249-16261

6. THIRD SU-8 MICROPROBE PROTOTYPE FOR SIMULTANEOUS DRUG DELIVERY AND NEURAL ACTIVITY RECORDING

In this chapter a step forward is given and the delivery function has been integrated into novel SU-8 probes. Although potentials are an important factor to determine neuronal activity, it is well known that complex biochemical reactions within cells are the major mechanism determining their functionality. Specifically, it is of huge relevance to deliver drugs to highly localized areas of neural tissue in precise quantities while monitoring the cell response *in vivo*. In this chapter a new design, fabrication procedure and packaging are developed in order to integrate electrodes and fluidic microchannels in a single device. Three probe designs are developed to best fit the application. Contrary to the fluidic probes developed in Chapter 4, a novel fabrication procedure is created to locate the electrodes at the probe surface and integrate the fluidic channel and electrodes in the same face of the probe. An advanced packaging is designed and fabricated to allow the simultaneous electric and fluidic connection of the probe with the outside. Previous to the experimental tests, impedance spectroscopy characterization is performed and as expected double layer behavior of the electrodes is confirmed. Finally, 0.5 μl of kainic acid are delivered in rat's hippocampus and an epileptic seizure is observed. First experimental attempts revealed recording and delivery capability of the third prototype.

Contents

6. THIRD SU-8 MICROPROBE PROTOTYPE FOR SIMULTANEOUS DRUG DELIVERY AND NEURAL ACTIVITY RECORDING	109
6.1 DESIGN	110
6.1.1 A tetrode and a fluidic channel integration	111
6.1.2 Eight electrodes and two fluidic channels integration.....	112
6.1.3 Eight electrodes and eight fluidic channels integration design	113
6.2 FABRICATION.....	114
6.2.1 Initial fabrication procedure	114
6.2.2 Modifications, problems and solutions related to the initial fabrication procedure	114
6.2.3 Final fabrication procedure.....	119
6.3 PACKAGING	121
6.4 CHARACTERIZATION.....	121
6.4.1 Impedance spectroscopy.....	121
6.5 EXPERIMENTAL PROCEDURES	122
6.5.1 Simultaneous neural activity recording and drug delivery by means of in vivo testing	122
6.6 CONCLUSIONS.....	123
6.7 REFERENCES.....	125

6.1 Design

Three types of probes were designed in relation with the number and configuration of the sensing sites and microfluidic channels. Several options were considered in order to know which of them best fits the application. The first design was a microprobe with a tetrode and a microchannel. The second one was a probe with eight electrodes in a row and two fluidic channels, and the third design consisted of integrating eight electrodes and eight channels in the probe. The three designs were thoroughly studied and, for that three main conditions were taken into account: 1) the dimensions of the insertion area in order to minimize the invasive effect, 2) limitations established by the microfabrication techniques and 3) the experience acquired with the first and second microprobe prototypes.

The starting point for the design of the probes presented in this chapter was established from the experimental conclusions obtained in Chapter 5. For example, the width of the insertion area of the tetrode probe and the diameter of the electrodes were maintained. However, among other changes, the current probes were designed shorter since some noise problems associated with an excessive length of the probe emerged during experimentation. Specifically, it was assumed that the probes tended to vibrate during experimental tests, such vibration being one of the sources of noise obtained during the electrical recording. Also, some achievements from the probes developed in Chapter 4 were taken into account while designing the current ones. It was demonstrated that a 50 μm wide channel can be perfectly created by bonding technique so the same size was chosen to guarantee at least the creation of one type of fluidic channel. The length between the connection head and the tip of the probe was 5 mm whereas the diameter of all the electrodes was set at 20 μm . Moreover, none of the probes had the

insertion area wider than 160 μm because undesirable tissue damages were predicted. Apart from these considerations based on experience, each type of probe presented its particular features held in the insertion area.

6.1.1 A tetrode and a fluidic channel integration

The first design was aimed to insert a tetrode close to the tip of the probe. The distance between the centers of the electrodes was set at 25 μm and the diameter was 20 μm in order to facilitate the discrimination of neurons. As a consequence of such sensing configuration, a 90 μm wide insertion area was designed, figure 6.1 b). In addition to the tetrode, a 50 μm wide fluidic channel was integrated. It was considered a proper size in order to guarantee the bonding in the proximities of the channel. The channel had an inlet and three outlets. An outlet was located in the center of the tetrode in order to deliver in an equidistant way respect to the four electrodes. The dimensions of the outlet were the largest possible so that it could fit in the area limited by the tetrode. This outlet was designed to be 11 μm long and 5 μm wide. One of the problems foreseen with the microfluidic was that the outlet may be partially or fully occluded while delivering in such an environment like the brain. Moreover, it was predicted that the outlet may not be well-defined by photolithography due to so reduced dimensions. Thereby, two more outlets were added to decrease the chances of a total obstruction of the microchannel. There was no room left in the center of the tetrode so both of them were located between the tetrode and the tip of the probe as seen in figure 6.1 b). Both, the electrodes and the outlets were located in the same side of the probe in order to deliver and record from the same piece of tissue, figure 6.1 c). Contrary to the outlets, the inlet was located in the connection head which was 7.6 mm long and 4.5 mm wide, figure 6.1 a). The design of the connection head was kept constant for all different probe designs presented in this chapter in order to maintain the same packaging tools for all of them. Also, the body length was kept constant in order to avoid misreading results due to the variations that may emerge during the experiments.

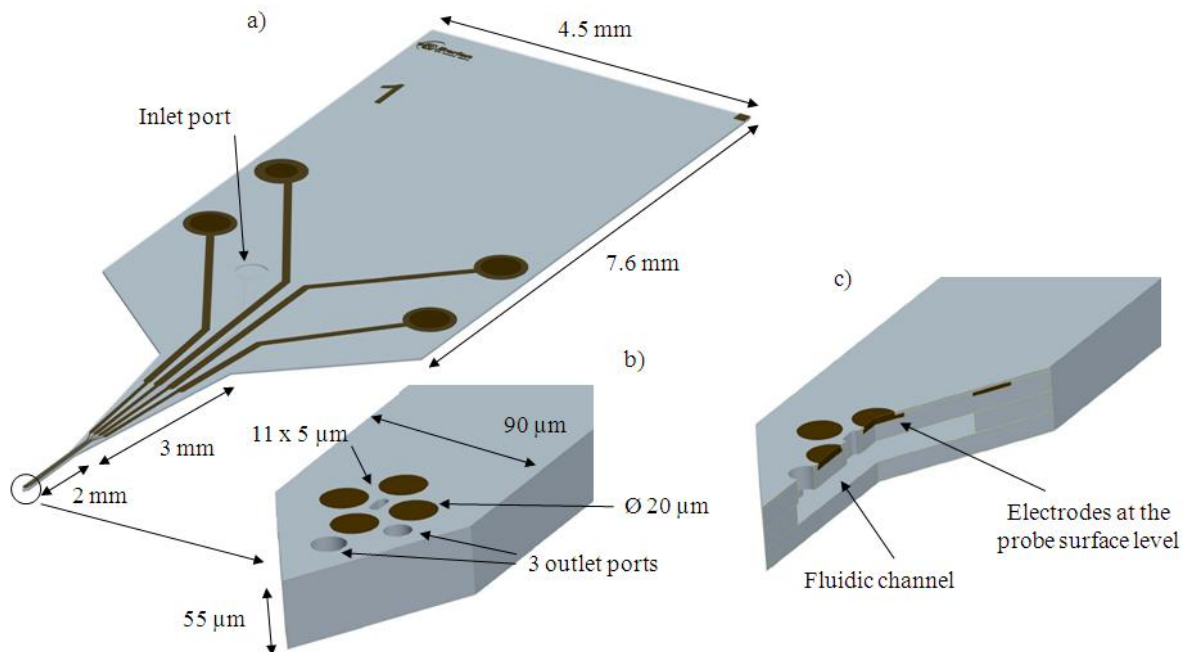


Figure 6.1 3D drawings of a microprobe with a tetrode and a microchannel integrated in it: a) the whole probe picture, b) a magnified picture of the tip and c) the transversal view of the fluidic channel

6.1.2 Eight electrodes and two fluidic channels integration

In the second design, eight electrodes in a row were placed along the insertion area at $100\ \mu\text{m}$ intervals, as shown in figure 6.2. As it is widely known, an ideal recording probe has a very small volume, so that tissue damage is minimized, but has very large number of monitoring sites so that the recorded spikes emanating from different neurons can be reliably separated. These competing demands limit the number of useful recording sites on a given probe. Thus, more than 10-12 recording sites require a probe wide enough to produce noticeable tissue damage and less favourable conditions for unit recording¹. In this case, the insertion area was $150\ \mu\text{m}$ wide so that 8 electrodes and two $40\ \mu\text{m}$ wide channels could fit in. Both channels had independent inlets and outlets in order to deliver more than a drug simultaneously. The diameter of the two outlets was $40\ \mu\text{m}$ and they were located between the third and fourth electrode, and the fourth and fifth one. The distance between the center of the outlet and the center of the closest electrode was $50\ \mu\text{m}$. The objective was to measure from two different firings in the hippocampus or to distinguish the recordings from the surface and depth layers of the cortex.

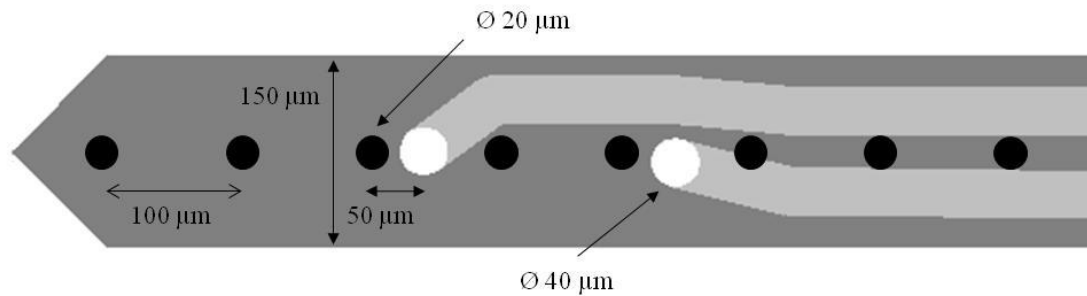


Figure 6.2 Schematic drawing of the eight electrodes in a row (black), two channels (light grey) and the outlets (white) located along the insertion area of the probe

6.1.3 Eight electrodes and eight fluidic channels integration design

In the third design eight electrodes in a row alternated with eight channels were designed as shown in figure 6.3. The width of the insertion area was set at 153 μm so that eight electrodes and eight fluidic channels could fit in. The distance between the center of the electrode and the center of the outlet was set at 50 μm . Each fluidic channel was designed to be 10 μm wide in order to be able to fit all the channels in the probe. Since the channels had to be so narrow, blocking problems during the fluidic tests were anticipated. In order to avoid so, different outlets were designed. The objective was to see which of those configurations was the most suitable for the application. The first fluidic channel was divided into three in the last stretch so that three outlets could be implemented between the first and the second electrode. The design was aimed to decrease the possibility to end up with a totally blocked channel once the probe was inserted. The second channel was widened up to 20 μm in the last stretch to get a wider outlet for the same reason. In the third channel, the outlet area was larger because it was extended along the channel. The fourth design consisted of creating a big pad with the aim of getting a larger outlet diameter. It was believed that the gliar scar formed during the experimental procedure could block such small outlets. In order to avoid the blocking effect a 40 μm diameter outlet was designed. In the next fluidic design, two outlets were placed along the channel also with the intention to minimize blocking effects. The last three channels did not have any significant features because the room was limited.

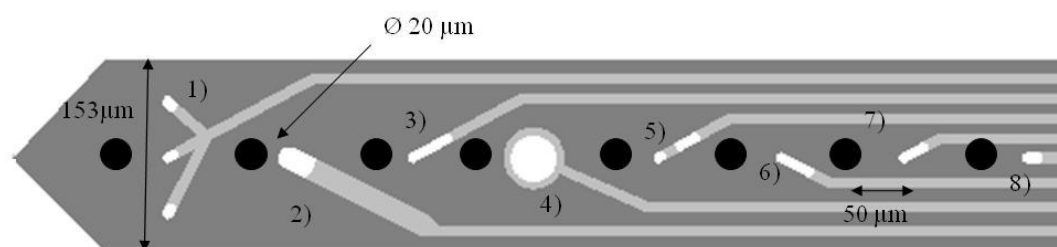


Figure 6.3 Schematic drawing of the eight electrodes in a row (black), eight channels (light grey) and the outlets (white) along the insertion area of the probe

6.2 Fabrication

6.2.1 Initial fabrication procedure

It was experimentally verified in Chapter 5 the importance of a close contact between the electrodes and the tissue, therefore, the novel sequence for the fabrication of the electrodes was reproduced. In addition, the standard bonding conditions developed in our lab were applied in order to integrate the fluidic function to the probe.

Briefly, once the aluminum sputtering was carried out and the wafer dehydrated, the passivation layer was processed in the conditions already reported in Chapter 5. The heating processes were increased up to 95°C and an UV dose of a 140 mJ/cm² was given. After this layer was developed, the sacrificial resin was processed and platinum sputtering was carried out. The electrodes were patterned by lift off technique. Next, the metallic tracks were covered with an SU-8 layer and, then, another SU-8 layer was processed in order to create the walls of the channels. The SB and PB processes were carried out at 95°C and the UV doses were of a 140 mJ/cm². The cover of the channel was fabricated on top of a Kapton™ film previously laminated on a Pyrex™ wafer. This layer was processed at 95°C and the bonding between both wafers was performed at a pressure of 1 bar and a temperature of 95°C. The release was done in two steps. First, the Kapton™ film was manually peeled off the Pyrex™ wafer. Next, the wafer was introduced in a saline solution, and the electrochemical etching of the aluminum was carried out in order to separate the probes from the wafer. Finally, the probes were rinsed with water and IPA and they were checked using an optical microscope.

6.2.2 Modifications, problems and solutions related to the initial fabrication procedure

Several drawbacks were seen in the initial fabrication procedure. There were problems to define the electrodes by lift off because the SU-8 was damaged in the ultrasonic bath. Various materials were

sputtered and adhesion and uniformity problems arose. Also, temperature and pressure parameters of the bonding needed optimization.

6.2.2.1 Electrodes patterning

In the fabrication procedure of the third prototype the lift off technique was used to pattern the metal instead of wet etching technique as repeatedly used in the second prototype fabrication. As explained in detail in Chapter 5, it was observed that by means of wet etching there were underetching problems and consequently, the process required some modifications. Furthermore, gold was the only noble metal that had an etchant available in our lab (platinum can be patterned using HF but this option was rejected because it was considered a risky process) and this fact limited the use of other metals. Thereby, it was believed the lift off to be a more versatile technique than the wet etching. In order to choose the best material, two criterions were taken into consideration: the good adhesion between the metal and SU-8 and the sensing capabilities of the metal. Thus, gold, platinum and iridium oxide were selected². Gold and platinum were sputtered following the standard recipe already reported in Chapter 3 and iridium oxide was sputtered following two different recipes based on the literature^{3,4}. As expected, the adhesion of the gold onto the SU-8 was not good, and an adhesion layer was necessary, figure 6.4 a). For the case of iridium oxide, sputtering by RF did not succeed due to the lack of adhesion as seen in figure 6.4 b), but DC sputtering seemed to be good enough, figure 6.4 c). Still, there was a lack of uniformity along the metallic tracks and, therefore, this material was discarded. Finally, it was observed that the adhesion and uniformity of platinum onto the SU-8 were excellent, figure 6.4 d). The platinum did not need an adhesion layer and that was another positive point because in this way, the wet etching process after the release of the probes could be avoided (this step was essential to get gold made electrodes in the second prototype fabrication procedure). Furthermore, platinum is a biocompatible material and have low electrode-electrolyte impedance compared with other materials⁵.

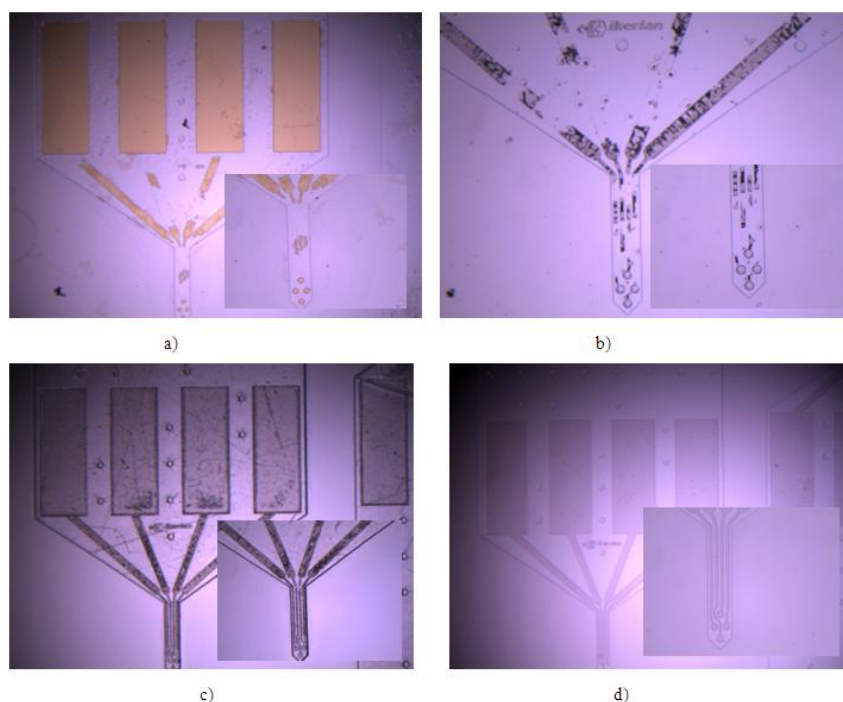


Figure 6.4 Metallization on top of the SU-8 5 layer by lift off technique: a) gold, b) iridium oxide by RF sputtering, c) iridium oxide by DC sputtering and d) platinum.

After these attempts, platinum patterning by lift off technique was implemented in the fabrication procedure of the third prototype but other problems emerged. A sacrificial resin was processed on top of the passivation layer in order to pattern the electrodes. OIR resin from Fujifilm⁶ was spin coated at 4000 r.p.m. and a 1.4 μm thick layer was obtained. OIR resin was chosen instead of S1818 because for the same spin rate a thinner layer was obtained and, at the same time, a higher photolithography resolution could be achieved. An exposure dose of a 100 mJ/cm^2 was given to pattern the OIR based on the technical report provided by the supplier⁶. Several developing durations were tested, but in all cases some grey figures were observed on the electrodes, figure 6.5 a). At first, it was thought that it was the resin that was not properly developed. Finally, it was realized that the developer affected the aluminum film. After keeping the wafer in contact with the developer up to a minute the aluminum started to disappear. This effect was undesirable because the aluminum was essential for the release of the probes as a final fabrication step. In order to solve this problem, the exposure dose of the resin was increased up to a 350 mJ/cm^2 . As expected, applying a higher dose the development was faster (down to 30 seconds), and the aluminum was not affected during the process, figure 6.5 b).

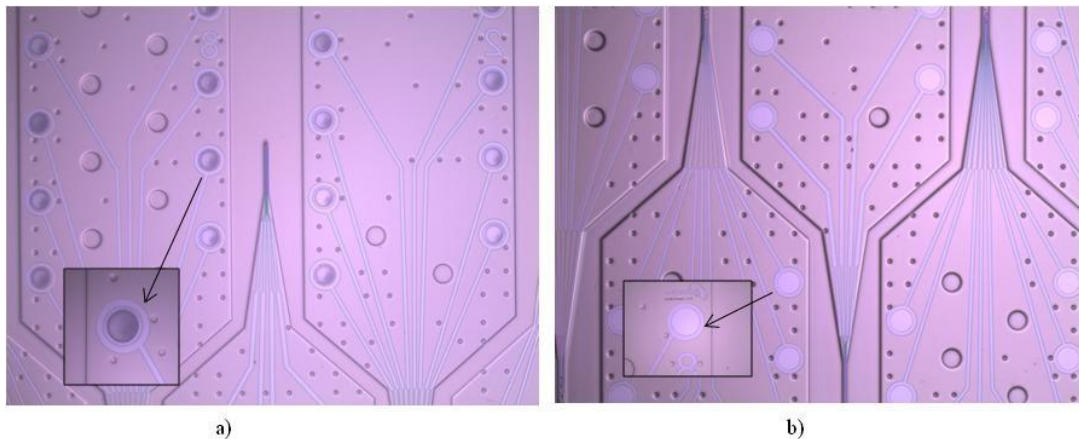


Figure 6.5 a) Grey figures on the electrode surface after the development of the OIR resin and b) the aluminum remains all over the wafer after the development of the OIR.

Another difficulty appeared during the lift off process itself. The 1.5 μm thick SU-8 5 passivation layer tended to break in the ultrasonic bath, figure 6.6 a). In order to address this issue, the process was carried out in cycles using the ultrasonic bath. Every 30 seconds the wafer was taken out from the ultrasonic bath and it was rinsed manually with methanol. As a result, a perfect lift off process was achieved as shown in figure 6.6 b).

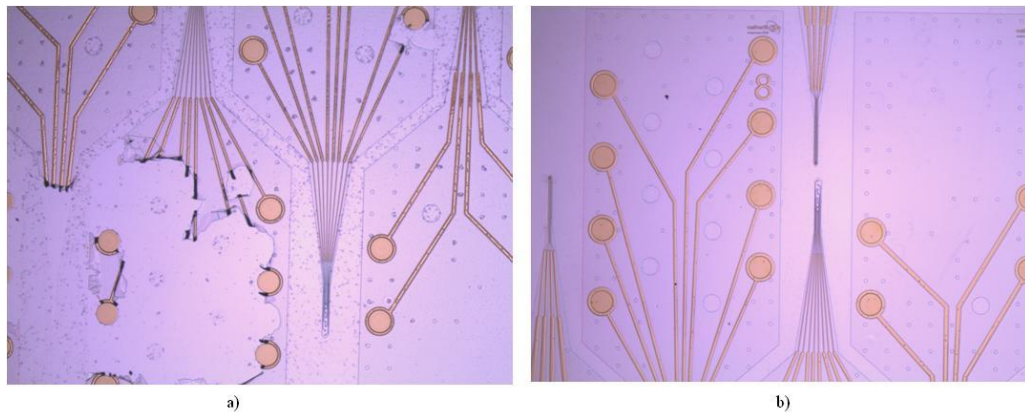


Figure 6.6 a) During the lift off process some SU-8 parts were broken and b) a suitable lift off process

6.2.2.2 Bonding and release processes

The first bonding attempt in order to create the cavities was carried out at 95°C applying 1 bar of pressure following the standard bonding conditions developed by the colleagues of Microsystems department in Ikerlan S. Coop.^{7,8,9}. It was observed that the SU-8 layers were perfectly bonded, but once the probes were detached from the substrate, the metallic areas that had been in contact with the aluminum, were separated from the probe and remained in the saline solution, figure 6.7 a). At first it was thought that the removal of the Pyrex™ and Kapton™ film was done in an aggressive way and that as a consequence, the electrode pads tended to detach from the probe. As a solution to this

problem, the SU-8 cover layer was processed on a Kapton™ film alone, avoiding the use of a Pyrex™ wafer. Finally, when the bonding finished the wafer was directly introduced in the electrolyte solution to etch the aluminum. In this way, any external force was not required during the release step. Additionally, some holes were made in the Kapton™ film once the SU-8 was developed. These holes helped to the saline solution to reach any part of the wafer and thus, increased the etching rate of the aluminum. However, this method was not the solution to the problem. Once the probes were separated from the substrate, the electrodes were still found detached from the probes. At last, it was realized that it was the stress of the SU-8 what made the electrodes peel off the SU-8. The platinum electrode had an aluminum layer underneath and an SU-8 layer on top. The sensing area was sandwiched by two different materials which have different mechanical response during the bonding process (where changes in temperature and pressure are applied). A new attempt was made changing the temperature of the bonding from its original value of 95°C down to 65°C, and keeping the pressure at 1 bar. To a certain degree, a slight advance was observed, since some of the probes present in the wafer had all the electrodes integrated. Nevertheless, the bonding area yield decreased, although the channels were still well defined. In order to increase the bonding yield, the pressure was increased up to 6 bar keeping the temperature at 62°C. As a result of this modification, a 70% yield was obtained. The fluidic channels were not collapsed, and most of the electrodes remained perfectly adhered to the probe. In order to get a 100% yield, another modification was performed in the fabrication procedure. Gold was added to the platinum electrodes under the assumption that being the gold a ductile metal, it could absorb the SU-8 internal tension and make the platinum keep stuck to the probe. It is difficult to demonstrate that the ductility of the gold was the cause, but what is true is that the deposition of 150 nm thick gold layer on top of the 50 nm thick platinum helped to reach a 100 % yield of well defined probes, figure 6.7 b).

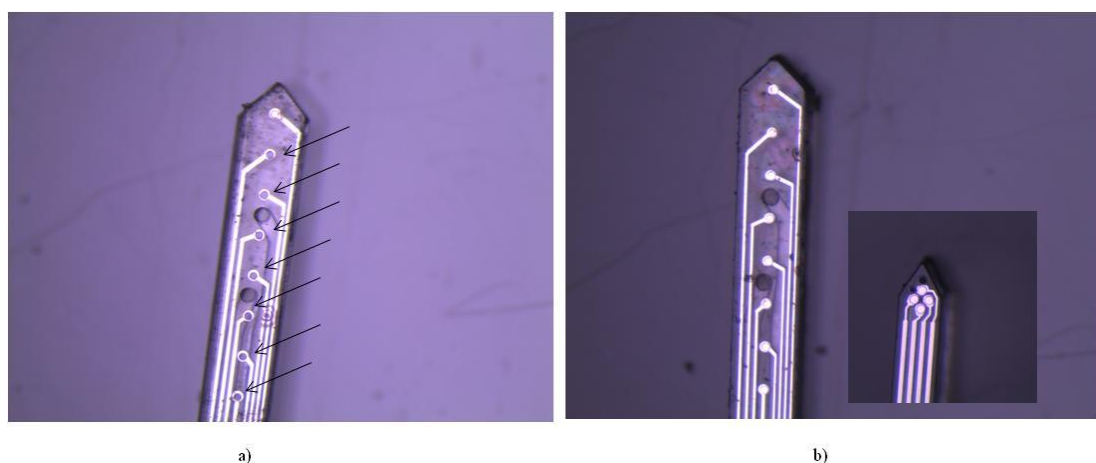


Figure 6.7 a) Seven electrodes out of eight detached from the probe (arrow) and b) all the electrodes (eight electrodes in a row and a tetrode) well stuck to the probe.

6.2.3 Final fabrication procedure

The final fabrication of the third SU-8 microprobe prototype was the result of the knowledge acquired from all the fabrication procedures of the previous prototypes. The technology developed for the fabrication of the first and second prototype was used; however, some processes had to be modified in order to integrate the microchannels into the probe. The fabrication procedure was carried out as follows.

The fabrication started with the deposition of an aluminum film on a silicon wafer by sputtering, figure 6.8 I). Then, the substrate was dehydrated for one hour at 200°C to improve the adhesion between the aluminum and the SU-8 layer. When the wafer cooled down, a 1.5 µm thick SU-8 passivation layer was spin coated and soft baked. The wafer was heated up to 65°C for 2 minutes and up to 95°C for 4 minutes. Then, a UV exposure of a 140 mJ/cm² was given using the mask which opened the inlets and outlets, and the sensing area. After the post bake, 2 minutes at 65°C and 4 minutes at 95°C, the layer was developed, figure 6.8 II). On top of this layer a sacrificial resin was processed in order to pattern the electrodes. Next, oxygen plasma treatment was applied on the SU-8 surface to improve the adhesion between the polymer and metal. Just after that, platinum (50nm) and gold (150 nm) were deposited by sputtering, figure 6.8 III). Next, the lift off technique was used for the definition of the electrodes, figure 6.8 IV). In order to cover the metallic tracks, a 10 µm thick SU-8 50 layer was spin coated, figure 6.8 V). The soft bake was carried out in a single step at 65°C for 20 minutes and a 140 mJ/cm² dose was given. After a post bake of 7 minutes at 65°C, another 20 µm thick SU-8 layer was spin coated on top, and processed in the same way to define the walls of the channels, figure 6.8 VI). Finally, both SU-8 layers were developed. Parallel to this procedure, another Pyrex™ wafer was used to fabricate the cover of the channel. A Kapton™ film was laminated on the Pyrex™ wafer, and a 40 µm thick SU-8 50 layer was spin coated, figure 6.8 VII). After a soft bake at 65°C for 20 minutes, a dose of a 140 mJ/cm² was given to pattern the shape of the probe. Contrary to previous fabrication procedures, the cover did not open any inlet or outlet. A post bake at 65°C was carried out for 7 minutes. As a last step, this layer was developed. Once both wafers were ready to be bonded, an oxygen plasma treatment was applied on both substrates to improve the bonding process. The bonding was carried out at 62°C and 6 bar for 20 minutes as already justified in the previous section, figure 6.8 VIII). When the wafers were cooled down, the Pyrex™ and Kapton™ were carefully removed, figure 6.8 IX). Finally, in order to separate the probes from the substrate, the wafer was connected to the power supplier to perform the aluminum electrochemical etching, figure 6.8 X). After four hours approximately, the probes were cleaned with IPA and water. SEM pictures show a typical fabrication result for each type of probe. In the tetrode version, figure 6.9 a), it can be observed that just an outlet was defined out of three. It was verified in the SEM that there were photolithography technique limitations to pattern so reduced figures. Some of the outlets of the third

design were not defined neither due to the dimensions, figure 6.9 c). On the other hand, the outlets that had a 40 μm diameter were perfectly defined as shown in figure 6.9 b). However, all the channels of the three designs were well-defined. They did not demonstrate any kind of deformation along the cavity.

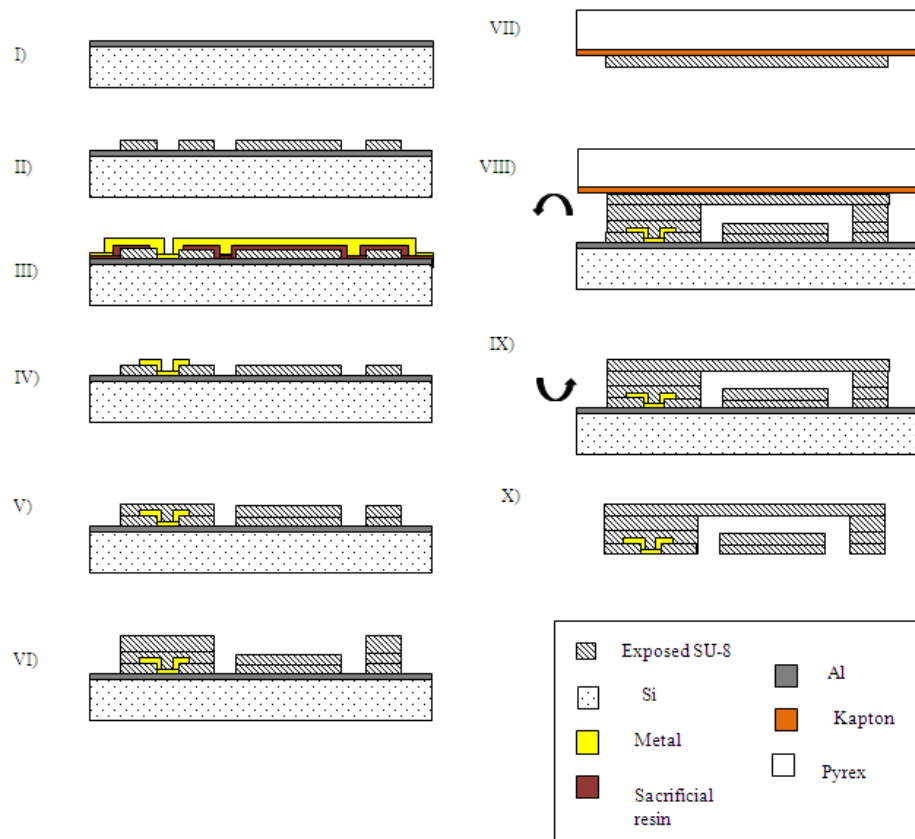


Figure 6.8 Schematic drawing of the third SU-8 microprobe prototype fabrication procedure sequence

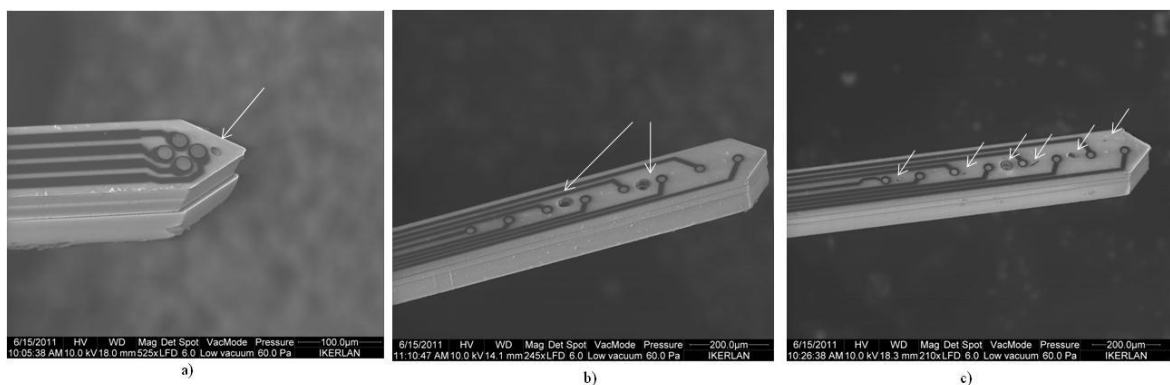


Figure 6.9 SEM figures of: a) the first probe design which includes a tetrode and a fluidic channel, b) the second design which includes eight electrodes in a row and two fluidic channels and c) the third

design which includes eight electrodes and eight fluidic channels. The outlets are indicated with arrows.

6.3 Packaging

An advanced package was developed for the housing of the third prototype probe to guarantee the electrical and fluidic connections with the outside. Stereolithography technique was used to create the package. As can be observed in figure 6.10 a) eight springs loaded pins were placed in the upper side of the package which connect the metallic pads of the probe and the socket. The socket is the piece that is fixed to the data acquisition equipment. Also, a fluidic connector with eight inlets was located on top of the deep red frame to fix the tubes and thus, ensure the delivery from the desired channel. This piece of the package allowed the simultaneous delivery even from eight independent channels. Owing to the probe placement, the bottom capsule included a pattern to fit the device in the base. Thus, any undesirable displacement was prevented. Once the probe was placed on the base it was perfectly aligned and fixed with two screws. In this way, electrical and fluidic connections were ensured. The figure 6.10 b) shows a probe fixed to the packaging ready to be used.

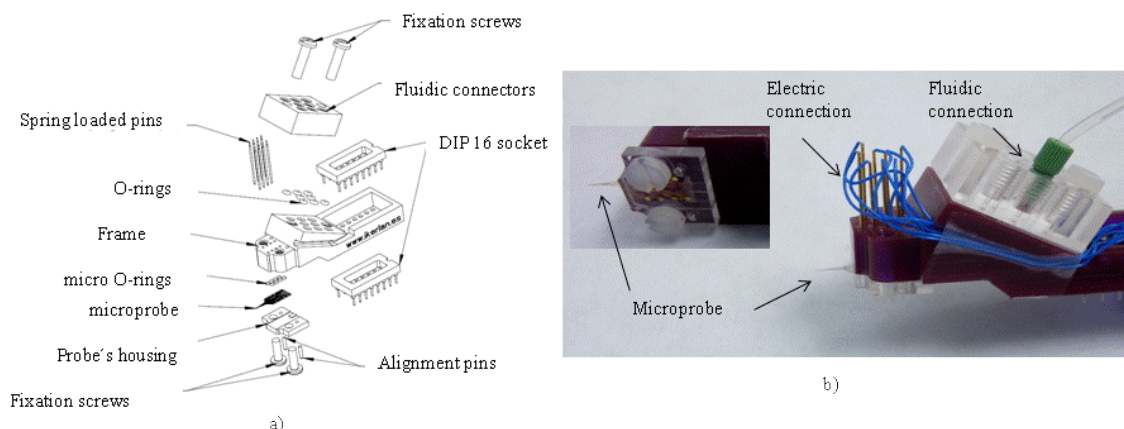


Figure 6.10 Microprobe packaging: a) Packaging drawing scheme and b) two pictures of an encapsulated probe

6.4 Characterization

6.4.1 Impedance spectroscopy

In the same way as with the second prototype probes, two-electrode impedance measurements were conducted using a commercial impedance analysis system (SI 1260, Solartron Analytical) in order to characterize the electrode-electrolyte interface impedance compared with a platinum reference electrode (Radiometer Analytical). Impedance modulus and phase were recorded from 6 probes at several discrete frequencies in the 10 Hz to 1 MHz range and all of them showed the same behavior. Here, the impedance values of a probe are shown as representative of any of them, figure 6.11. During

characterization, the microprobes were immersed in physiological saline solution (0.9 wt. % NaCl, with a nominal resistivity of $71.3 \Omega \cdot \text{cm}$ at 25°C) and impedance spectroscopy was carried out. Impedance modulus and phase behavior were similar to the second prototype version reported in Chapter 5. The current result showed again a great dependence of the frequency which corresponds to a capacitive behavior of the electrode double layer. Also, the capacitance is very low which can be explained by the surface roughness of the electrode. This result was considered suitable for the next experimental tests.

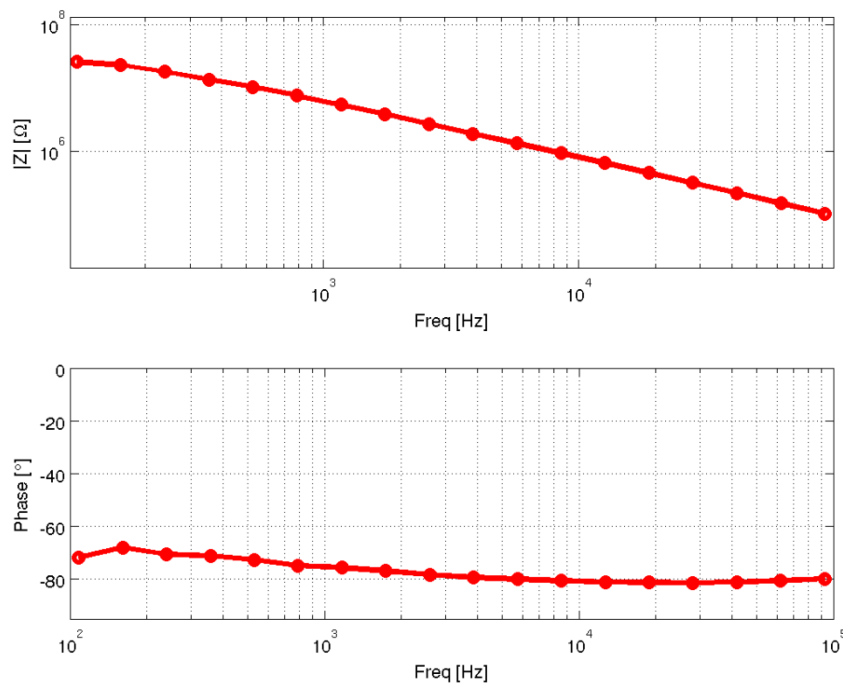


Figure 6.11 Impedance modulus and phase shift of the third prototype probes. Four probes with eight electrodes in a row and two tetrodes were characterized.

6.5 Experimental procedures

6.5.1 Simultaneous neural activity recording and drug delivery by means of *in vivo* testing

Experimental tests were then performed to deliver drugs into neural tissue using SU-8 probes with microchannels. The second probe design which had 8 electrodes in a row and two fluidic channels was chosen for this application. To this purpose, a small volume ($0.5 \mu\text{l}$) of kainic acid was delivered into the *in vivo* anesthetized preparation at a concentration of $0.4 \text{ mg}/0.2 \text{ ml}$ saline and it was delivered continuously over a period of 10 seconds. Kainic acid is a convulsive chemical known to elicit epileptic seizures when it is delivered locally in the hippocampus¹⁰.

Immediately after delivery started, it was observed that the activity increased near the electrodes close to the channel outlet, followed by a mechanical stimulation, figure 6.12. About 10 seconds after

completing delivery, local field potentials started to exhibit an increase of activity in the high frequency band (>20 Hz) followed by a rhythmic pattern of spikes-and-waves characteristic of epileptic seizure. This experiment confirmed us that drugs can be adequately delivered using integrated microchannels in SU-8 based probes. However, it was observed that the associated mechanical effects sometimes affected the recording capability of the electrodes after delivery. Also, in this first attempt the electrical response was recorded from six electrodes instead of the eight that the probe had. At present, we are actively working to improve delivery protocols and to reduce invasive capacity of the third prototype probes.

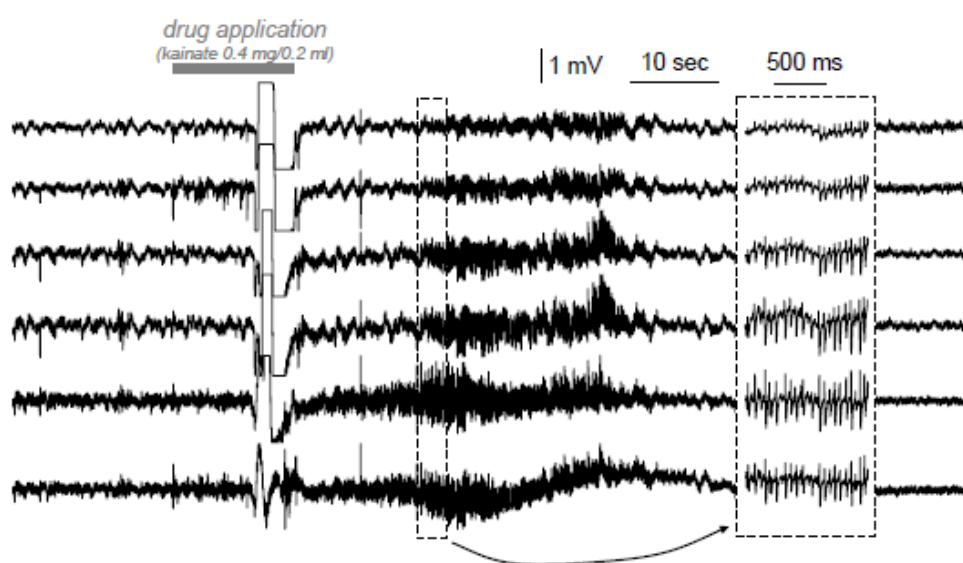


Figure 6.12 Typical example of drug delivery test. Kainic acid, a convulsive known to elicit local seizures in the hippocampus, was gently delivered through one of the microchannels (the probe which had two fluidic channels and 8 electrodes was used in this experiment). A typical seizure was recorded in the following few second after drug deliver.

6.6 Conclusions

In this chapter remarkable improvements of SU-8 probes in terms of design, fabrication, packaging and application have been demonstrated. Three designs have been developed varying the configuration and dimensions of the sensing sites and fluidic channels. The fabrication procedure results have shown that the best option is the one that integrates two fluidic channels. It was observed that the rest of the fluidic configurations are limited by the photolithography resolution. Platinum electrodes have been implemented in the current fabrication procedure because the sputtering results were superior to gold and iridium oxide ones. Bonding parameters also needed to be modified. It was verified a pressure of 6 bar and a temperature of 62 °C being the best parameters to obtain well-defined cavities and facilitate the release of the probes. A clear relation between the bonding conditions and a suitable release was observed. Additionally, an advanced packaging was developed which guaranteed the simultaneous

electrical and fluidic function of the probe. Finally, kainic acid solution was delivered in the rat hippocampus with the aim to detect a change in the neural activity. First attempts proved the functionality of the probe because as expected a clear increase in the activity was recorded. Nevertheless, a further investigation is essential to confirm the results. At present, more experimental trials are being performed.

6.7 References

- ¹Csicsvari, J., Henze, D.A., Jamieson, B., Harris, K.D., Sirota, A., Barthó, P., Wise, K.D., Buzsáki, G. Massively parallel recording of unit and local field potentials with silicon-based electrodes (2003) *Journal of Neurophysiology*, 90 (2), pp. 1314-1323
- ²Cogan, S.F. Neural stimulation and recording electrodes (2008) *Annual Review of Biomedical Engineering*, 10, pp. 275-309
- ³Lee, S.H., Jung, J.H., Chae, Y.M., Suh, J.-K.F., Kang, J.Y. Fabrication and characterization of implantable and flexible nerve cuff electrodes with Pt, Ir and IrOx films deposited by RF sputtering (2010) *Journal of Micromechanics and Microengineering*, 20 (3), art. no. 035015
- ⁴Van Ooyen, A., Topalov, G., Ganske, G., Mokwa, W., Schnakenberg, U. Iridium oxide deposited by pulsed dc-sputtering for stimulation electrodes (2009) *Journal of Micromechanics and Microengineering*, 19 (7), art. no. 074009
- ⁵Ivorra, A., Gómez, R., Noguera, N., Villa, R., Sola, A., Palacios, L., Hotter, G., Aguiló, J. Minimally invasive silicon probe for electrical impedance measurements in small animals (2003) *Biosensors and Bioelectronics*, 19 (4), pp. 391-399
- ⁶http://photoresist.com/wp-content/uploads/2010/11/OiR_908.pdf
- ⁷Agirregabiria, M., Blanco, F.J., Berganzo, J., Arroyo, M.T., Fullaondo, A., Mayora, K., Ruano-López, J.M. Fabrication of SU-8 multilayer microstructures based on successive CMOS compatible adhesive bonding and releasing steps (2005) *Lab on a Chip - Miniaturisation for Chemistry and Biology*, 5 (5), pp. 545-552
- ⁸Arroyo, M.T., Fernández, L.J., Agirregabiria, M., Ibañez, N., Aurrekoetxea, J., Blanco, F.J. Novel all-polymer microfluidic devices monolithically integrated within metallic electrodes for SDS-CGE of proteins (2007) *Journal of Micromechanics and Microengineering*, 17 (7), art. no. 011, pp. 1289-1298
- ⁹Blanco, F.J., Agirregabiria, M., Garcia, J., Berganzo, J., Tijero, M., Arroyo, M.T., Ruano, J.M., Aramburu, I., Mayora, K. Novel three-dimensional embedded SU-8 microchannels fabricated using a low temperature full wafer adhesive bonding (2004) *Journal of Micromechanics and Microengineering*, 14 (7), pp. 1047-1056
- ¹⁰Cavalheiro, E.A., Riche, D.A., Le Gal La Salle, G. Long-term effects of intrahippocampal kainic acid injection in rats: A method for inducing spontaneous recurrent seizures (1982) *Electroencephalography and Clinical Neurophysiology*, 53 (6), pp. 581-589

7. CONCLUSIONS AND FUTURE WORK

In this thesis, the research leading towards the creation of functional SU-8 microprobes has been presented. This research has been conducted from initial predictions and applications concerning the bioMEMS in Chapter 1, followed by the state of the art of microprobes, polymer SU-8 and microfabrication techniques reported in Chapter 2. In Chapter 3, the SU-8 microprobe for the monitorization of living tissues has been introduced. Then, the first neural SU-8 probe is addressed in Chapter 4 in order to prove the viability of the SU-8 technology for neural applications. In Chapter 5, the recoding capability of the probes has been optimized for fine-scale neural measurements. In Chapter 6, the technology already proved in Chapter 5 is used and multiple fluidic channels are integrated for neural drug delivery applications. In the current chapter, the most relevant conclusions with respect to the technology developed in previous chapters are first dealt. Then, costs' evaluation is reported looking towards the commercialization of the SU-8 probe. Next, the most relevant features concerning SU-8 and silicon probes are discussed and finally, some suggestions for future work are given.

Contents

7.1 GENERAL CONCLUSIONS	127
7.2 COSTS' EVALUATION	130
7.3 DISCUSSION	130
7.4 FUTURE WORK.....	132
7.5 REFERENCES.....	135

7.1 General conclusions

- The behavior of polymer SU-8 has been studied in the fabrication procedures and reported in Chapter 3, 4, 5 and 6. The ideal parameters of the heating processes such as soft bake, post bake and hard bake were found in order to obtain a flat surface, improve adhesion and change the polymerization state of the polymer when necessary. Moreover, UV exposure dose has been varied to fulfill those requirements. It was concluded in Chapter 3 that the adhesion between two layers that are in contact improves when the exposure dose increases and thus, delamination is prevented. In addition, it was seen in Chapter 4 that a controlled post bake (50°C) was required to develop the un-exposed SU-8 as a final step. Also, it was demonstrated in Chapter 6 that a particular design of masks (the design that avoids lightening the resin repeatedly) is essential to get a flat SU-8 device.
- The already well-established sputtering technique has been optimized in this thesis in order to metalize on top of the SU-8. Controlled recipes for the deposition of Ti, Pt, Cr and Au have been created in order to avoid damaging the SU-8 as explained in Chapter 3. Moreover, first attempts were carried out to obtain iridium films in Chapter 6. Nevertheless, iridium sputtering recipe needs improvements. It was seen that the sputtering has to be performed in cycles in order to avoid damaging the resin. Furthermore, it was verified that plasma treatment on top of the SU-8 and a previous hard bake (10 minutes at 95°C) are advisable steps to get a perfect adhesion between the resin and metal.
- Wet etching and lift off techniques were employed to structure the metal. In Chapter 5 it was seen the necessity of etching the gold in the spin coater in order to avoid underetching. In Chapter 6 the lift off technique was employed with especial care and avoiding the use of the ultrasonics for a long time to prevent against SU-8 damages.
- The bonding process was optimized in Chapter 4 and 6 in order to integrate perfect channels. Although the fabrication procedure was not the same, it was seen in both cases that low temperature (50-60°C) and high pressure (3-6 bar) are the best choice to create well-defined channels.

- Two positive resins, S1818 and OIR were used to pattern the electrodes. In Chapter 3 it was seen that using a primer and processing the resin S1818 for 20 minutes at 90°C is the best option to get a high resolution. In Chapter 6 the resin OIR was used because for the same spin rate a thinner layer was obtained and, as a result, the resolution was even better. Additionally, it was concluded that the developer of OIR can damage aluminum.
- Among microfabrication techniques, dicing techniques are commonly used to separate each microdevice individually as a final step. In the current work, alternative release methods have been used. The Kapton™ film resulted very useful because of its low adhesion to the SU-8 as explained in Chapter 3, 4 and 6. Once the fabrication of the probes finished, they were manually separated from the film easily. Nevertheless, it was verified in Chapter 5 and 6 the electrochemical release being the ideal method to release thin and narrow probes without breaking them.
- In addition, electrochemical deposition of platinum black was optimized in order to reduce the electrode-electrolyte interface impedance and, consequently, improve the sensing behavior of the electrodes. This process was demonstrated in Chapter 3 and 5. First attempts concerning the SWNTs coating were carried out, however, it was concluded in Chapter 5 that more tests are required to verify the viability of the process.
- Four suitable designs (one for the living tissue monitoring and three for neural applications) have been developed in this thesis. Each dimension has been thoroughly studied in order to get a minimally invasive microdevice and guarantee insertion in tissue at the same time. Nevertheless, some mechanical problems arose in Chapter 5. A 70 μm thick SU-8 layer was a drawback for the SWNTs deposition on top of the electrodes. Finally, it was observed that replacing the 70 μm thick layer by 4 layers of 20 μm and adjusting the fabrication procedure were the solution. Another critical point of the design was the configuration of the electrodes. The configuration was always designed to achieve the highest signal-to-noise ratio possible. The diameter of the electrodes (20 μm) for neural applications was experimentally verified being a suitable option because apart from recording from high peak-to-peak amplitudes (400-500 μV), different neuronal sources were recorded in each electrode.
- A novel sequence of fabrication steps was developed in Chapter 5 in order to place the electrodes at the probe surface level and hence improve neuron-electrode contact. Sputtering on top of a 1.5 μm thick passivation SU-8 layer was the key in order to reach this objective.

Experimental trials revealed that a close contact between the electrode and neural tissue was essential to detect action potentials with high peak-to-peak amplitude.

- A flexible packaging was developed for the monitorization of the ischemia in Chapter 3. The encapsulation resulted in a high yield procedure and an easy handling ensemble of probe and packaging was obtained. Stereolithography technique was then employed for the neural probes housing. Electrical and fluidic connections were successfully fixed and there were no problems during experimental tests. Also, a typical PCB was slightly modified for the neural activity recording in Chapter 5. Finally, a more complex packaging was developed with multiple fluidic connections for simultaneous neural activity recording and drug delivery in Chapter 6. As a general conclusion, it was demonstrated the ability to design and fabricate a suitable packaging for each probe prototype and application.
- Impedance spectroscopy technique was repeatedly used in this thesis. It resulted in an ideal method to predict the behavior of the electrodes before the experimental tests as already dealt in Chapter 3, 5 and 6. Additionally, this technique was used to detect an ischemia episode. It was demonstrated in Chapter 3 that the chemical and electrical changes that an ischemia causes in a living tissue can be monitorized using this technique.
- The functionality of all the SU-8 based microprobes developed in this thesis has been demonstrated. *In vivo* ischemia-reperfusion episode in rat's kidney was detected by real time measurements in Chapter 3. An increase of impedance was seen as a reliable indicator of anoxic edema due to ischemic cell swelling. In addition, multiple neural applications were carried out in rat's hippocampus. The first neural probe prototype developed in Chapter 4 demonstrated being capable of delivering into neural surroundings. First *in vitro* tests were carried out in Chapter 5 and it was demonstrated the capability of the probe to record from action potentials. The quality of the next *in vitro* recordings reported also in Chapter 5 increased due to a better electrode-neuron contact and the platinization process. Finally, *in vivo* trials were performed in rat's hippocampus and action potentials with peak-to-peak amplitude of 400-500 μV were measured over noise background. Furthermore, the correct configuration of the sensing site was confirmed. The tetrode distinguished from different neural sources.
- Few tests were performed with reference to the mechanical behavior of the SU-8 probes. First results reported in Chapter 4 verified the damage evoked to the neural tissue being lower with regards to standard rigid probes.

- Simultaneous neural activity recording and drug delivery application was for the first time carried out using SU-8 based microprobes. An epileptic seizure was recorded after 0.5 μ l of kainic solution was delivered into rat's hippocampus. Probe functionality was verified. Nevertheless, more tests are necessary to confirm this promising result.

7.2 Costs' evaluation

Evaluation of costs has been performed in order to calculate the price of a SU-8 probe as a final product. In addition, the final price of the SU-8 probe has been somehow compared with price of the commercial silicon based probes. The probes developed by Neuronexus Technologies, Inc.¹ have the highest impact among electrophysiologist at present and that is the reason of choosing as a reference to make the comparison. The standard and cheapest probe supplied by Neuronexus with 8 electrodes in a row costs 185\$. The next price concerns to a probe with 16 electrodes placed in 1, 2 or 4 rows, which costs 305\$. The price then increases up to 510 \$ when 32 electrodes are integrated in a narrow probe shank and the probes made for chronic applications range between 330 and 655 \$ approximately.

In the present thesis an evaluation of costs has been added which has been previously developed by Microliquid². It has been considered that 4 wafers which have 250 probes each can be processed in a week. However, a success of the 70% is estimated, thus, 700 probes would be fabricated in a week. The costs have been distributed as follows: 1000€ the use of the clean room, 2000€ staff costs, 350€ assembly costs and 5250 € packaging process and delivery costs. The sum of all these costs and the subsequent division with 700 gives the result of 12.3€, which is the cost of a single probe. The packaging costs 4.5€, consequently the probe and the packaging sum increases up to 16.8 €. Considering that the profit is the double of its initial price, the final price would be of 33.6 €. It has to be considered that marketing costs have not been added to this final price. Even so, the price of commercial probes is an order of magnitude higher comparing to SU-8 based probe's price. Therefore, it has been concluded that the fabrication of SU-8 probes is a low cost process.

7.3 Discussion

Once all the results and costs' evaluation have been highlighted, a brief comparison respect the most important features of the SU-8 neural probes and the probes developed by Neuronexus Technologies, Inc. are reported in the current section.

- Recording capability: best results were obtained with the tetrode developed in Chapter 5. Action potentials and local field potentials were captured by the tetrode immediately upon penetration of the CA1 cell layer. Peak-to-peak amplitudes of 400-500 μ V were recorded. This result is considered similar to conventional silicon-based tetrodes³.

- Noise: typically, the noise level over normal unit recording bandwidth for the Neuronexus probe is of $15 \mu\text{V}_{\text{RMS}}$ ¹. The initial noise level using the $20 \mu\text{m}$ embedded electrode was of $27 \mu\text{V}_{\text{RMS}}$ ⁴. However, in the last experiments, where the best recording was obtained, the noise level was qualitatively appreciated to be lower⁵. In the future, more tests have to be done in order to confirm quantitatively the current noise level.
- Impedance: Neuronexus probes have impedance values between approximately 0.5 to $3 \text{ M}\Omega$ (at 1 kHz) depending on the geometrical size of the electrode site. The probes developed in this thesis have impedance values between 0.5 and $6 \text{ M}\Omega$. Nevertheless, probes with impedance values inferior to $3 \text{ M}\Omega$ were used in all the experiments.
- Fluidic integration: Neuronexus offers probes with combined fluidic and electrophysiological recording functionality. The fluidic tubes are attached to the lower side on the microelectrode array and the delivery port is at the distal end of the fluidic tube. The probe fluidic port is made of fused silica and the outer and inner diameters are of $165 \mu\text{m}$ and $100 \mu\text{m}$ respectively. Contrary to this design, the SU-8 technology enables the integration of more than one fluidic channel in the same probe. Moreover, the outports of the channels can be located at the required deep of the probe. Thus, it is confirmed the versatility of the SU-8 technology.
- Damage in tissue: since high peak-to-peak amplitudes have been recorded ($400\text{-}500 \mu\text{V}$) with the SU-8 probes, it can be concluded that this probes are not remarkably invasive. Recording from high amplitudes means that the electrode is near the neuron and that the probe has not damage the neuron. In order to make a comparison with silicon based probes a further study would be required.
- Biocompatibility: already reported studies confirm the biocompatibility of the polymer SU-8. Anyway, further studies are required to know the scope of the SU-8^{6,7,8}.
- Costs: in the previous section it has been estimated that the price of a single SU-8 probe would be initially lower than the probes of Neuronexus.
- Use: it has been experimentally proved that silicon based probes tend to break whereas SU-8 based probes are not broken so easily during experimental tests. It can be concluded that the SU-8 probe is a reusable device because it can stand repetitive experimental trials and keep the accuracy in the consecutive recordings.

7.4 Future work

The present section deals with some of the most relevant topics in this thesis that would require improvements, followed by possible applications and modifications of the microprobes developed within and, finally, the current state of the probes will be explained.

One of the most critical point of the microprobes has been their sensing capability. Particular dimensions of the electrodes were designed for each prototype in order to increase signal-to-noise ratio. Moreover, the diameter of the electrode was designed to sort multi-neuronal activities into their single-neuron components. Nevertheless, the sensing behavior needs to keep improving. Platinum black electrochemical coating resulted in a potential method for initial monitorization tests but there were impedance variations along the time. Also, SWNTs deposition was tested but the few attempts realized were not enough to get an idea of the possibilities of this technique. We should continue working with SWNTs and optimize the procedure in order to fill the entire gap between the electrode and the tissue. Moreover, it should be proved if it is possible to cover the electrodes when these ones are placed at the probe surface and there is no gap between the electrode and the outside. Another option could be to increase the roughness of the electrode. For that, the sputtering process should be optimized and metal grain size measured each time until an ideal morphology is achieved. Inversely, instead of creating a rough metal surface an alternative should be to perform the sputtering of the metal on top of a rough surface. It has been already reported a fabrication procedure where the electrodes are placed on top of a polysilicon rough film⁹. It was concluded that the electrode-electrolyte interface impedance was lowered by a factor of approximately 50 compared to smooth surfaces.

The mechanical behavior of the polymer probe has also been dealt in this work. The behavior of the SU-8 microprobes for living tissue monitoring was compared with Si and SiC probes in an already reported work¹⁰. It was demonstrated how the high flexibility of the SU-8 avoids damaging the tissue when the external probe cap is laterally pushed or pulled. When a lateral force was applied to the inserted probe the Si or SiC lacerated the tissue due to its rigidity, which could cause slight hemorrhage and affect the accuracy of the impedance measurement. In such situations, the SU-8 probe deflected at the surface of the organ causing no damage and minimizing potential measurement errors. Owing to these results, no more mechanical test will be done in the near future. The first SU-8 neural probes developed in Chapter 4 also demonstrated that the damage evoked into neural tissue is lower comparing with conventional rigid probes. Nevertheless, up to now any specific study has not been performed for example after a long-term testing. In the near future further tests should be carried out to know the lesion that the latest neural SU-8 prototype evokes.

In addition to the electrical and mechanical optimal behavior of the probe, any device intended for short and especially long-term *in vivo* application has to fulfill rigorous biocompatibility and biostability requirements¹¹. First, it should not induce toxicity in the surrounding tissues, and should not damage local tissue due to induced mechanical stress. Second, the drug-eluting capabilities of the device should not be compromised by the surrounding tissue. Specifically, the implant must tolerate long-term exposure to the physiological environment, as well as resist the impact of the surrounding tissue on its function (biofouling)^{12,13}. With this in mind, biocompatibility and biofouling level of the SU-8 has been already reported in the literature. There are some reports that guarantee an adequate biocompatibility and reduced biofouling^{6,8}. However, studies of long-term stability should be carried out specifically once the properties of the SU-8 have been modified during the fabrication procedure of the probes.

In vitro and *in vivo* experimentation has been carried out in this thesis in order to prove the viability of the microprobes. Short-term preliminary attempts have been realized due to their little complication of the procedure. Moreover, a huge knowledge has been obtained as a result. In spite of having promising results, long-term *in vitro* studies and chronic *in vivo* tests would be a perfect complement to show the behavior of the probe along the time. In addition, stimulation function can be added to the probes and for that, other sensing materials could be tested. For example, polymer poly(3,4-ethylenedioxythiophene) (PEDOT) could be studied as a new material for simultaneous neural recording and stimulation. *In vivo* chronic testing of microelectrode arrays implanted in rat's cortex revealed that using PEDOT coated electrodes a high signal-to-noise ratio and charge injection is obtained.

Although multiple options can be numbered in this section, the real situation is that little changes are being done in the last prototype design or fabrication procedure. As mentioned in Chapter 6, 8 independent fluidic channels were designed for the probe but some of them were collapsed due to the high aspect ratio and photolithography limitations. This issue should be solved in the near future. The dimensions and shapes of the outlets might be designed again and the fabrication procedure adjusted.

The most attractive application at the present is the simultaneous neural activity recording and drug delivery. Preliminary tests have demonstrated a promising future, however, more tests have to be carried out and repetitive results have to be reached in order to confirm the good results shown in this thesis. At this moment, drug delivery tests are being carried out in order to get the best of the technology already optimized.

Briefly, future work will be mainly focused on making the probes known in the scientific community. They have been experimentally tested and initial tests showed their suitable functionality. As a general

conclusion and looking toward the future, it is believed that the field of application of the SU-8 microprobes can be extended.

7.5 References

¹<http://www.neuronexus.com/>

²<http://www.microliquid.com/>

³Csicsvari, J., Henze, D.A., Jamieson, B., Harris, K.D., Sirota, A., Barthó, P., Wise, K.D., Buzsáki, G., 2003. Massively parallel recording of unit and local field potentials with silicon-based electrodes. *Journal of Neurophysiology* 90(2), 1314-1323.

⁴Altuna, A., Gabriel, G., De La Prida, L.M., Tijero, M., Guimerá, A., Berganzo, J., Salido, R., Villa, R., Fernández, L.J. SU-8-based microneedles for in vitro neural applications (2010) *Journal of Micromechanics and Microengineering*, 20 (6), art. no. 064014

⁵ Altuna, A., De La Prida, L.M., Gabriel, G., Guimerá, A., Berganzo, J., Villa, R., Fernández, L.J. SU-8 based microprobes with integrated planar electrodes for enhanced neural depth recording, sent to *Biosensors&Bioelectronics*

⁶Kotzar, G., Freas, M., Abel, P., Fleischman, A., Roy, S., Zorman, C., Moran, J.M., Melzak, J. Evaluation of MEMS materials of construction for implantable medical devices (2002) *Biomaterials*, 23 (13), pp. 2737-2750

⁷Voskerician, G., Shive, M.S., Shawgo, R.S., Von Recum, H., Anderson, J.M., Cima, M.J., Langer, R. Biocompatibility and biofouling of MEMS drug delivery devices (2003) *Biomaterials*, 24 (11), pp. 1959-1967

⁸Cho, S.-H., Lu, H.M., Cauller, L., Romero-Ortega, M.I., Lee, J.-B., Hughes, G.A. Biocompatible SU-8-based microprobes for recording neural spike signals from regenerated peripheral nerve fibers (2008) *IEEE Sensors Journal*, 8 (11), art. no. 4658118, pp. 1830-1836

⁹Paik, S.-J., Park, Y., Cho, D.-I.D. Roughened polysilicon for low impedance microelectrodes in neural probes (2003) *Journal of Micromechanics and Microengineering*, 13 (3), pp. 373-379

¹⁰Tijero, M., Gabriel, G., Caro, J., Altuna, A., Hernández, R., Villa, R., Berganzo, J., Blanco, F.J., Salido, R., Fernández, L.J. SU-8 microprobe with microelectrodes for monitoring electrical impedance in living tissues (2009) *Biosensors and Bioelectronics*, 24 (8), pp. 2410-2416

¹¹Anderson, J.M., Langone, J.J. Issues and perspectives on the biocompatibility and immunotoxicity evaluation of implanted controlled release systems (1999) *Journal of Controlled Release*, 57 (2), pp. 107-113

¹²Anderson, J.M. Inflammation and the foreign body response (1994) *Problems in General Surgery*, 11 (2), pp. 147-160

¹³Voskerician, G., Shive, M.S., Shawgo, R.S., Von Recum, H., Anderson, J.M., Cima, M.J., Langer, R. Biocompatibility and biofouling of MEMS drug delivery devices (2003) *Biomaterials*, 24 (11), pp. 1959-1967